5 Lock Wall Simulation

In Chapter 4, it was shown that the extended hyperbolic model accurately predicts the interface response for a variety of experimental stress paths applied in the laboratory. It is desirable, however, to evaluate the accuracy and applicability of this new model for SSI analyses of lock walls. There are little data on lock wall response during construction and operation of locks that can be used to perform such an evaluation. The IRW at Virginia Tech provides a unique opportunity to model key aspects of lock wall construction and operation within a controlled experimental environment.

The IRW was originally developed to study the earth pressures induced by compaction of backfill. Factors such as type of backfill, compaction procedure, and lateral movements of the wall were analyzed by Sehn (1990) and Filz (1992) using the IRW. As result of their work, methods were developed for estimation of compaction-induced earth pressures against retaining walls (Duncan et al. 1991; Filz and Duncan 1997; Filz, Duncan, and Ebeling 1997).

For this investigation, a test was performed in the IRW that modeled placement and compaction of the backfill, application and removal of surcharge, and movements of the water table behind a lock wall. Light Castle sand was used as backfill material for the test. Finite element analyses of all the stages of the test were performed using the updated version of SOILSTRUCT-ALPHA, which contains the formulation of the extended hyperbolic model for interfaces. Analyses of the backfill and surcharge stages served to calibrate the backfill properties for use in analyses of the inundation stage. The test results indicate that the extended hyperbolic model provides accurate approximations of the response of the wall-backfill interface for the type of loading induced during the test.

This chapter describes the experimental procedures, results of the IRW test, and analyses of the IRW test. The chapter is divided into the following sections:

a. The IRW facility.

b. Testing procedures.

c. Test results.

d. Discussion of test results.

e. Finite element analysis procedures.

f. Calibration analyses.

g. Analysis of backfill inundation.

h. Summary and conclusions.

The first section describes the characteristics of the IRW and the modifications that were necessary to accommodate simulation of a lock wall. In subsequent sections, the testing procedures and results are described in detail. Some observations are presented regarding the backfill response to external loading and compaction that are relevant for the finite element analyses of the IRW. Details of the analyses performed using SOILSTRUCT-ALPHA are also presented. Finally, the accuracy of the extended hyperbolic model is evaluated based on comparisons of the results of the analyses and the test data.

5.1 The IRW Facility

A complete description of the components of the IRW was presented by Sehn (1990). This section summarizes the features of the IRW that are relevant for this investigation.

5.1.1 Components of the IRW

Figure 5-1 is a general view of the IRW. It is composed of a backfill area, the instrumented wall, and a reinforced concrete U-frame structure that supports the wall and encloses the backfill area. The IRW is located inside a building, isolated from the direct action of the elements. An overhead crane facilitates movement of heavy equipment and materials. The floor of the backfill area is approximately 0.90 m below the floor level of the surrounding areas in the building. The top of the instrumented wall is approximately 1.20 m above the floor level of the building. The backfill area is 1.83 m wide by 3.05 m long. A 1.83-m-wide ramp leading into the area provides access for the equipment necessary for placement and compaction of the backfill.

A cross section of the IRW is shown in Figure 5-2. The instrumented wall is composed of four 0.73-m-wide by 2.13-m-high concrete panels. Each of the panels is supported vertically by two cantilever-type load cells (Sehn 1990), which consist of a 0.1-m-long cantilever beam bolted to a support bracket at the bottom of the panel. On the free end of the beam, a roller bearing wheel allows movement on a hardened steel pad attached to the concrete floor. Each of the panels is supported horizontally by three horizontal load cells. Each of the load cells consists of a steel bar, supported on both ends by spherical bearings to minimize bending moments. The forces on the vertical and horizontal load cells are measured by strain gauges bonded to their surface at appropriate locations.

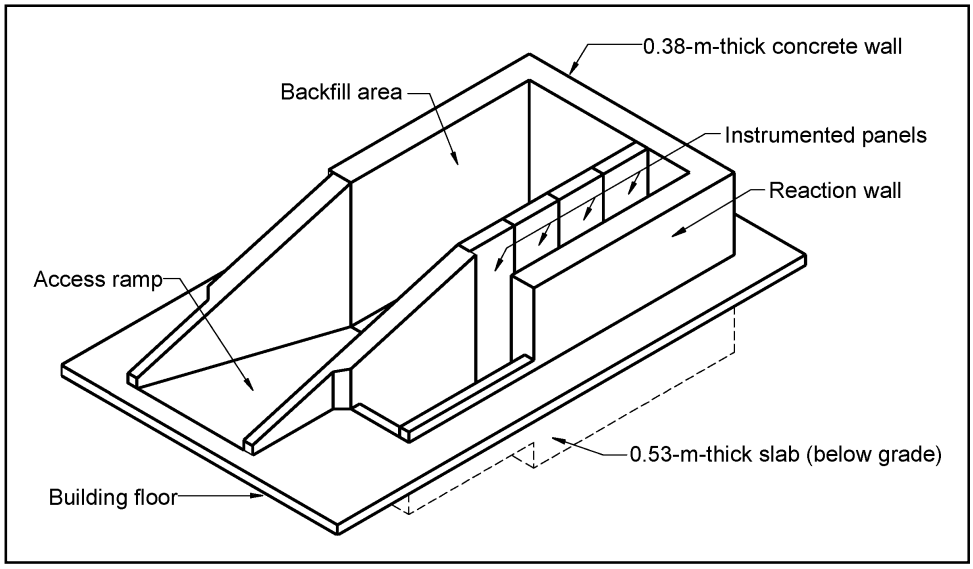

Figure 5-1. The IRW test facility (after Sehn 1990)

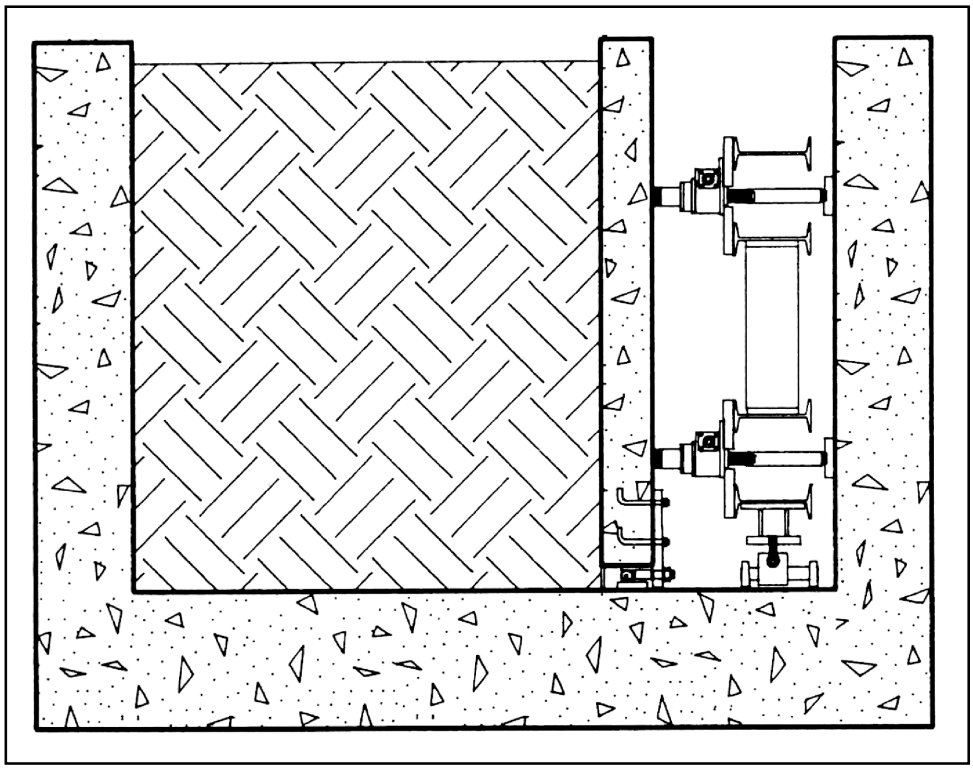

Figure 5-2. Cross-section of the IRW (after Sehn 1990)

The horizontal loads from the panels are transmitted by the load cells to a steel frame behind the panels. The frame is supported vertically by bearings that allow horizontal movements. Four screw jacks allow the application of horizontal displacements to the instrumented wall. This feature of the IRW was not used in

the lock wall simulation. The concrete panels were kept in place throughout the test.

The displacements of each of the panels during testing are monitored by two LVDTs, located at the top and bottom of the panel. The LVDTs are attached to a fixed reference beam located behind the panels.

As illustrated in Figure 5-3, the two central panels of the instrumented wall contain a variety of pressure cells for local measurements of earth pressures. Sehn (1990) presents a detailed description of the type of pressure cells embedded in the panels. For this investigation, pressures were measured using only the Gloetzl cells. The Gloetzl cells are mounted flush with the exposed wall surface. The surface of each of the cells is coated with a cement grout that resembles the surface texture of the wall. It was found that the Gloetzl cells did not provide accurate data, especially during inundation of the backfill. Filz (1992) recognized that these pressure cells may be especially sensitive to moisture migration in the surrounding mass of concrete. Nevertheless, pressure data collected during backfilling operations of the IRW provided qualitatively useful information on compaction-induced earth pressures.

A series of thermocouples are installed on both sides of the instrumented wall. The thermocouples provide data necessary for corrections of pressure and deformation readings, which may be needed when large temperature fluctuations take place during the test.

5.1.2 Preparations for the test

Simulation of a lock wall in the IRW required compaction of the backfill, application of a surcharge on the backfill surface, and inundation of the backfill. The IRW was not originally designed for surcharge application and inundation of the backfill. This section contains a description of the work performed to accommodate this type of testing in the IRW.

5.1.2.1 Construction of Bulkhead. To allow full inundation of the backfill, a bulkhead was built at the bottom of the access ramp. The bulkhead consisted of a rigid, wooden frame capable of withstanding the earth pressures generated during compaction, surcharge, and inundation. A 19-mm- (3/4-in.-) thick plywood facing was attached to the bulkhead on its backfill side. The bulkhead was pre-assembled outside the IRW and laid in place using the overhead crane. Tight tolerances were required to minimize the width of the gaps between the bulkhead and the existing concrete walls. The bulkhead was tightly attached to the walls and floor of the ramp with fifteen 12.5-mm- (1/2-in.-) steel bolts.

5.1.2.2 Water seal. To prevent significant leaks during inundation of the backfill, a sealant was applied to all the gaps existing between the instrumented panels, between the panels and the floor, and along the edges of the bulkhead. All the gaps had a maximum width of approximately 12.5 mm (0.5 in.). Caulking strips were introduced in all gaps to serve as support for the sealant. A

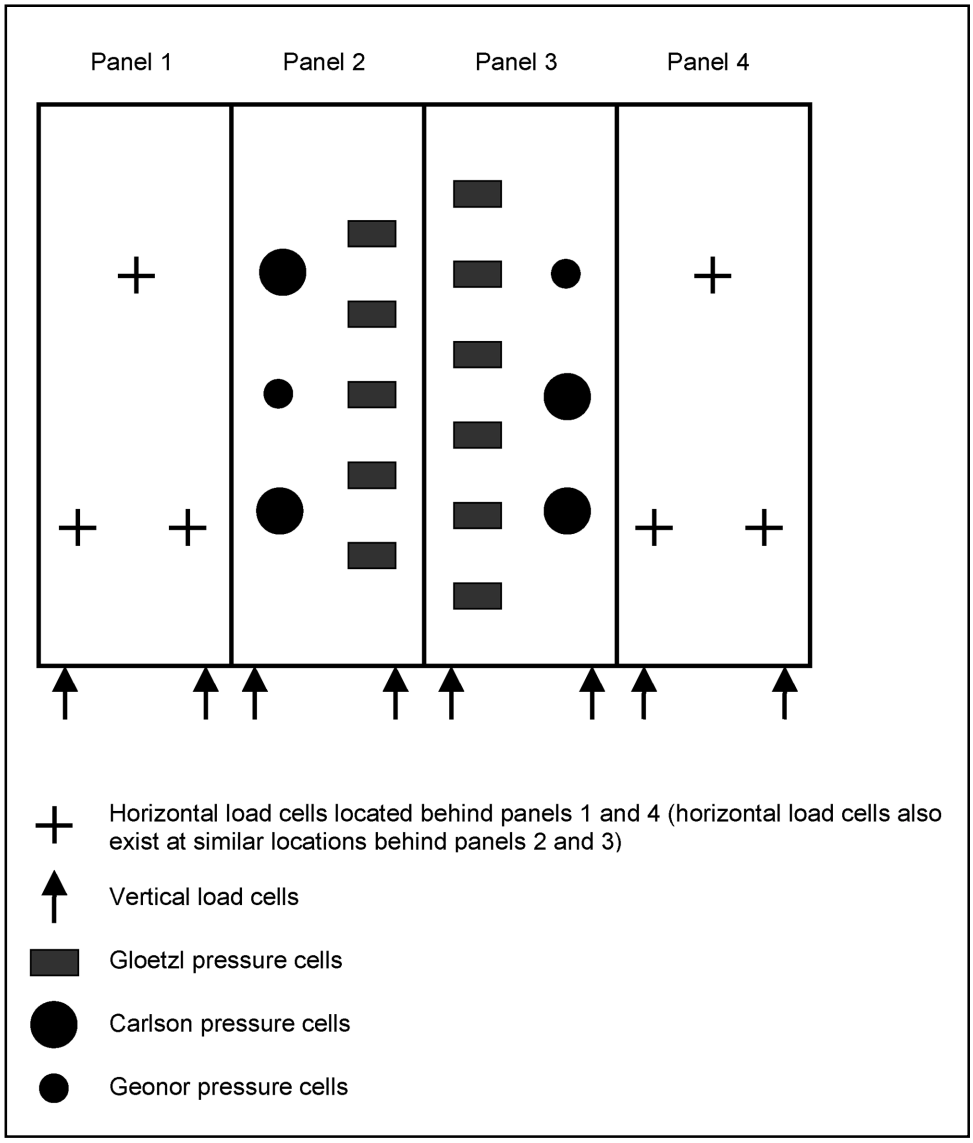

Figure 5-3. IRW panels (after Sehn 1990)

polyurethane-based, elastomeric sealant (Sikaflex-1a) was applied over the support strips with a thickness of approximately 12.5 mm (0.5 in.), and left to cure for 1 week. Once cured, the sealant has a relatively high strength and an elastic modulus ranging from 0.275 to 0.551 MPa. Application of the sealant to the bottom gap of the panels may have some influence on the force measurements of the load cells. However, this influence is minimal because the elastic modulus of the sealant is comparatively small, as confirmed by measurements performed before and after application of the sealant.

5.1.2.3 Inundation/drainage system. A simple system was devised to allow controlled inundation and drainage of the backfill. Two polyvinyl chloride (PVC) pipes were placed in the corners of the backfill area farthest from the instrumented panels. The pipes had an internal diameter of 150 mm (6 in.) and were

approximately 2.5 m (8 ft) long. The pipes were perforated and entirely covered with a geotextile fabric. In this way, inundation and drainage were possible without causing migration of fines from the soil.

One of the pipes, referred to herein as the well pipe, was selected for introduction and removal of the water during inundation and drainage. The other pipe, referred to herein as the piezometer, was used to monitor the water level inside the backfill. For drainage of the backfill, a submersible electrical pump was introduced into the well pipe.

5.1.2.4 Data acquisition. A data acquisition system was installed in the IRW, consisting of a Keithley 500A system connected to a personal computer (PC) equipped with a 486 processor. The Keithley 500A system allows use of up to ten 16-bit data acquisition cards designed for specific types of instrumentation. Table 5-1 lists some details regarding the data acquisition setup for the lock wall simulation.

Table 5-1
Features of the Data Acquisition System for the Lock Wall Simulation

Instruments	Card type	Voltage Range	Accuracy	Sampling Frequency Hz
Horizontal load cells	AIMM3a	±0.01 V	±0.22 kN	5
Vertical load cells	AIMM3a	±0.05 V	±0.07 kN	5
Gloetzl pressure cells	AIMM3a	±0.05 V	Not determined	5
LVDTs	AMM2	±0.5 V	±0.01 mm	5
Thermocouples	AMM7	±0.25 °C	±0.01 V	0.2

The data acquisition software provided with the Keithley 500 allows sampling of the instrumentation according to a predetermined sequence and sampling frequency. The digital output from the cards is converted into physical quantities according to calibration factors determined before the test. The software also allows graphic representation of the data.

The instruments were calibrated in situ before the test. The vertical and horizontal load cells were calibrated by the incremental application of forces of known magnitude at the load cell locations. Calibration of the load cells was verified after application of the sealant around the edges of the panels. It was found that the load absorbed by the sealant was negligible compared to the total loads applied to the panels. The Gloetzl pressure cells and LVDTs were calibrated following the procedures described by Sehn (1990). Several loading cycles were applied to the load cells and pressure cells to verify the repeatability of the measurements. No calibration was required for the thermocouples.

5.2 Testing Procedures

As illustrated in Figure 5-4, the test was performed in three stages:

a. Stage 1, backfilling.

b. Stage 2, surcharge.

c. Stage 3, inundation.

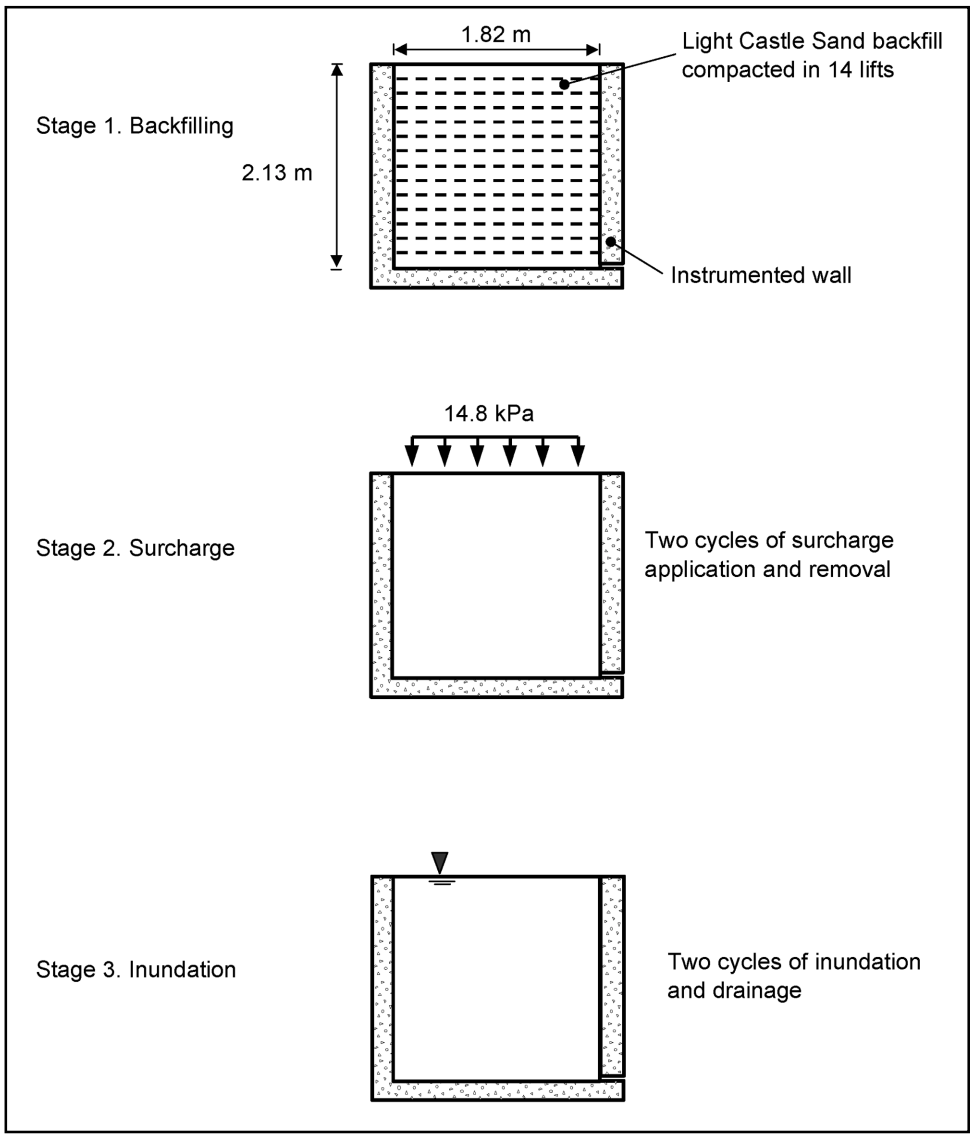

Figre 5-4. Stages of the lock wall simulation performed in the IRW test facility

The following sections describe each of the stages of the test.

5.2.1 Stage 1, Backfilling

Before the start of the backfilling operation, a nonfrictional lining was applied to the fixed walls and the bulkhead to minimize boundary effects. The lining consisted of an automotive grease coating and plastic film. Care was taken to avoid contaminating the surface of the instrumented panels or the floor of the backfill area during this process.

The backfill material was Light Castle sand. The properties of Light Castle sand are presented in Chapter 3, and Appendices A and B. The sand was air-dried to a water content below 0.2 percent, and stored inside the building until the start of the backfilling operation. The backfill was placed and compacted in 14 lifts, each with a compacted thickness of approximately 150 mm as illustrated in Figure 5-4. The sand was poured into the IRW using a hopper with bottom discharge as shown in Figure 5-5a. The weight of each batch of soil was carefully measured and recorded before pouring.

Each lift was compacted with two passes of a vibrating plate compactor as shown in Figure 5-5b. The compactor was a hand-operated Wacker model BPU2440A. After compaction of each lift, the total backfill thickness was determined by measuring the distance from the top of the backfill to a reference beam at twelve points distributed on the backfill surface. The thickness of the backfill was calculated based on the average of these readings. Measurements of horizontal and vertical forces, normal stresses, deformations, and temperatures were made after placement and after compaction of each lift.

a. Backfill placement b. Backfill compaction c. Surcharge application

Figure 5-5. View of the IRW at different stages of the lock wall simulation

The average density of the backfill at the end of compaction was 16.8 kN/m^3 (107 lb/ft^3), which corresponds approximately to the maximum density determined in the laboratory (Table 3-1). Previous investigators reported slightly lower density values for the Light Castle sand backfill in the IRW following identical compaction procedures (Filz 1992). It is possible that the confinement provided by the wooden bulkhead helped to increase the compacted density of the backfill above the previous value. As discussed in a subsequent section, a beneficial consequence of the large backfill density was the minimization of hydrocompression effects during inundation.

5.2.2 Stage 2, Surcharge

After completion of the backfilling operation, a surcharge was placed on the surface of the backfill. The surcharge consisted of a 1.07-m (3.5-ft) wooden container filled with Light Castle sand in a loose condition. Figure 5-5c is a view of the IRW during application of the surcharge. The total weight of the sand plus the container induced a vertical pressure on the backfill surface of 14.8 kPa (310 lbf/ft^2).

Two cycles of placement and removal of the surcharge were applied. After the box was carefully placed on the surface of the backfill, it was filled with sand. A uniform, horizontal surface was kept during filling to maintain a uniform surcharge on the backfill. After completion of the surcharge application, the sand was slowly removed from the box through a side opening. An identical procedure was followed for the second cycle. A precise record of the weight of sand inside the box was kept during this stage of the test. Instrumentation readings were made before, during, and after each loading cycle.

5.2.3 Stage 3, Inundation

Inundation of the backfill followed removal of the surcharge. After full inundation of the backfill, a submersible pump was introduced in the well pipe for drainage of the backfill. Two cycles of inundation and drainage were performed.

Instrumentation readings were made at several intermediate stages during inundation and drainage. Prior to each reading, the flow of water was arrested, and the water level in the pipes was monitored until equilibrium was reached. This prevented errors in the measurement of the water level inside the backfill.

Careful monitoring of flow rates during the test made possible estimation of the rate of leakage through the instrumented wall. It was found that the rate of leakage was negligible for practical purposes.

5.3 Test Results

The results of the test are summarized in Tables 5-2 to 5-5. Al the data reported in the tables correspond to measurements in the two central panels (panels 2 and 3) of the instrumented wall. It is assumed that panels 2 and 3 are relatively free from any significant boundary effects induced by the presence of the endwall and the bulkhead in the IRW. Consequently, data from these panels may most closely represent a plane strain condition that can be modeled with SOILSTRUCT-ALPHA. This section discusses the results obtained from each of the three stages of the test.

Table 5-2
Summary of the Force Measurements during Stage 1 of the IRW Test (Backfilling)[1]

Height of Backfill, H, m	Total Horizontal Load per Panel[2] kN		Total Vertical Force per Panel[2] kN		Effective Overburden kN/m	F'_x kN/m	F_v kN/m	K_h	K_v
	Panel 2	Panel 3	Panel 2	Panel 3					
0.00	0.000	0.000	0.000	0.000	0.000	0.000	0.000	-	-
0.15	0.096	0.126	0.027	-0.001	0.195	0.146	0.017	0.747	0.086
0.30	0.527	0.643	0.143	0.115	0.781	0.767	0.169	0.982	0.217
0.46	0.671	1.057	0.037	0.008	1.757	1.134	0.030	0.645	0.017
0.61	1.166	1.640	-0.083	-0.057	3.124	1.841	-0.091	0.589	-0.029
0.76	1.827	2.514	0.240	0.143	4.881	2.848	0.251	0.583	0.051
0.91	2.362	3.190	0.271	0.146	7.029	3.643	0.274	0.518	0.039
1.07	3.151	3.852	0.355	0.265	9.567	4.596	0.407	0.480	0.043
1.22	4.139	4.736	0.584	0.505	12.495	5.824	0.715	0.466	0.057
1.37	5.115	5.646	0.847	0.769	15.814	7.061	1.060	0.446	0.067
1.52	6.245	6.923	1.315	1.191	19.524	8.640	1.644	0.443	0.084
1.52	6.459	6.984	1.419	1.313	19.524	8.821	1.793	0.452	0.092
1.68	7.988	8.447	1.838	1.681	23.624	10.785	2.309	0.457	0.098
1.83	9.031	9.598	2.227	2.067	28.114	12.224	2.818	0.435	0.100
1.98	10.420	10.499	2.734	2.486	32.995	13.726	3.425	0.416	0.104
2.13	11.478	11.562	3.191	2.936	38.266	15.118	4.020	0.395	0.105
2.13	11.222	11.394	3.183	2.904	38.266	14.840	3.994	0.388	0.104

[1] See Notation (Appendix F) for definition of symbols.
[2] Measurements made after placement and before compaction of each lift are omitted.

5.3.1 Results from stage 1

5.3.1.1 Force measurements. Table 5-2 summarizes the vertical and horizontal force data measured in the two central panels during compaction of the backfill. The data collected after placement and before compaction of each lift have been omitted for clarity. Measurements were made before and after any interruptions of the backfill placement process. They are also included in the table. The total horizontal and total vertical loads per panel correspond to the sum of the individual load cells readings in each panel. The effective overburden

Table 5-3
Data From Gloetzl Pressure Cells at the End of Stage 1 (Backfilling)

Gloetzl Cell Number	Position of Cell[1] m	Horizontal Pressure, σ_h KPa	
		Measured	Corrected [2]
G1	1.778	12.44	10.64
G7	1.626	11.29	9.65
G2	1.473	8.83	7.55
G8	1.321	No response	-
G3	1.168	10.20	8.72
G9	1.016	9.76	8.34
G4	0.864	8.31	7.11
G10	0.711	10.15	8.68
G5	0.559	9.53	8.15
G11	0.406	8.48	7.25
G6	0.253	No response	-

[1] Measured from bottom of backfill to center of each cell.
[2] Obtained by dividing the measured pressure by 1.17.

Table 5-4
Summary of the Results of Stage 2 of the IRW (Surcharge)[1]

Applied Surcharge, q_s, kPa	Total Horizontal Load per Panel kN		Total Vertical Force per Panel kN		F'_x kN/m	F_v kN/m	$F_{v,q}$ kN/m	$K_{v,q}$
	Panel 2	Panel 3	Panel 2	Panel 3				
0.0 [2]	11.22	11.39	3.18	2.90	14.84	3.99	0.000	-
0.3	11.31	11.63	3.21	2.95	15.05	4.04	0.048	0.079
0.3	11.82	11.97	3.35	3.10	15.61	4.23	0.236	0.388
9.2	12.67	13.76	4.11	4.00	17.34	5.32	1.324	0.067
18.2	13.32	14.91	4.86	4.81	18.52	6.35	2.351	0.061
0.3	10.75	11.07	3.49	3.25	14.32	4.42	0.427	0.704
18.2	12.82	13.56	4.99	4.75	17.30	6.39	2.397	0.062
18.2	13.03	13.60	5.03	4.80	17.48	6.45	2.459	0.063
0.00	10.86	11.05	3.48	3.23	14.38	4.40	0.411	-

[1] See Notation (Appendix F) for definition of symbols.
[2] Corresponds to end of backfilling (last row of Table 5-2).

values are determined using Equation 1-1. The values of F'_x and F_v correspond to the horizontal and vertical forces, respectively, per unit length of wall. Definitions of the earth pressure coefficients, K_h and K_v, are presented in Chapter 1. According to Equations 1-2 and 1-3, the values of K_h and K_v are calculated by dividing the values of F'_x and F_v, respectively, by the effective overburden.

Table 5-5
Summary of the Results of Stage 3 of the IRW (Inundation)[1]

Cycle		D_2, m	D_2 / H	D_1, m	F_w kN/m	Total Horizontal Force per Panel, kN		Total Vertical Force per Panel, kN		F_x kN/m	F'_x kN/m	F_v kN/m	K_v	C_{wt}
						Panel 2	Panel 3	Panel 2	Panel 3					
1[2]	Inundation	0.00	0.00	2.13	0.00	10.86	11.05	3.48	3.23	14.38	14.38	4.40	0.115	1.000
		0.60	0.28	1.54	1.75	10.85	10.63	2.46	2.23	14.09	12.35	3.07	0.083	0.721
		0.95	0.45	1.18	4.45	12.04	11.69	1.79	1.43	15.57	11.13	2.11	0.060	0.522
		1.32	0.62	0.81	8.55	14.48	13.50	1.28	1.11	18.36	9.81	1.56	0.049	0.422
		1.52	0.71	0.61	11.38	15.67	14.90	1.12	1.08	20.06	8.68	1.44	0.048	0.416
		1.50	0.71	0.63	11.10	14.89	14.42	1.10	1.07	19.24	8.14	1.43	0.047	0.408
		1.83	0.86	0.30	16.39	17.54	16.46	0.81	0.92	22.31	5.92	1.13	0.043	0.371
		2.06	0.96	0.08	20.74	18.97	17.83	0.57	0.81	24.14	3.40	0.91	0.039	0.335
	Drainage	1.77	0.83	0.37	15.27	16.59	15.61	0.93	1.16	21.13	5.86	1.37	0.049	0.428
		1.60	0.75	0.53	12.55	15.15	14.10	0.94	1.13	19.19	6.65	1.36	0.045	0.394
		1.40	0.65	0.74	9.56	14.70	13.51	1.06	1.21	18.51	8.94	1.49	0.046	0.400
		1.19	0.56	0.94	6.98	13.83	12.51	1.34	1.49	17.29	10.31	1.86	0.054	0.470
		0.72	0.34	1.41	2.57	11.73	10.19	1.88	1.99	14.38	11.81	2.54	0.067	0.585
		0.65	0.30	1.49	2.06	11.87	10.15	1.83	1.91	14.45	12.39	2.45	0.064	0.560
		0.36	0.17	1.77	0.64	11.82	9.78	2.24	2.27	14.17	13.53	2.96	0.075	0.655
		0.33	0.15	1.80	0.53	11.57	9.25	2.55	2.55	13.66	13.13	3.35	0.085	0.741
2	Inundation	0.88	0.41	1.26	3.76	12.33	10.14	2.07	2.14	14.74	10.98	2.76	0.075	0.652
		1.70	0.80	0.43	14.19	16.86	15.17	1.18	1.40	21.02	6.83	1.70	0.059	0.514
		2.13	1.00	0.01	22.31	20.09	18.53	0.75	1.05	25.35	3.04	1.18	0.053	0.458
	Drainage	1.66	0.78	0.48	13.46	16.66	14.91	1.16	1.39	20.71	7.25	1.67	0.057	0.497
		1.11	0.52	1.02	6.05	13.76	12.11	1.93	2.06	16.97	10.92	2.62	0.075	0.650
		0.61	0.29	1.52	1.82	11.81	10.07	2.52	2.65	14.36	12.54	3.39	0.089	0.770
		0.32	0.15	1.81	0.51	12.01	9.83	2.93	3.03	14.33	13.82	3.91	0.099	0.864

[1] D_1 = Thickness of backfill above the water table;, D_2 = height of water behind the wall; F_w = hydrostatic force on wall. See Notation (Appendix F) for definitions of other symbols.
[2] Corresponds to end of surcharge cycle (last row of Table 5-4).

It can be observed that the magnitudes of vertical and horizontal forces are similar for the two panels. They are also similar to the values reported by Filz (1992) for a previous IRW test using the Light Castle sand backfill.

5.3.1.2 Pressure measurements. The data from the Gloetzl pressure cells at the end of backfilling are presented in Table 5-3. Integration of these pressure values over the height of the wall yields a horizontal force magnitude of 17.35 kN per meter run of wall. This value is approximately 17 percent greater than the value of 14.84 kN/m obtained from the load cell measurements presented in Table 5-2. Table 5-3 also shows the corrected values of normal pressure, which were obtained by dividing the pressure data by 1.17.

The error in the pressure measurements suggests that Gloetzl cells do not provide data that is usable for accurate analyses of the response of the wall-backfill system. However, they provide an important insight for SSI analyses of the IRW, as discussed in the section on the interpretation of the test results.

5.3.2 Results from stage 2

Table 5-4 summarizes the data from the two cycles of application and removal of the surcharge. The vertical force increment due to surcharge application $F_{v,\,q}$ and the vertical shear force coefficient for sloping backfill and surcharge $K_{v,\,q}$ are defined in Chapter 2. The value of $F_{v,\,q}$ is the difference between the values of F_v

after and before the application of the surcharge. Rearranging terms in Equation 2-16 gives the following expression for the determination of $K_{v\,q}$ from the IRW data:

$$K_{v,q} = \frac{F_{v,q}}{q_s \cdot H} \tag{5-1}$$

The magnitudes of the vertical shear load before and after this stage of the test are very similar. This suggests that there is little or no degradation of the vertical shear loads with cycles of application and removal of the surcharge.

5.3.3 Results from stage 3

5.3.3.1 Force measurements. The data collected during the inundation cycles of the IRW test are summarized in Table 5-5. The hydrostatic force on the wall F_w is calculated from the following expression:

$$F_w = \frac{\gamma_w \cdot D_2^{\,2}}{2} \tag{5-2}$$

The effective horizontal force F_x' is calculated by subtracting the hydrostatic force F_w from the total horizontal force F_x. The definition of the correction factor C_{wt} for a post-construction rise in the water table was presented in Chapter 2. The value of C_{wt} for the IRW test was calculated as the ratio between the K_v values during inundation and the K_v value immediately before the start of inundation (Equation 2-20).

It can be seen that the magnitude of the vertical shear force F_v decreases as the height of water in the backfill D_2 increases during inundation. Conversely, the magnitude of F_v increases as D_2 decreases during drainage. Drainage of the backfill was carried out until D_2 reached a value of approximately 0.3 m. Further lowering of the water table was not practical because the time required for full drainage of the backfill ($D_2 = 0$) was too long. However, extrapolation of the vertical force data collected during the two drainage stages reveals that the value of F_v for full drainage ($D_2 = 0$) is similar to its initial value before the start of inundation ($F_v = 4.40$ kN/m). This suggests that there is no significant degradation of the vertical shear force with cycles of inundation for the conditions of this test in the IRW.

5.3.3.2 Hydrocompression. During inundation, the elevation of the surface of the backfill was measured periodically with an accuracy of ±1 mm. No significant changes in the backfill height were detected during inundation. This is consistent with the analysis of the hydrocompression properties of the Light Castle sand presented in Appendix A. Therefore, for the analyses of the IRW, it was assumed that hydrocompression of the backfill is negligible.

5.4 Discussion of Test Results

In this section, the backfill response observed during the test and its relevance for the finite element analyses of the IRW are discussed.

5.4.1 Response of the wall-backfill system to backfilling

5.4.1.1 Evolution of lateral earth pressures during backfilling. The values of the lateral earth pressure coefficient K_h listed in Table 5-2 are plotted against the height of the backfill in Figure 5-6. It can be seen that the value of K_h decreases as the height of the backfill increases. A value of K_h of approximately 0.4 was obtained at the end of backfilling.

For comparison, the value of the at-rest coefficient K_o determined using the approximation suggested by Jaky (1948) for an internal friction angle of the backfill of 47 deg is also illustrated in the figure. The at-rest coefficient does not account for compaction-induced lateral earth pressures behind walls with rough interfaces. Therefore, the value of K_o should be identical to the value of K_h in a nonmoving wall retaining a normally consolidated backfill and with a smooth backfill-to-wall interface. The value of K_h in the IRW is larger than the value of the at-rest coefficient throughout the backfilling stage because significant lateral stresses are locked in during compaction of the backfill.

Figure 5-7 shows the pressure distribution at the end of backfilling in the IRW test. Data from a similar test performed previously in the IRW (Filz 1992) are also shown. It can be seen that the pressure distribution on the wall is not linear and that large horizontal pressures develop throughout the height of the wall. As discussed by Duncan et al. (1991), compaction-induced earth pressures are much greater than the at-rest values near the surface of a compacted backfill. At large depths, the overburden pressure induced by the weight of the overlying backfill is significantly larger than the vertical stresses applied during compaction. Therefore, in short walls such as the IRW, the magnitude of the total horizontal force on the wall may be controlled by compaction-induced earth pressures.

In higher walls, the total horizontal force on the wall may be controlled by the at-rest pressures for normally consolidated soil backfills. As the height of the backfill increases, the value of K_h decreases. For lock walls, which are typically 12 m (40 ft) or higher and have smooth wall-to-backfill interfaces, the K_h values approach Jaky's K_o value, since the stresses induced by the overburden exceed the stresses induced by compaction.

To perform accurate analyses of short walls such as the IRW, it is necessary to account for the relatively large pressures that develop at shallow depths inside the backfill.

5.4.1.2 Evolution of vertical shear forces during backfilling. The values of the vertical force coefficient K_v measured during stage 1 of the test are plotted in Figure 5-8 against the height of the backfill. The value of K_v increases with the

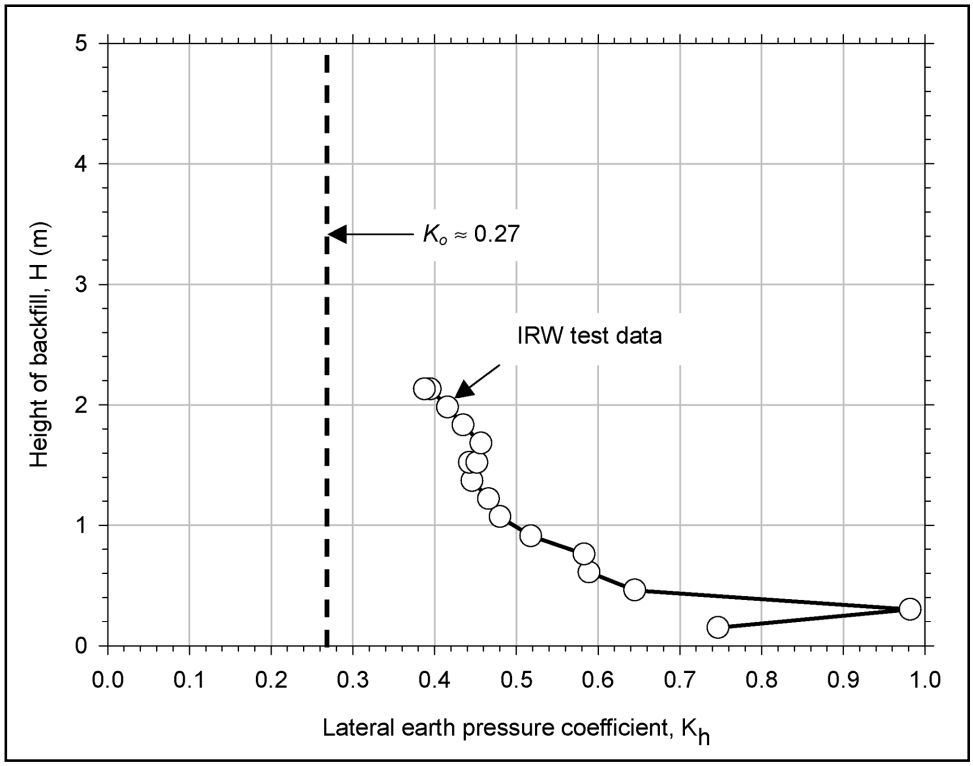

Figure 5-6. Evolution of the lateral earth pressure coefficient K_h during backfilling in the IRW

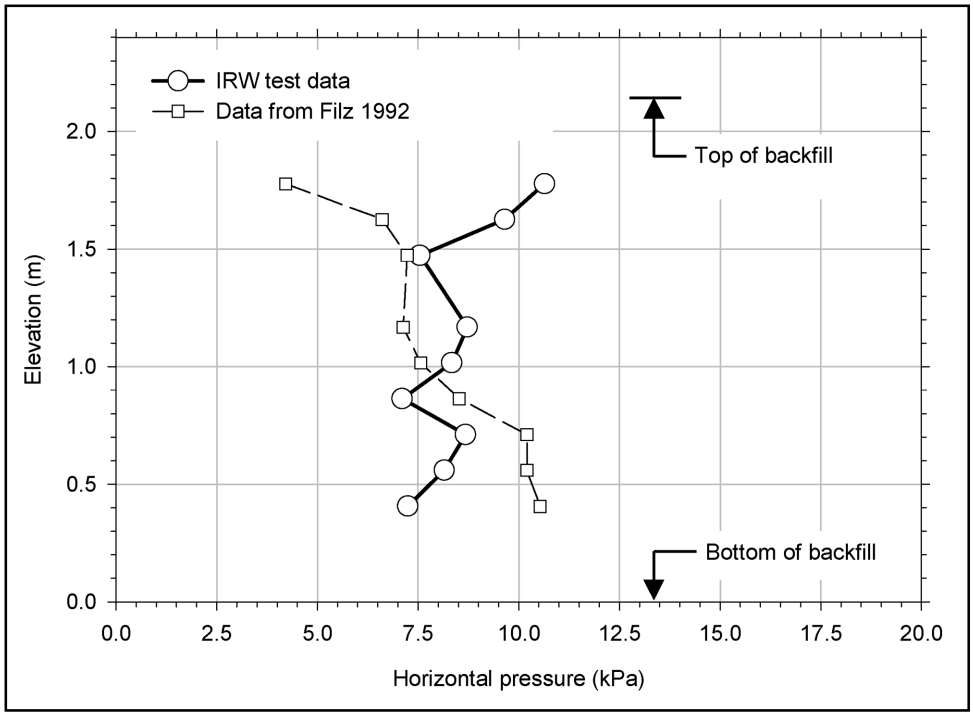

Figure 5-7. Lateral pressure distribution at the end of backfilling

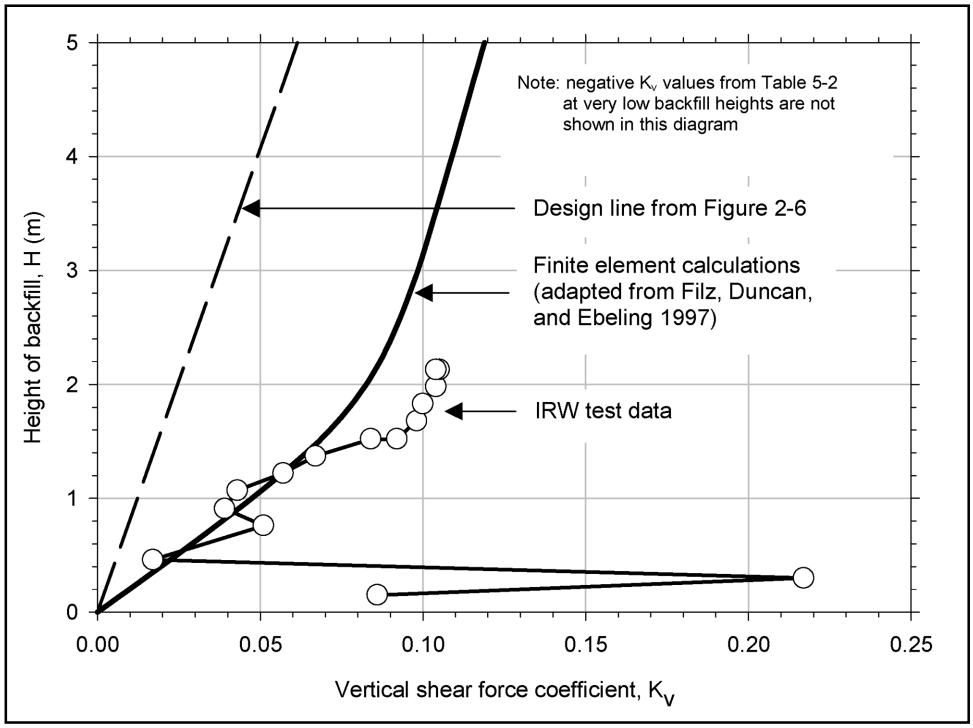

Figure 5-8. Evolution of the vertical shear force coefficient K_v during backfilling in the IRW

height of the backfill to a final value of 0.10 at the end of backfilling. This value is consistent with the results of a previous test performed in the IRW (Filz 1992).

A discussion of the development of vertical shear forces in nonmoving walls was presented by Filz and Duncan (1997) and Filz, Duncan, and Ebeling (1997). From a series of finite element analyses, they developed a set of K_v versus backfill height curves for different densities of the backfill. Figure 2-6 reproduces the results of their analyses. The calculated values of K_v for dense, granular backfills are reproduced in Figure 5-8, together with the design line recommended in Appendix F of Engineer Manual 1110-2-2100 (HQUSACE, in preparation).

It can be observed that the calculated and measured K_v values follow similar trends of variation with backfill height. However, the measured K_v values at the end of backfilling are somewhat higher than the calculated values.

The design line shown in Figure 5-8 provides conservative estimates of K_v, according to the IRW data.

5.4.2 Response of the wall-backfill system to surcharge

Values of the earth pressure coefficient for surcharge $K_{v,\,q}$ determined from force measurements in stage 2 are listed in Table 5-4. Neglecting the extreme values for low surcharge magnitudes, the average value of $K_{v,\,q}$ is 0.063. In the

IRW test, the backfill surface is horizontal and the distance from the surcharge to the wall is zero. Therefore, the concept of $K_{v,\,q}$ is equivalent to the concept of $K_{v,\,q,\,ref}$ discussed in Chapter 2. The average value of $K_{v,\,q}$ from the test is represented in a $K_{v,\,q,\,ref}$ versus backfill height diagram in Figure 5-9.

The $K_{v,\,q}$ values obtained by Filz, Duncan, and Ebeling (1997) from finite element analyses of nonmoving walls with dense backfills are also represented in Figure 5-9. These analyses were performed using the same backfill properties as those used in their backfilling analyses discussed in the previous section. From the theoretical plots, a value of $K_{v,\,q}$ of approximately 0.12 is obtained. This value is larger than the $K_{v,\,q}$ value determined from the IRW data. This difference between calculated and measured $K_{v,\,q}$ values occurs because the compressibility of the backfill assumed for the analyses is larger than the compressibility of the compacted Light Castle sand, as discussed in Sections 5.5.3 and 5.6.2.

The design line recommended in Appendix F of Engineer Manual 1110-2-2100 (HQUSACE, in preparation) is also reproduced in Figure 5-9. It provides a slightly conservative estimate of the value of $K_{v,\,q}$, according to the IRW data.

5.4.3 Response of the wall-backfill system to inundation

The values of the correction factor C_{wt} listed in Table 5-5 are plotted against the normalized height of water D_2/H in Figure 5-10. The test data follow a curvilinear path reaching an average final value of C_{wt} of approximately 0.4 after full inundation of the backfill ($D_2/H = 1$). The design line, recommended in Appendix F of Engineer Manual 1110-2-2100 (HQUSACE, in preparation), is also represented in the figure. It yields a good approximation to the C_{wt} values from the IRW test for D_2/H ratios lower than 0.5. For D_2/H ratios between 0.5 and 1, the design line yields conservative values of the correction factor.

5.4.4 Special considerations for finite element analyses of the IRW

A method to incorporate compaction effects into finite element analyses was developed by Seed and Duncan (1986). The compaction of each lift was modeled as the temporary application of compaction stresses on the surface of the backfill. They used a hysteretic soil model, which provided reasonable estimations of the residual earth pressures after removal of the compaction stresses.

The implementation of such a model in SOILSTRUCT-ALPHA may be a lengthy process, and it is beyond the scope of this investigation. Therefore, a simpler, alternative procedure was followed to model the response of the wall-backfill system to all types of loading applied during the test. For the analyses, different backfill property values were assigned for backfilling and for surcharge placement. The effect of compaction on the lateral pressures was modeled by assigning a larger Poisson's ratio and a lower modulus to the backfill material for stage 1 (backfilling) than for stage 2 (surcharge).

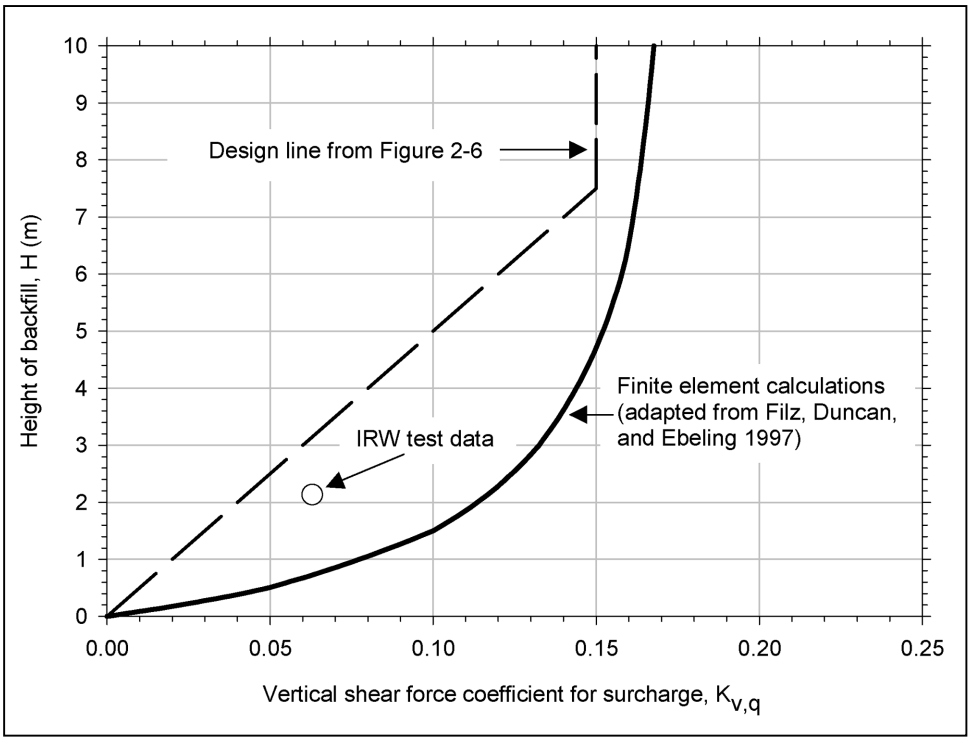

Figure 5-9. Vertical shear force coefficient for surcharge $K_{v,\,q}$ in the IRW

In previous sections of this report, it was observed that at the end of backfilling in the IRW, large horizontal pressures exist throughout the height of the instrumented wall, and that the pressure distribution is not linear with depth. To obtain accurate values of vertical and horizontal forces from finite element analyses of the IRW, it is necessary to account for this type of lateral pressure distribution. Finite element analyses in SOILSTRUCT-ALPHA do not provide the type of horizontal pressure distribution observed in the IRW test. In the analyses, the distribution tends to be linear, and pressures are low at shallow depths in the backfill. Consequently, the effect of the confining pressures on the backfill response to loading is not accurately modeled in the analyses. Additional adjustments of the backfill properties are required to account for the larger confining pressures that occur due to compaction.

For these reasons, limited information on the accuracy of the extended hyperbolic model can be expected from the analyses of the IRW for the backfilling and surcharge stages. The analyses of stages 1 and 2 were performed to obtain a reasonable estimate of the backfill properties and of the state of stresses existing prior to inundation. The backfill properties and state of stresses obtained from these calibration analyses were used for the analysis of inundation. The comparison between the results of the inundation analysis and the test data is the basis for the evaluation of the extended hyperbolic model.

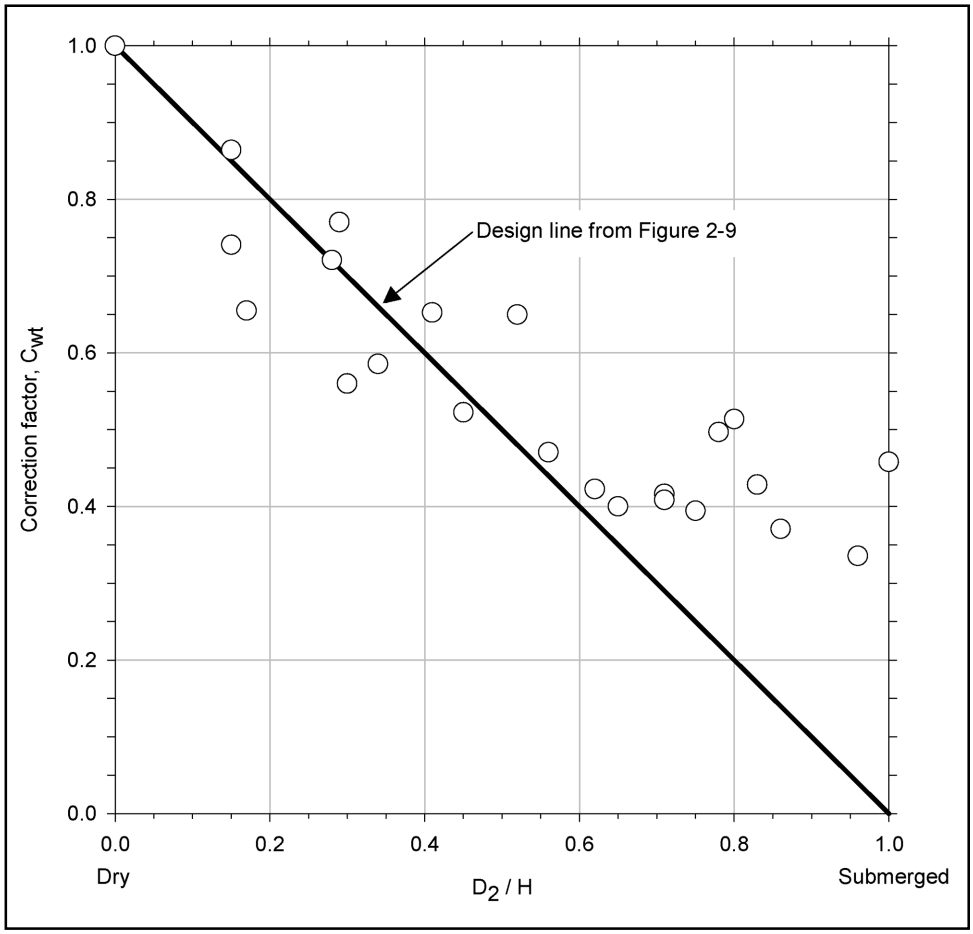

Figure 5-10. Values of the correction factor C_{wt} during inundation of the backfill in the IRW

These issues regarding the limitations of SOILSTRUCT-ALPHA analyses of the IRW may not be applicable to most lock walls. In lock walls of moderate to large height, the earth pressures are largely controlled by the self-weight of the backfill. A single set of material properties that produces reasonable estimates of earth pressures for backfilling may also produce reasonable estimates for surcharge application and for post-construction rise of the groundwater table.

5.5 Finite Element Analysis Procedures

Finite element analyses were performed to model the IRW test using the updated version of the program SOILSTRUCT-ALPHA, which contains the extended hyperbolic model presented in Chapter 4. The following steps were followed for the analyses:

a. Selection of tentative material properties for the backfill.

b. Calibration analyses.

c. Inundation analysis.

Tentative values of backfill properties were determined from the results of the triaxial and consolidation tests on the Light Castle sand. These values were adjusted during the calibration analyses to match the force values measured at the end of the backfilling and surcharge stages. Finally, these adjusted properties were used for the analyses of the inundation stage.

This section summarizes features of SOILSTRUCT-ALPHA that are relevant for the analyses performed. The criteria followed for the selection of the material property values and procedures used for the calibration and backfill inundation analyses are described in detail. Finally, the analysis results are compared to the data collected during the IRW test, and the accuracy of the extended hyperbolic model for interfaces is discussed.

5.5.1 Summary of features of SOILSTRUCT-ALPHA

The program SOILSTRUCT was developed by Clough and Duncan (1969) for finite element analyses of earth retaining structures. It is a general-purpose finite element program for two-dimensional analysis of plane strain problems of soil-structure interaction. It calculates stresses and displacements due to incremental construction and/or load application, and can model nonlinear stress-strain material behavior. Two types of finite elements are used in SOILSTRUCT: two-dimensional elements for soil and structural materials, and joint elements for the interfaces between the different materials. SOILSTRUCT has undergone a continuous evolution as new developments have been introduced in soil and interface models. SOILSTRUCT-ALPHA is the latest result of this process (as described in Ebeling and Wahl 1997 and Ebeling, Pace, and Morrison 1997).

In SOILSTRUCT-ALPHA, the nonlinear response of soils to primary loading is modeled using the hyperbolic formulation by Duncan and Chang (1970). For unloading-reloading, a stress-dependent, linear response is assumed (Ebeling, Peters, and Clough 1992). The Alpha method (Ebeling, Duncan, and Clough 1990; Ebeling et al. 1992) implemented in the code allows analyses of lock walls undergoing base separation. Base separation is not a relevant issue for the IRW analyses, and it is not discussed further in this report.

As indicated in Chapter 4, the updated version of SOILSTRUCT-ALPHA, which was developed during this investigation, contains the formulation for yield-inducing shear and unloading-reloading Version II of the extended hyperbolic model for interfaces.

5.5.1.1 Incremental analysis techniques. In SOILSTRUCT-ALPHA, analyses are performed following the incremental techniques described by Clough and Duncan (1969). In the analyses, the backfill elements and structure-to-backfill

interface elements take on three different states during the analyses: air, fluid, and solid. In the initial condition before the start of backfilling, all the backfill and interface elements are assigned the properties of air and of structure-to-air interface, respectively.

Each newly placed lift is modeled as a dense fluid, with a unit weight equal to the unit weight of the compacted backfill. The pressures exerted by the new lift on the existing backfill and on the structural elements are calculated and transformed into nodal loads. The interface elements between the structure and the newly placed lift are assigned a low value of shear stiffness and, as discussed in Chapter 2, a large value of normal stiffness. Zero nodal displacements are prescribed at the surface of the newly placed lift to prevent buildup of displacements in the overlying air elements.

The value of the at-rest pressure coefficient K_o assigned to the fluid elements is usually assumed equal to one. It determines the magnitude of the lateral pressures between the fluid elements and between the fluid elements and the retaining wall.

Upon addition of subsequent lifts to the mesh, the previously fluid elements take on a solid state. At this time, the complete set of properties of the compacted backfill and of the structure-to-backfill interface are assigned to the backfill and interface elements.

For soil and backfill, the incremental changes in stresses are related to the incremental strains through the linear relationship:

$$\begin{Bmatrix} \Delta\sigma_x \\ \Delta\sigma_y \\ \Delta\tau_{xy} \end{Bmatrix} = \frac{3 \cdot B}{9 \cdot B - E_t} \begin{bmatrix} (3 \cdot B + E_t) & (3 \cdot B - E_t) & 0 \\ (3 \cdot B - E_t) & (3 \cdot B + E_t) & 0 \\ 0 & 0 & E_t \end{bmatrix} \cdot \begin{Bmatrix} \Delta\varepsilon_x \\ \Delta\varepsilon_y \\ \Delta\gamma_{xy} \end{Bmatrix} \qquad (5\text{-}3)$$

where

$\Delta\sigma_x$ = horizontal stress increment

$\Delta\sigma_y$ = vertical stress increment

$\Delta\tau_{xy}$ = shear stress increment

B = bulk modulus of the soil

E_t = tangent modulus of the soil

$\Delta\varepsilon_x$ = horizontal strain increment

$\Delta\varepsilon_y$ = vertical strain increment

$\Delta\gamma_{xy}$ = shear strain increment

For interface elements, the incremental changes in stresses and displacements are related according to the following expression:

$$\begin{Bmatrix} \Delta\tau \\ \Delta\sigma_n \end{Bmatrix} = \begin{bmatrix} K'_{st} & 0 \\ 0 & K_n \end{bmatrix} \cdot \begin{Bmatrix} \Delta_s \\ \Delta_n \end{Bmatrix} \tag{5-4}$$

where

$\Delta\tau$ = shear stress increment

$\Delta\sigma_n$ = normal stress increment

K'_{st} = tangent interface shear stiffness

K_n = interface normal stiffness

Δ_s = interface shear displacement

Δ_n = interface normal displacement

5.5.1.2 Soil properties. The tangent Young's modulus E_t of the soil for use in each load increment is computed from the following equation:

$$E_t = E_i \cdot \left(1 - R_f \cdot SL\right)^2 \tag{5-5}$$

where E_i is the initial Young's modulus of the soil.

In effective stress analyses, the initial Young's modulus E_i is determined from

$$E_i = K \cdot p_a \cdot \left(\frac{\sigma'_3}{p_a}\right)^n \tag{5-6}$$

The stress level SL in soils is determined from:

$$SL = \frac{\left(\sigma_1 - \sigma_3\right)}{\left(\sigma_1 - \sigma_3\right)_f} \tag{5-7}$$

where

σ_1 = major principal stress

σ_3 = minor principal stress

For a frictional backfill with *zero* cohesion intercept, the deviator stress at failure $(\sigma_1-\sigma_3)_f$ is determined from:

$$\left(\sigma_1 - \sigma_3\right)_f = 2\frac{\sigma'_3 \cdot \sin\phi'}{1 - \sin\phi'} \tag{5-8}$$

where ϕ' is the internal friction angle of the soil.

In this formulation, the parameters K, n, R_f, and ϕ' are the hyperbolic parameters defined by Duncan and Chang (1970) for modeling the response of the soil to primary loading. During unloading-reloading, a linear, stress-dependent soil response is assumed. The value of the Young's modulus for unloading-reloading E_{ur} is calculated from the following expression:

$$E_{ur} = K_{ur} \cdot p_a \cdot \left(\frac{\sigma'_3}{p_a}\right)^n \tag{5-9}$$

where K_{ur} is the unload-reload modulus number.

According to the hyperbolic formulation by Duncan and Chang (1970), the bulk modulus B of the soil is calculated from the equation:

$$B = K_b \cdot p_a \cdot \left(\frac{\sigma'_3}{p_a}\right)^m \tag{5-10}$$

where m is the bulk modulus exponent.

In SOILSTRUCT-ALPHA, the following approximate formulation is used to calculate the bulk modulus number (Ebeling, Pace, and Morrison 1997):

$$K_b = \frac{K}{3 \cdot \left(1 - 2 \cdot \upsilon_{nom}\right)} \tag{5-11}$$

In Equation 5-11, it is implicitly assumed that the values of modulus exponent n and the bulk modulus exponent m are identical. The nominal Poisson's ratio ν_{nom} is related to Poisson's ratio ν according to the following expression (Ebeling, Pace, and Morrison 1997):

$$\upsilon = \frac{1 - \left(1 - 2 \cdot \upsilon_{nom}\right) \cdot \left(1 - R_f \cdot SL\right)^2}{2} \tag{5-12}$$

The at-rest pressure coefficient K_o, used only for the analysis of the stresses induced by the newly placed lift, is usually assumed equal to one. The unit weight of the soil γ is assumed equal to the moist unit weight γ_{moist} for the portion of the backfill above the water table, and to the saturated unit weight γ_{sat} for the portion below the water table. Table 5-6 is a summary of the properties required to model soils in SOILSTRUCT-ALPHA analyses.

5.5.1.3 Interface properties. The shear stiffness K'_{st} of the interface is determined according to the formulations for yield-inducing shear and for unloading-reloading in Version II of the extended hyperbolic model introduced in Chapter 4. The normal stiffness K_n is assigned a large value to prevent overlapping of adjacent elements in the mesh.

Table 5-6
Summary of Soil Properties Required in SOILSTRUCT-ALPHA Analyses

Soil Property	Definition
K	Modulus number
n	Modulus exponent
K_{ur}	Modulus number for unloading-reloading
R_f	Failure ratio
ϕ'	Internal friction angle
ν_{nom}	Nominal Poisson's ratio
K_o	At-rest earth pressure coefficient for fluid backfill
γ_{moist}, γ_{sat}	Moist and saturated unit weight, respectively

5.5.2 Finite element mesh

Figure 5-11 shows the mesh used for the finite element analyses of the IRW. It is composed of the following elements:

a. 224 two-dimensional elements for modeling the backfill.

b. 32 two-dimensional elements for modeling the instrumented panels.

c. 46 joint elements for modeling the interfaces between the backfill and the walls, and between the backfill and the floor of the IRW.

d. 3 elastic springs to model the vertical and horizontal load cells.

The far field interface was assigned a very low stiffness to model the non-frictional lining applied to the far field wall. The instrumented wall elements were assigned common properties of reinforced concrete. The stiffness values of the springs used to model the horizontal load cells were determined from experimental load-deformation data of previous tests. The stiffness of the vertical load cell was calculated theoretically from the geometry and material properties of the load cells.

Table 5-7 lists property values that are representative of the structural materials in the IRW. These values were used for all the analyses. The following section discusses the selection of property values for the backfill and interfaces.

5.5.3 Tentative soil properties

As described in Chapter 3, hyperbolic parameter values for the Light Castle sand were determined from triaxial and consolidation tests performed on specimens compacted to relative densities of 50 and 80 percent. A relative density of approximately 100 percent was attained during compaction of the backfill in the

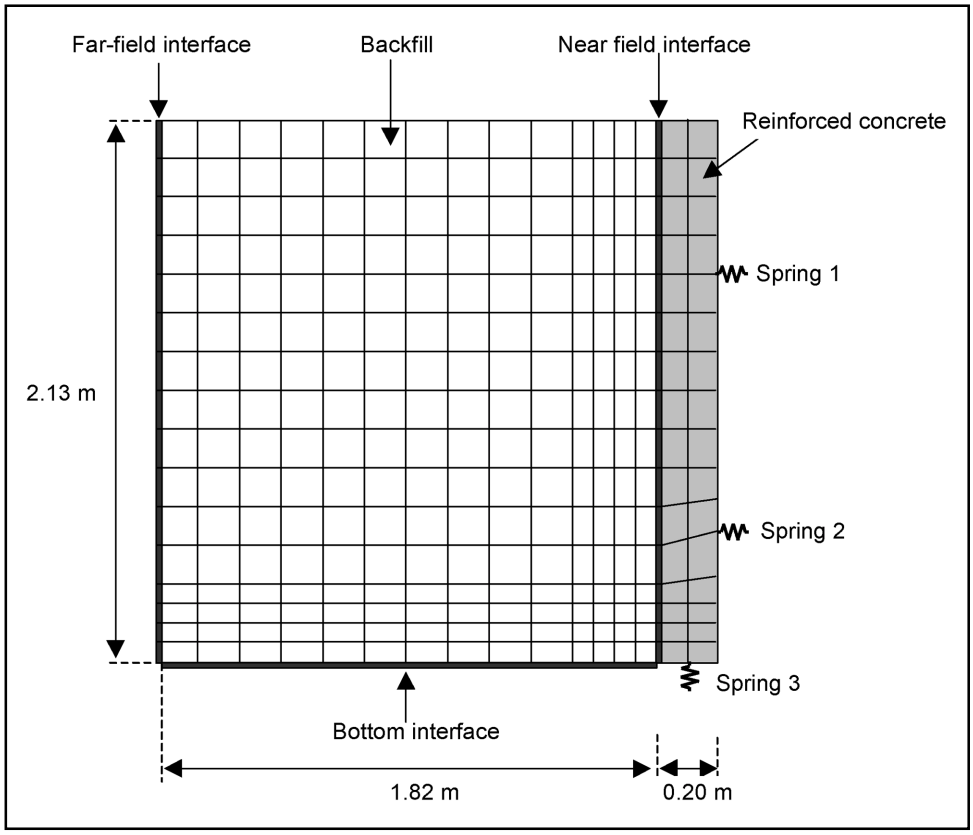

Figure 5-11. Finite element mesh used for the analyses

Table 5-7
Summary of Property Values for Structural Materials in the IRW Analyses

Material	Property	Value
Reinforced concrete	Poisson's ratio ν	0.2
	Unit weight γ	23.6 kN/m^3
	Young's modulus E	20.7 x 10^6 kPa
Spring 1	Stiffness per meter run of wall	13150 kN/m
Spring 2	Stiffness per meter run of wall	17810 kN/m
Spring 3	Stiffness per meter run of wall	24160 kN/m

IRW; consequently, no direct experimental data were available on the compacted backfill properties. Tentative property values of the compacted backfill for use in the calibration analyses were determined following the procedures described in the following paragraphs.

5.5.3.1 Estimation of stiffness number *K*. Duncan et al. (1980) reported hyperbolic parameter values for a number of granular soils. They noted that there is a direct relationship between the relative density of the soil and the value of

stiffness number K. The results of the tests performed on the Density sand and the Light Castle sand confirm these observations, as shown in Figure 3-3. Therefore, it is possible to estimate the value of K by extrapolation of the values determined from the triaxial tests.

A range of tentative values of K determined from extrapolation is listed in Table 5-8. Both the test results and the data reported by Duncan et al. (1980) were used for this extrapolation. These values were adjusted during the analyses of backfilling and surcharge, to account for the effects of compaction on the lateral stresses in the backfill. This is discussed in the section on calibration analyses.

5.5.3.2 Estimation of stiffness exponent *n*. According to Duncan et al. (1980), the value of n does not vary significantly with relative density. Therefore, the average value of n from the triaxial tests can be used directly. However, additional considerations need to be made for the selection of n in finite element analyses of the IRW.

Table 5-8
Tentative Property Values for the Light Castle Sand Backfill

Property[1]	Tentative Value
K	800 - 1600
n	0.20
R_f	0.85
ν_{nom}	0.3 - 0.40
K_{ur}	800-1600
ϕ'	47°
γ	16.8 kN/m^3

[1] Material parameters are listed and defined in the Notation (Appendix F).

As discussed previously, the lateral stress distribution in the compacted backfill in the IRW is not linear. Relatively large horizontal stresses exist at shallow depths inside the backfill that are induced by the stresses applied during compaction. On the other hand, finite element analyses using SOILSTRUCT-ALPHA do not model compaction effects and produce stress distributions that tend to be linear, with lateral stresses at shallow depths being relatively small.

Figure 5-12 shows the lateral earth pressures measured at the end of backfilling in the IRW. The solid line is the pressure distribution assumed for the purposes of the following discussion. For comparison, the pressure distribution obtained from a SOILSTRUCT-ALPHA analysis is also shown. Both distributions produce approximately the same magnitude of lateral force F'_x. In the upper portion of the wall, the measured lateral stresses are larger than the stresses from the finite element analyses (Figure 5-12a). Conversely, the lateral stresses from the analyses are larger than the measured stresses in the lower portion of the wall. Although no measurements were made of the lateral stresses in the backfill away from the wall, it is reasonable to assume that a similar situation occurs throughout the soil mass.

Figure 5-12b is a hypothetical diagram of an arbitrary stress-dependent property versus confining pressure. The solid line corresponds to the relationship

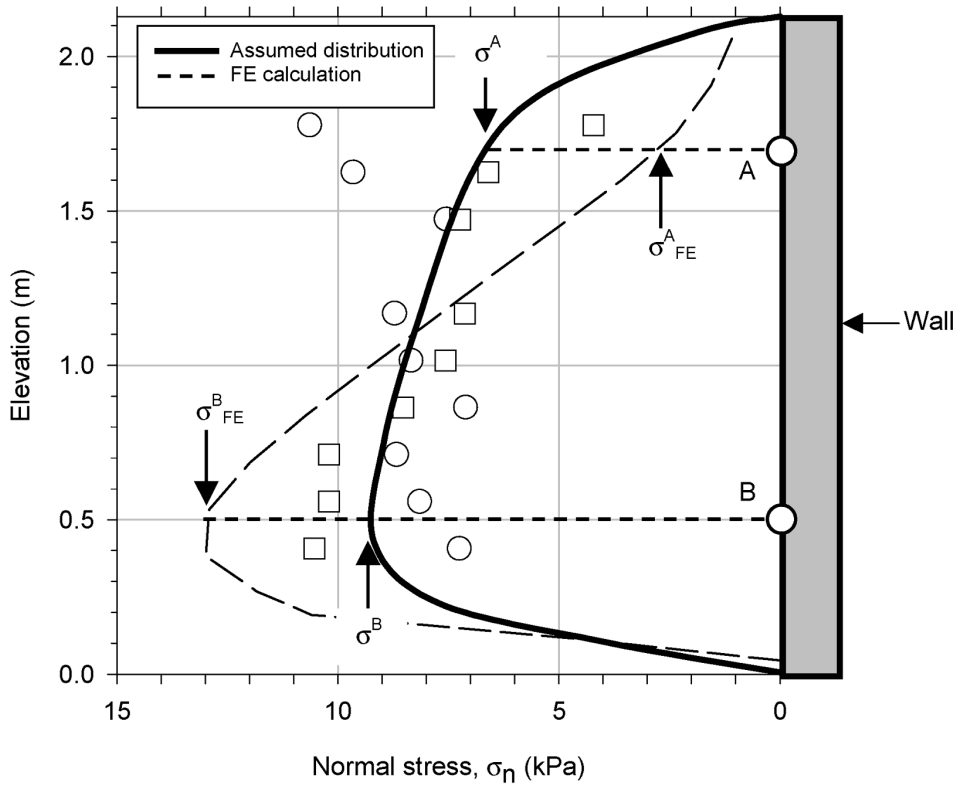

a. Comparison between measured and calculated normal pressures on the instrumented panels

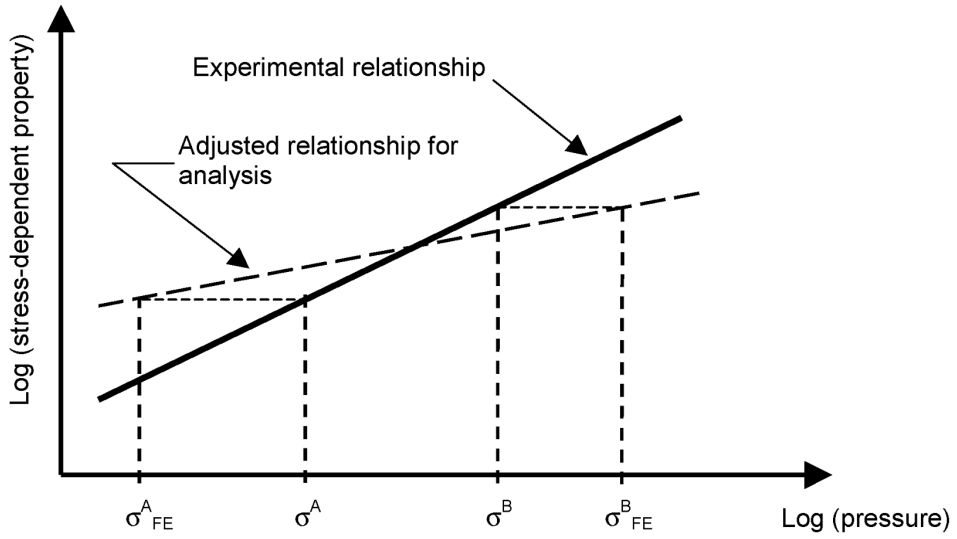

b. Adjustment of stress-dependent property value

Figure 5-12. Adjustment of stress-dependent backfill property for finite element analyses of the IRW

determined from hypothetical laboratory tests. Soil properties such as the Young's modulus and the bulk modulus follow this type of relationship, as discussed in Chapter 3. The property values are inaccurate if they are determined using the solid line and the stresses from the finite element analysis. An adjusted relationship with a shallower slope, shown as a dashed line in the figure, allows estimation of approximate property values using the confining stresses from the analyses.

In order to illustrate the determination of the adjusted relationship, two points, *A* and *B*, are represented in Figure 5-12b. Point *A* is located in the upper portion of the backfill. Point *B* is located in the lower portion of the backfill. As illustrated in Figure 5-12b, the property value corresponding to the lateral stress σ^A at a point such as *A* is assigned to the lower value of stress $\sigma_{FE}{}^A$, calculated from the finite element analyses. Conversely, the property value corresponding to the lateral stress σ^B at a point such as *B* is assigned to the larger value of stress $\sigma_{FE}{}^B$, calculated from the finite element analyses. The resulting relationship has a shallower slope. If the stress-dependent property plotted in the diagram is the initial Young's modulus E_i of the soil, the slope of the relationship corresponds to the value of the modulus exponent *n*. Therefore, a lower value of *n* than that determined from the triaxial tests is required for the finite element analyses of the IRW.

Stress distributions, obtained from a series of preliminary analyses using SOILSTRUCT-ALPHA, were compared to the results of the IRW test. Based on these comparisons, an apparent value of *n*, listed in Table 5-8, was determined for the analyses. No further adjustments were made to the value of *n* during the analyses.

It must be noted that this procedure for the determination of the value of *n* applies only to the case of the IRW or any other walls of similar height. In lock walls, backfill heights are typically larger than 12 m (40 ft) and the lateral stresses induced by the overburden exceed the stresses induced by compaction. Consequently, adjustment of the value of *n* is not necessary for SOILSTRUCT-ALPHA analyses of lock walls.

5.5.3.3 Estimation of the failure ratio R_f. Duncan et al. (1980) noted that the value of R_f does not vary significantly with relative density. This was confirmed by the results of the triaxial tests performed on the Density sand and Light Castle sand, as observed in Table 3-3. The value of R_f assigned to the compacted backfill for the analyses is the average of the R_f values determined from the laboratory tests. No further adjustments were made to this value during the analyses.

5.5.3.4 Estimation of the nominal Poisson's ratio ν_{nom}. The value of ν_{nom} for analysis cannot be estimated directly from the results of laboratory tests. The one-dimensional (1-D) column analysis procedure described by Ebeling and Wahl (1997) was used for a preliminary estimation of ν_{nom}. In the 1-D column procedure, finite element analyses of a column of backfill are performed. The column is free to deform in the vertical direction under the imposed loads but fully restrained in the horizontal direction. Compaction-induced stresses are not modeled in 1-D column analyses.

The 1-D column method does not provide accurate values of ν_{nom} for analyses of the IRW because significant compaction-induced lateral stresses take place in walls of low height. Additionally, vertical shear forces on the wall-backfill interface are comparatively large. A range of tentative values of ν_{nom} for analysis of the IRW is presented in Table 5-8. These values correspond to lateral loads in the 1-D column that are equal to or larger than the measured loads in the IRW. Adjustment of these tentative values of ν_{nom} was required to account for compaction effects in the IRW. For lock walls, 1-D column analyses may provide ν_{nom} values that are adequate for analysis because, due to the larger height of the lock walls, the effects of compaction on the magnitude of lateral stresses are not as significant as in the IRW.

5.5.3.5 Estimation of the unload-reload modulus K_{ur}. As discussed previously, the assumed response of the soil to unloading-reloading is linear and stress-dependent in SOILSTRUCT-ALPHA. It was assumed that a value of K_{ur} identical to the value of K may provide a reasonable approximation to the modulus value during hysteretic unload-reload cycles. The values of K and K_{ur} were adjusted simultaneously in the calibration analyses of the IRW.

5.5.3.6 Estimation of the friction angle ϕ'. There is a direct relationship between the value of ϕ_o and the relative density of the soil (Duncan et al. 1980). The value of ϕ_o of the compacted backfill was estimated by extrapolation from Figure 3-3. The extrapolated value of ϕ_o and the average value of $\Delta\phi$ were used to determine the internal friction angle of the backfill according to Equation 3-1. The magnitude of the confining stress σ_3' used for calculation of ϕ' was the average of the horizontal stress measurements in the IRW test.

5.5.4 Near-field interface properties

Property values were determined for the interface between dense Light Castle sand and concrete as described in Chapter 4. Soil specimens for interface tests were prepared with relative densities of 80 percent; therefore, no direct experimental data are available on the interface properties corresponding to the Light Castle sand compacted to 100 percent of relative density.

There are no established criteria to predict the interface parameters based on the density of the soil. The results reported by Peterson et al. (1976) suggest that interface properties may or may not vary with relative density. In some cases, lower stiffness values were observed in dense specimens than in medium dense specimens of the same soil. In other cases, the variation in interface properties was not substantial for large changes in the soil void ratio.

Based on this information, the interface property values for the compacted backfill were assumed identical to those determined from the interface tests on the dense Light Castle sand against concrete interface. These values, listed in Table 5-9, were used for all the analyses without further adjustments.

As discussed previously, the earth pressure distribution on the wall calculated from finite element analyses differs from the pressures measured in the IRW. For the backfill, an adjusted value of n was determined as illustrated in Figure 5-12 to account for the effect of the pressure distribution on the value of the Young's modulus. Similar analyses can be performed to determine an adjusted value of n_j that accounts for the effect of the pressure distribution on the value of interface stiffness. However, sensitivity analyses showed that n_j has negligible influence on the magnitude of the forces acting on the wall. Consequently, the value of n_j determined from the interface tests was used for the analyses.

Table 5-9
Property Values of the Wall-Backfill Interface used for the Finite Element Analyses of the IRW

Parameter [1]	Value (Determined in Chapter 4)
K_I	20700
n_j	0.79
R_{fj}	0.79
δ	33.7°

[1] Material parameters are listed and defined in the Notation (Appendix F) and Appendix B.

5.6 Calibration Analyses

A series of preliminary analyses were performed for the backfilling and surcharge stages of the IRW test. The purposes of these analyses were

a. To adjust the tentative backfill parameter values determined from the laboratory tests on Light Castle sand specimens.

b. To provide a reasonable approximation of the stresses existing in the wall-backfill system before the start of the inundation stage.

The values of horizontal and vertical forces F_x' and F_v, measured in the IRW at the end of compaction and at the end of surcharge, were the target values for the calibration analyses. The backfill property values were adjusted until the results of the analyses were approximately equal to the target values. The adjusted parameter values for the surcharge stage were used for the analysis of backfill inundation.

5.6.1 Analysis of backfilling

During the backfilling analyses, the target magnitudes of F_v and F_x' at the end of backfilling were attained by adjusting the values of modulus number K and nominal Poisson's ratio ν_{nom}. An increase in the value of K produces a decrease in vertical displacements in the backfill and, consequently, a decrease in the shear force at the wall-backfill interface. An increase in ν_{nom} produces an increase in the horizontal force magnitude. A trial-and-error process is necessary because changes in K and ν_{nom} also induce changes in F_x' and F_v, respectively.

Table 5-10
Backfill Property Values Determined from Calibration Analyses of Stage 1 of the IRW Test

Property[1]	Value
K	1000
n	0.20
R_f	0.85
ν_{nom}	0.36
K_{ur}	-
ϕ'	47°
γ	16.8 kN/m^3

[1] Material parameters are listed and defined in the Notation (Appendix F)

Table 5-10 lists the property values determined from this iteration process. Figure 5-13 compares the measured and calculated values of F'_x and F_v.

The analysis showed that varying K and ν_{nom} within their expected range of values listed in Table 5-8 produces large variations in the results of the analyses. Therefore, it is not possible to make first-order predictions of backfilling in the IRW using the property values obtained from laboratory tests. However, once the target values of the forces at the end of backfilling are attained, the results of the analysis for intermediate backfill heights are in excellent agreement with the test data, as shown in Figure 5-13. This suggests that the procedures followed for the analyses are adequate, and that the models of soil and interface provide reasonable approximations to their actual response.

5.6.2 Analysis of surcharge application and removal

The analysis of the surcharge stage was performed consecutively after the backfilling analysis. Therefore, the initial forces acting on the wall before surcharge application corresponded to the values measured at the end of backfilling. The surcharge analyses were performed in two steps:

a. The values of K and ν_{nom} were adjusted during the analyses to match the target values of F_v and F'_x for full surcharge application.

b. An analysis of surcharge removal was performed using the same parameter values determined in Step 1 and assuming a value of K_{ur} identical to the value of K.

The parameter values of the backfill determined from these analyses are listed in Table 5-11. It can be observed that a larger value of K is necessary to model surcharge application than to model backfilling. Conversely, a smaller value of ν_{nom} is necessary to model surcharge application than to model backfilling. As discussed previously, the differences in the values of K and ν_{nom} between backfilling and surcharge application are due to the existence of compaction effects during backfilling that are not modeled in SOILSTRUCT-ALPHA. The values of K and ν_{nom} in Table 5-10 were selected to account for these compaction effects, and they are not representative of the properties of the compacted backfill. The soil property values listed in Table 5-11, on the other hand, are believed to be representative of the compacted backfill, and were used for the analysis of inundation described in the following section.

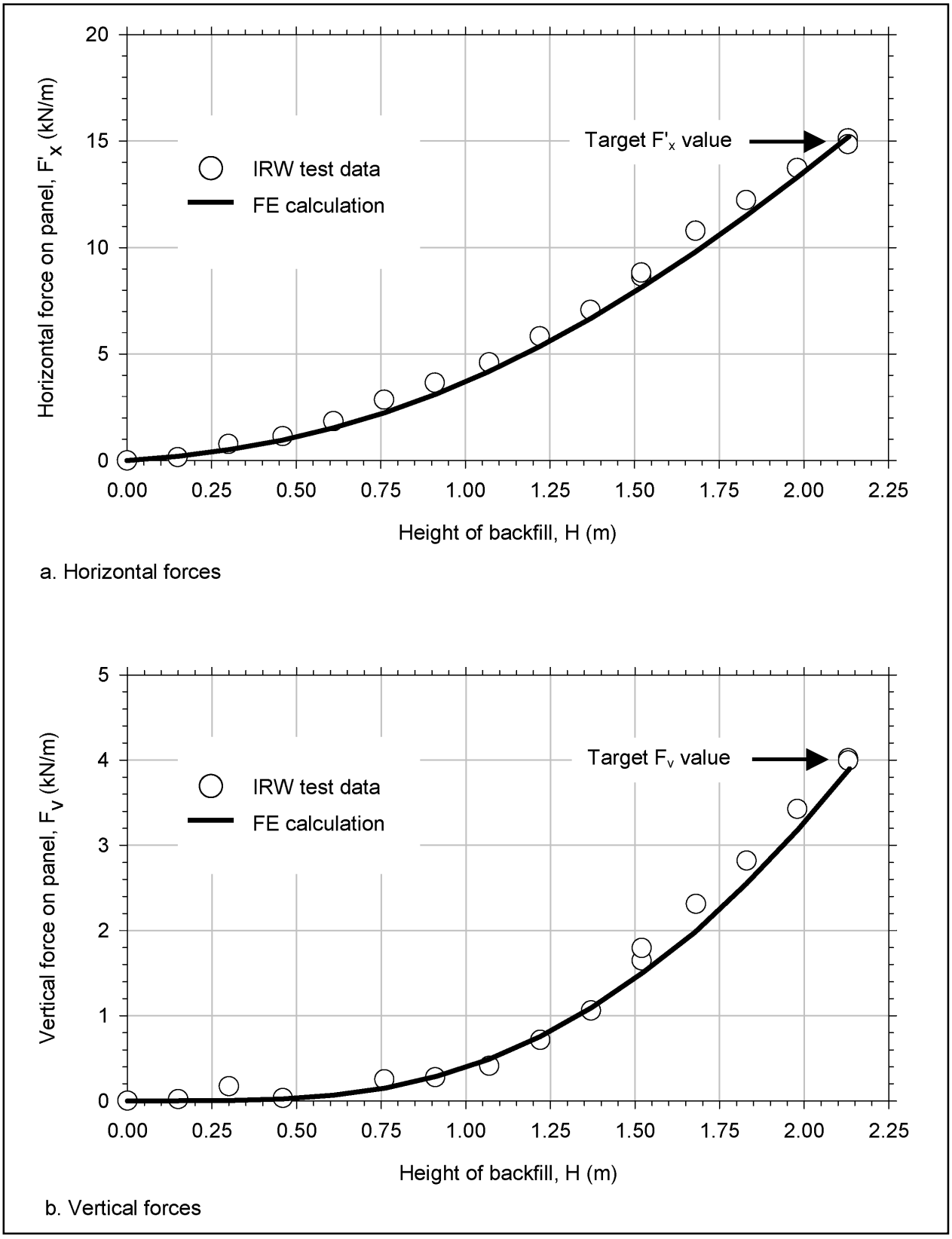

Figure 5-13. Results of calibration analyses of backfilling and comparison of IRW test data

The value of K obtained from these analyses is larger than the expected value from the laboratory tests. This may be due to the following:

a. The laboratory specimens were prepared by pluviation, whereas the backfill was compacted by vibration. The difference in the preparation procedures may account for differences between the properties of the laboratory specimens and the compacted backfill.

b. Compaction stresses applied to each lift induce preloading of the backfill. Because the height of the IRW is relatively small, it is possible that these preloading stresses are not exceeded throughout the soil mass during subsequent application of the surcharge. Consequently, surcharge application may correspond to reloading and induce a stiffer backfill response, especially at shallow depths.

Table 5-11
Backfill Property Values Determined from Calibration Analyses of Stage 2 of the IRW Test

Property[1]	Value
K	2500
n	0.20
R_f	0.85
ν_{nom}	-0.06
K_{ur}	2500
ϕ'	47°
γ	16.8 kN/m^3

[1] Material parameters are listed and defined in the Notation (Appendix F).

The value of ν_{nom} is negative. It must be recalled that ν_{nom} does not have direct physical meaning. Considering an average stress level of the backfill of 0.23, determined from the analyses, and using Equation 5-12, an average value of the Poisson's ratio ν of 0.14 is obtained.

Figure 5-14 compares the measured and calculated values of F'_x and F_v. In the finite element analyses, the initial values of F'_x and F_v are different from the residual values after removal of the surcharge because the responses of the backfill and the interface are different during primary loading from those during unloading. Due to the scatter of the test data, it is unclear if this aspect of the analyses is representative of the actual response of the wall-backfill system.

5.7 Analysis of Backfill Inundation

An analysis was performed of the inundation stage of the IRW test consecutively after the analysis of backfilling and surcharge described in the previous section. The backfill property values listed in Table 5-11 were used for the analysis. The rise of the water level from the bottom to the top elevation of the wall was modeled in 14 incremental steps.

The results of the analyses are represented graphically in Figure 5-15 and compared to the test data. The analysis provides a very good approximation to the values of F'_x and F_v measured during the test. Three important conclusions can be made from the analysis results:

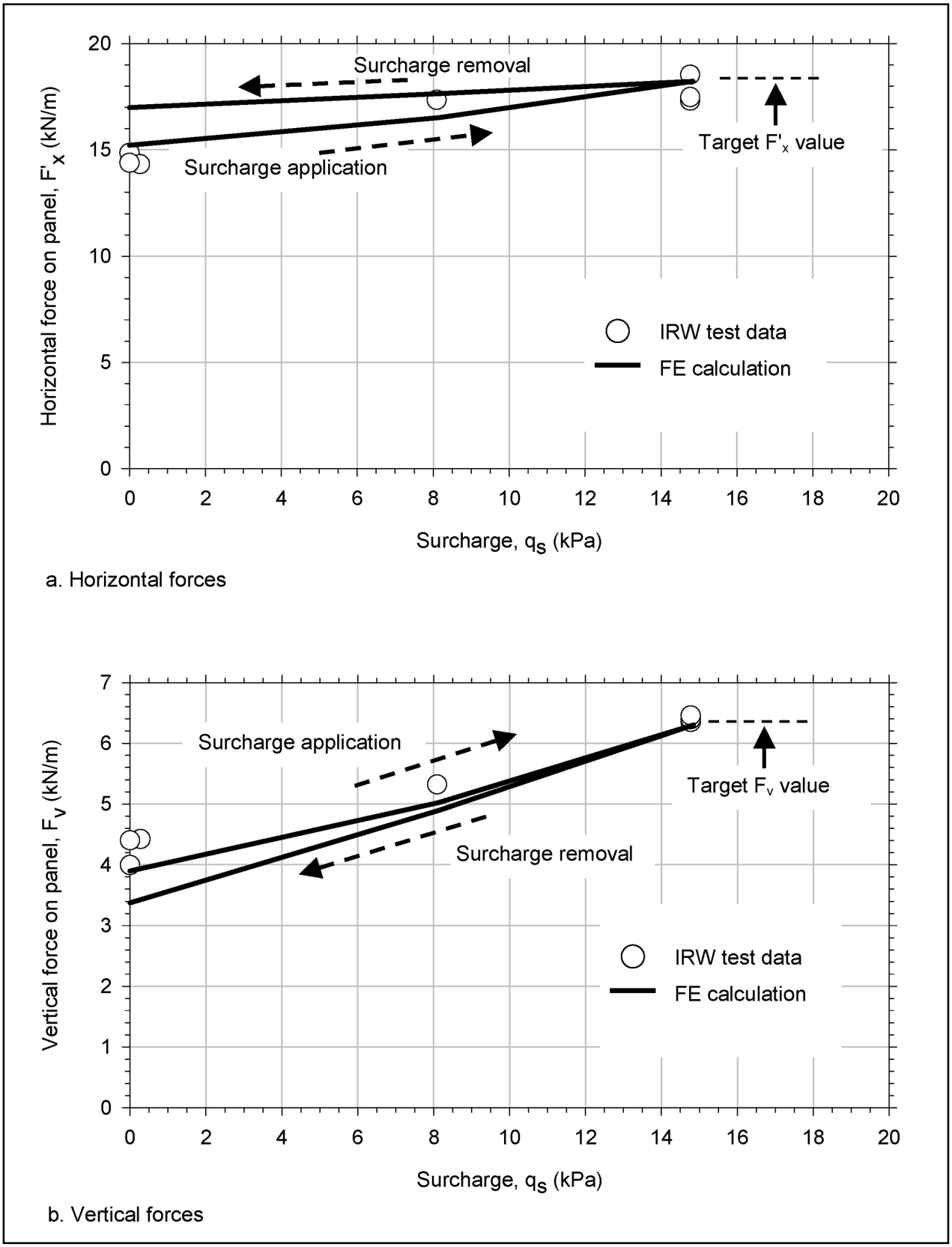

Figure 5-14. Results of calibration analyses of surcharge and comparison to IRW test data

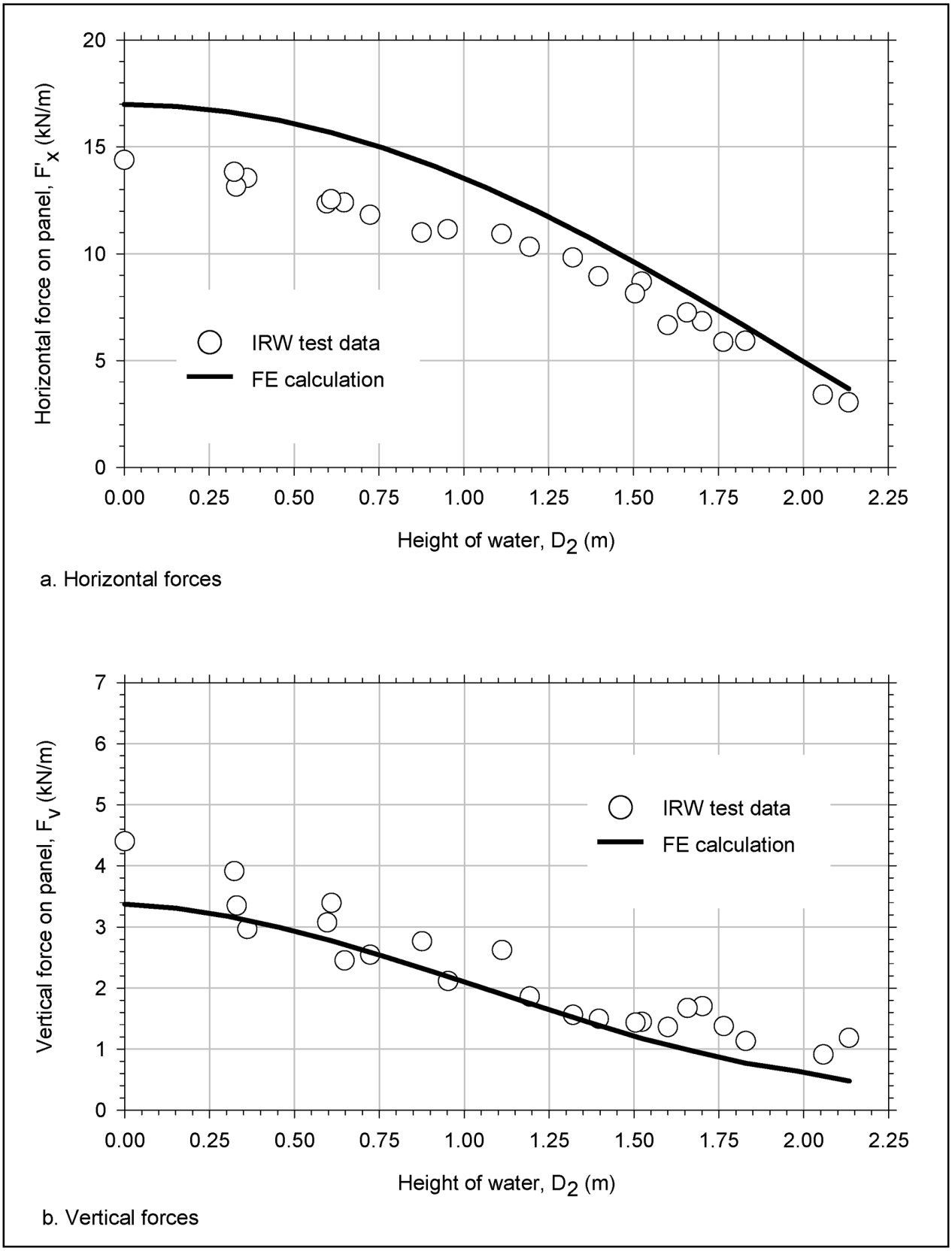

Figure 5-15. Results of finite element analyses of inundation and comparison to IRW test data

a. The implementation of the extended hyperbolic model in SOILSTRUCT-ALPHA was successful.

b. The soil and interface models used in the analyses are accurate for the type of loading that takes place during inundation of the IRW backfill.

c. It may be inferred that the interface model may be accurate for analyses of actual lock walls of greater height. Therefore, use of the interface model for lock wall analyses is recommended for further validation of its accuracy and advantages.

5.8 Summary and Conclusions

A pilot-scale test was performed in the IRW to simulate construction and operation of a lock wall. The test was carried out in three stages: backfilling, surcharge application, and backfill inundation. Light Castle sand was used as backfill material for the test. The properties of the backfill and of the wall-backfill interface were estimated from the results of the laboratory tests described in Chapter 3.

The IRW was not originally designed for surcharge application and inundation of the backfill. Consequently, preparations were necessary to accommodate the intended simulation. To allow full inundation of the backfill, a wooden bulkhead was designed and constructed at the bottom of the access ramp. A sealant was applied to all the gaps existing between the instrumented panels, between the panels and the floor, and along the edges of the bulkhead to prevent significant leaks during inundation of the backfill. Two perforated polyvinyl chloride pipes were installed for inundation and drainage of the backfill. A soil box was prepared to contain the soil used as surcharge. Before the start of the test, all the instruments were calibrated in situ and a data acquisition system was installed in the IRW.

The test results show that a significant vertical shear force develops at the wall-backfill interface during placement and compaction of the backfill. This shear force increases significantly during surcharge application, and decreases during inundation of the backfill. However, it was observed that the final magnitude of the vertical shear force at the end of the test, after drainage of the backfill, was similar to the shear force at the end of backfilling. This suggests that there is no significant degradation of the vertical shear force with cycles of surcharge application and backfill inundation.

The vertical shear force coefficient K_v was calculated from the vertical force measurements during backfilling. It was found that it increases with increasing backfill height. The measured values of K_v are greater than the values predicted using the design line recommended in Appendix F of Engineer Manual 1110-2-2100 (HQUSACE, in preparation). This is a result of the conservatism employed in establishing the design line and the relatively large effect of compaction-induced stresses in short walls such as the IRW. It is not recommended here that the K_v values given by the design line be exceeded for design of lock walls.

The vertical shear force coefficient for surcharge $K_{v,q}$ was determined from the test measurements from the surcharge application stage. It was found that the design line (Appendix F of Engineer Manual 1110-2-2100 (HQUSACE, in preparation)) provides a slightly conservative approximation to the measured $K_{v,q}$ value.

The correction factor C_{wt} for determining the vertical shear force coefficient during inundation was determined from the vertical force measurements during inundation and drainage of the backfill. It was found that the design line (Appendix F of Engineer Manual 1110-2-2100 (HQUSACE, in preparation)) provides a good approximation of the C_{wt} value for water-to-wall height ratios D_2/H that are less than 0.5. For larger ratios, the design values are conservative.

Compaction-induced stresses are significant in the IRW because of its short height. Because the influence of compaction on the stresses decreases with increasing wall heights, accurate finite element analyses of lock walls do not commonly require modeling the stresses applied during compaction. However, for the finite element analyses of the IRW, it is important to account for these compaction effects.

The finite element analyses of the IRW were performed using the updated version of SOILSTRUCT-ALPHA, which contains the extended hyperbolic model for interfaces. For finite element analyses of the IRW, different properties were assigned to the backfill during backfilling than were assigned during surcharge application. For the backfilling analysis, a lower modulus and larger Poisson's ratio than suggested by laboratory test data were assumed, which provided appropriate vertical and horizontal stresses at the wall-backfill interface. For the surcharge placement analysis, a stiffer backfill with a reduced Poisson's ratio were assumed. The properties of the backfill were adjusted by trial and error until the analysis results matched the target values of F_v and F'_x measured in the IRW at the end of compaction and surcharge application. It was found that, once a match to the target F_v and F'_x values was obtained from the analyses, the analysis results for intermediate stages also matched the test data. This suggests that the procedures followed for the analyses are adequate, and that the models of soil and interface provide reasonable approximations to their actual response.

A finite element analysis of backfill inundation was performed using the backfill properties determined from the calibration analysis of surcharge placement. The analysis provides a very good approximation to the values of F'_x and F_v measured during the test. It can be concluded that the implementation of the extended hyperbolic model in SOILSTRUCT-ALPHA was successful, and that the soil and interface models used in the analyses are accurate for inundation analyses of the IRW. It may be inferred that the model may be accurate for analyses of actual lock walls of greater height. Therefore, use of the model for lock wall analyses is recommended for further validation of its accuracy and advantages.

6 Summary and Conclusions

An earth retaining structure such as a lock wall may be subjected to a significant downdrag force generated during placement of the backfill. This downdrag force has a stabilizing effect that could produce a substantially more economical design if accounted for in the design of the wall. Accurate estimation of the downdrag force requires use of an appropriate model for the interface between the backfill and the wall. The model must provide accurate predictions of the interface response to the type of loading applied during placement of the backfill, inundation of the lock, and subsequent operational stages.

The hyperbolic formulation developed by Clough and Duncan (1971) has been used extensively in soil-structure interaction (SSI) analyses for modeling the interface response under monotonic loading. However, it is not applicable to cases where the interface undergoes unloading-reloading or simultaneous changes in shear and normal stresses such as in the backfill-to-structure interface in lock walls. An extended hyperbolic model was developed during this investigation that can predict the interface response to simultaneous changes in shear and normal stresses as well as unloading-reloading and staged shear.

The accuracy of the model was evaluated against the results of interface tests performed for this investigation. In addition, the model was implemented in the finite element program SOILSTRUCT-ALPHA. A pilot-scale test was performed at the Instrumented Retaining Wall (IRW) at Virginia Tech to simulate backfilling, application and removal of surcharge, and changes in the elevation of the water table behind a lock wall. Finite element analyses of all the stages of the test were performed using SOILSTRUCT-ALPHA. Comparisons between the test measurements and the results of the finite element analyses indicate that the extended hyperbolic model provides accurate approximations of the interface response.

This chapter summarizes the activities performed and the conclusions from this investigation. The advantages and limitations of the extended hyperbolic model are presented, as well as recommendations regarding future work on interface modeling for lock wall analyses.

6.1 Summary of Activities

This section summarizes all the activities completed for this investigation: literature review, laboratory testing, the extended hyperbolic model, and lock wall simulation.

6.1.1 Literature review

The literature review (Chapter 2) focused on interface testing, interface modeling, and SSI analyses of retaining walls.

In the experimental work reviewed, the direct shear box (DSB) and the direct simple shear (DSS) are the devices most frequently used for testing sand-to-concrete and sand-to-steel interfaces. Most of the previous work on interfaces investigated monotonic shear of the interface under constant normal stress. Some investigations have been published concerning cyclic shear of interfaces under conditions of constant normal stress or constant normal stiffness. No previous studies of interface response under staged shear were found in the literature.

All of the interface testing devices described in the literature present limitations. The interface sizes are limited and do not allow the determination of the residual interface strength in all cases. In addition, end effects may be present, inducing errors in the measurement of the pre-peak and peak interface response. The Large Direct Shear Box (LDSB) at Virginia Tech allows testing of interfaces as large as 711 mm by 406 mm under monotonic or cyclic shear. The size of the interface minimizes end effects and permits maximum interface displacements of 305 mm, allowing the determination of the residual interface strength. The large displacement capabilities of the LDSB also make possible shearing of the interface in several stages with changing normal stress.

Two types of elements are commonly implemented for modeling interfaces: the joint element and the thin layer element. The joint element, developed by Goodman, Taylor, and Brekke (1968), appears to be used most frequently due to the simplicity of its formulation.

Several models of interface response under shearing have been described in the literature. The hyperbolic formulation by Clough and Duncan (1971) was described in detail in Chapter 2. It has been widely used for modeling the interface response to monotonic shear under constant normal stress. It is a simple model that incorporates the most important aspects of interface behavior using parameters that have physical meaning. However, the Clough and Duncan (1971) hyperbolic formulation was not developed to model interface response under cyclic loading or staged shear. None of the other interface models found in this literature review accounts for simultaneous changes in shear and normal stresses.

Several studies have been published concerning SSI analyses of retaining structures. From these studies, it may be concluded that the downdrag force acting on the back of a retaining wall can contribute significantly to the stability of the

structure. In typical lock walls, the downdrag develops during fill placement. During this stage, the shear and normal stresses acting on the backfill-to-structure interface are changing simultaneously. During submergence and operation of the lock, the shear stresses may be reduced or even reversed. Hence, it is important to model accurately the interface response under staged shear, unloading-reloading, and shear reversals.

A detailed description of a simplified method (Appendix F of Engineer Manual 1110-2-2100 (HQUSACE, in preparation) to estimate the downdrag force was presented in Chapter 2. It is based on a number of SSI analyses of typical lock structures. The simplified method is useful to illustrate the importance of an adequate estimation of the downdrag force in design.

6.1.2 Laboratory testing

The following laboratory and field activities (Chapter 3) were performed for this investigation:

a. Modifications to the LDSB.

b. Selection of sand specimens for interface testing.

c. Grain size distribution, minimum/maximum density, specific gravity, consolidation testing, and triaxial testing on the Density sand and Light Castle sand.

d. Field survey of existing concrete retaining walls to determine a range of representative surface textures for the concrete specimen.

e. Design and construction of a soil box and concrete slab.

f. Development of appropriate testing procedures.

g. Interface tests following a variety of laboratory stress paths to investigate the constitutive behavior of interfaces and to determine the interface response under field conditions for lock walls.

The LDSB was modified specifically to accommodate soil-to-concrete interface testing for this investigation. A special aluminum soil box was designed and constructed that allows compaction of the sand sample directly onto the concrete specimen and minimizes the disturbance of the interface during test setup operations.

A field survey of concrete walls was performed. A concrete specimen was prepared with surface features similar to those observed in the field. The concrete specimen was contained in a frame, which was designed and constructed to act as an external reinforcement for the concrete and to minimize its deformations during interface shear.

A fine, rounded, silica sand (Density sand), and a fine, angular sand (Light Castle sand) were selected for interface testing. A series of basic laboratory tests,

such as minimum/maximum density and grain size analyses, were performed on these sands. Consolidation and CD triaxial tests were also performed to determine sets of hyperbolic parameter values for these soils for a range of relative densities representative of the backfill in lock walls.

An interface testing program was carried out that included initial loading tests, staged shear tests, unload-reload tests, and multidirectional stress path tests. Three types of interfaces were tested: dense Density sand against concrete, medium-dense Density sand against concrete, and dense Light Castle sand against concrete.

From the results of the interface tests, it was found that the average ratio between the values of interface friction angle and internal friction angle of the soil was 0.8. Displacement softening was observed in all tests. The displacements required for the development of the residual condition were as large as 20 mm.

Staged shear tests were performed by increasing the normal pressure in steps during shear. The staged shear tests provided important information about the behavior of sand-to-concrete interfaces and were used to define the yield surfaces implemented in the extended hyperbolic model. It was found that it is possible to determine a complete residual strength envelope from staged shear tests, as long as the displacement capability of the equipment is enough for the development of the residual condition.

Several unload-reload tests were performed during which a complete loading cycle was applied between two predetermined stress levels. These tests follow stress paths similar to field stress paths in which the shear stresses may decrease as a consequence of a rise of the water table behind a lock wall. A substantial increase in the interface shear stiffness was observed during unloading and reloading. It was observed that compression takes place during unloading, followed by dilation during subsequent reloading of the interface. In some tests, one or more cycles of shear were performed upon mobilization of the residual strength. Similar shear stress-displacement response and residual strength values were obtained for both directions of shear in all tests.

Multidirectional stress path tests were performed on all three types of interfaces. The purpose of these tests was to provide a basis for a performance evaluation of the extended hyperbolic model under complicated loading paths. They also modeled certain aspects of the type of loading expected at the backfill-structure interface during backfill placement and operation of a lock wall. The extended hyperbolic model was validated against the results of these tests.

6.1.3 Extended hyperbolic model

An extended hyperbolic model for interfaces was developed during this investigation (Chapter 4). The model captures important aspects of interface response under the type of loading expected to occur in a wall-backfill interface. The material parameters required for implementation of the model are the same as those introduced by Clough and Duncan (1971).

A procedure for normalization of interface test data was developed that facilitated the study of interface response under a variety of experimental stress paths. Based on this study, the concepts of yield surfaces and loading regions were introduced. Two yield surfaces are defined by the past maximum and past minimum stress levels during shear. Two transition surfaces are defined by the past-maximum and past-minimum shear stresses on the interface.

Three types of loading are considered in the extended hyperbolic model: yield-inducing shear, unloading-reloading, and transition loading (Table 4-1). Yield-inducing shear occurs if the stress path reaches one of the yield surfaces. Transition loading in the first quadrant of the τ-σ_n plane occurs if the stress level is lower than the past maximum stress level and the shear stress is equal to or greater than the past maximum shear stress. Conversely, transition loading in the fourth quadrant occurs if the stress level is greater than the past minimum stress level and the shear stress is equal to or lower than the past minimum shear stress. Unloading-reloading takes place if the stress level is lower than the past maximum stress level and greater than the past minimum stress level, and if the shear stress is lower than the past maximum shear stress and greater than the past minimum shear stress.

A formulation for yield-inducing shear was developed in which the interface stiffness is determined by the normal stress, the stress level, and the rate of change of the normal stresses during shear, i.e., the inclination of the stress path. The formulation was found to predict the interface response accurately under a variety of experimental, yield-inducing stress paths.

For unloading-reloading or transition loading, one of three versions of the model can be applied, depending on the accuracy required for the analysis. In Version I, a linear, normal stress-dependent response of the interface is assumed both for unloading-reloading and for transition loading. This version does not model the hysteretic response of the interface under unloading-reloading. Comparisons of the calculated interface response with test data showed that this version may provide reasonable predictions of the interface response for unloading-reloading cycles that are not too large. It is inaccurate for modeling the interface response to large unload-reload loops or interfaces subjected predominantly to transition loading. Version I is the simplest to implement and use in SSI analyses.

In Version II, a nonlinear, hyperbolic response is assumed for unloading-reloading and transition loading that accurately models the hysteretic behavior of interfaces subjected to large unload-reload loops. It provides accurate or reasonable estimates of interface response for most of the experimental stress paths considered in this investigation. However, it does not provide accurate estimates for cases in which the interface is subjected predominantly to transition loading. Although the formulation of Version II introduces some additional state variables, it is simple to implement in SSI analyses of retaining walls.

In Version III, the interface stiffness for unloading-reloading is determined in the same way as in Version II. For transition loading, on the other hand, the interface stiffness is determined by interpolation from the normalized stiffness diagram. Two normalized stiffness values are used for the interpolation: the

normalized stiffness of the interface at the onset of transition loading and the normalized stiffness at yield. This version provides the most accurate estimates of interface response for all the experimental stress paths considered. It is particularly useful for cases where the interface is subjected predominantly to staged shear. Version III is the most difficult to implement in SSI analyses because it introduces several additional state variables with respect to the other two versions.

The principal advantages of the extended hyperbolic model are as follows:

a. It has a simple mathematical formulation.

b. Hyperbolic parameter values for different types of interfaces are available in the literature.

c. It captures the main features of the interface response under simultaneous changes in shear and normal stress and unloading-reloading.

d. It provides accurate estimates of the interface response for the experimental stress paths considered in this investigation.

e. It is relatively easy to implement in SSI analyses.

f. It establishes a framework for future work on plasticity-based interface models.

The formulations for yield-inducing shear and for unloading-reloading Version II of the extended hyperbolic model were implemented in the finite element program SOILSTRUCT-ALPHA, which is commonly used by the U.S. Army Corps of Engineers for analyses of lock walls. Finite element analyses of the IRW lock wall simulation suggest that these formulations are effective for prediction of vertical shear forces in retaining structures.

The model has several limitations:

a. It does not model displacements normal to the interface, and the interface thickness is implicitly assumed as zero. Consequently, in finite element analyses, a large normal stiffness must be assigned to interface elements in order to minimize overlapping of adjacent two-dimensional elements. In addition, it cannot model the generation of normal stresses due to restrained dilation of the interface during shear between two stiff, rough media. This may not be important for analyses of stiff retaining structures that have relatively compressible backfills.

b. It does not model displacement softening of the interface. According to the experimental data collected during this investigation, displacement softening may take place in interfaces subjected to relative displacements of 6 to 20 mm. Therefore, in cases where larger magnitudes of interface displacement take place, the model cannot provide accurate predictions of the softening response.

c. The model predicts interface stiffness values that are zero or negative for certain loading combinations. For implementation of the model in finite

element programs, it is then necessary to use appropriate stiffness values and adequate numerical procedures to prevent numerical problems. It is believed that the model predictions for these cases are correct. However, if finite element analyses of lock walls show that these types of loading are common, it may be necessary to perform additional experimental work to verify the model predictions.

As discussed in Chapter 5, the model was used successfully for the estimation of vertical shear forces in the IRW lock wall simulation. However, it has not yet been used for routine analyses of actual lock walls.

6.1.4 Lock wall simulation

A pilot-scale test was performed in the IRW to simulate construction and operation of a lock wall (Chapter 5). The test was carried out in three stages: backfilling, surcharge application, and backfill inundation. Light Castle sand was used as backfill material for the test.

The IRW was not originally designed for surcharge application and inundation of the backfill. Consequently, preparations were necessary to accommodate the intended simulation. To allow full inundation of the backfill, a wooden bulkhead was designed and constructed at the bottom of the access ramp and all the gaps between the instrumented panels were sealed. Two perforated polyvinyl chloride pipes were installed for inundation and drainage of the backfill. A soil box was prepared to contain the soil used as surcharge. Before the start of the test, all the instruments were calibrated in situ and a data acquisition system was installed in the IRW.

The test results show that a significant vertical shear force develops at the wall-backfill interface during placement and compaction of the backfill. This shear force increases significantly during surcharge application, and decreases during inundation of the backfill. However, it was observed that the final magnitude of the vertical shear force at the end of the test, after drainage of the backfill, was similar to the shear force at the end of backfilling. This suggests that there is not a significant degradation of the vertical shear force with cycles of surcharge application and backfill inundation.

The vertical shear force coefficient K_v was calculated from the vertical force measurements during backfilling. It was found to increase with increasing backfill height. The measured values of K_v are greater than the values predicted using the design line recommended in Appendix F of Engineer Manual 1110-2-2100 (HQUSACE, in preparation). This is a result of the conservatism employed in establishing the design line and the relatively large effect of compaction-induced stresses in short walls such as the IRW. It is not recommended here that the K_v values given by the design line be exceeded for design of lock walls.

The vertical shear force coefficient for surcharge $K_{v,q}$ was determined from the test measurements from the surcharge application stage. It was found that the design line (Appendix F of Engineer Manual 1110-2-2100 (HQUSACE, in

preparation)) provides a slightly conservative approximation of the measured $K_{v,q}$ value.

The correction factor C_{wt} for determination of the vertical shear force coefficient during inundation was determined from the vertical force measurements during inundation and drainage of the backfill. It was found that the design line (Appendix F of Engineer Manual 1110-2-2100 (HQUSACE, in preparation)) provides a good approximation of the C_{wt} value for water-to-wall height ratios D_2/H less than 0.5. For larger ratios, the design values are conservative.

Compaction-induced stresses are significant in the IRW because of its short height. Because the influence of compaction on the stresses decreases with increasing wall heights, accurate finite element analyses of lock walls do not commonly require modeling the stresses applied during compaction. However, for the finite element analyses of the IRW, it is important to account for these compaction effects.

The finite element analyses of the IRW were performed using the updated version of SOILSTRUCT-ALPHA, which contains the extended hyperbolic model for interfaces. For finite element analyses of the IRW, different properties were assigned to the backfill during backfilling than were assigned during surcharge application. For the backfilling analysis, a lower modulus and larger Poisson's ratio than suggested by laboratory test data were assumed, which provided appropriate vertical and horizontal stresses at the wall-backfill interface. For the surcharge placement analysis, a stiffer backfill and a reduced Poisson's ratio were assumed. The properties of the backfill were adjusted by trial and error until the analysis results matched the target values of F_v and F_x' measured in the IRW at the end of compaction and surcharge application. It was found that, once a match to the target F_v and F_x' values was obtained from the analyses, the analysis results for intermediate stages also matched the test data. This suggests that the procedures followed for the analyses are adequate, and that the models of the soil and interface provide reasonable approximations to their actual response.

A finite element analysis of backfill inundation was performed using the backfill properties determined from the calibration analysis of surcharge placement. The analysis provided a very good approximation to the values of F_x' and F_v measured during the test. It can be concluded that the implementation of the extended hyperbolic model in SOILSTRUCT-ALPHA was successful, and that the soil and interface models used in the analyses are accurate for inundation analyses of the IRW. It may be inferred that the model may be accurate for analyses of actual lock walls of greater height. Therefore, use of the model for lock wall analyses is recommended for further validation of its accuracy and usefulness.

6.2 Recommendations for Future Work

According to the findings from this investigation, the following recommendations are presented for future work on interface modeling and SSI analyses of lock walls:

a. It is recommended that the updated version of the program SOILSTRUCT-ALPHA be used for analyses of lock walls to further verify the applicability of the extended hyperbolic model for interfaces. Such analyses would also serve to detect numerical problems, if any, arising from the implementation of the extended hyperbolic model in SOILSTRUCT-ALPHA.

b. The relative significance of Versions I, II, and III could be assessed by adding Versions I and III to SOILSTRUCT-ALPHA and then comparing the results of analyses of lock walls.

c. The extended hyperbolic model does not account for displacement softening of interfaces. If peak strengths are used in cases where displacement softening takes place at the wall-backfill interface, SOILSTRUCT-ALPHA analyses may overestimate the magnitude of the downdrag force. It is therefore recommended to calculate the range of relative displacement magnitudes at the interface between backfill and interface from the results of SOILSTRUCT-ALPHA analyses of typical lock walls with varying foundation conditions. Such analyses may reveal the type of lock wall configurations where displacement softening behavior of the wall-backfill interface needs to be modelled to obtain accurate estimates of downdrag forces. According to the results of the interface tests performed during this investigation, displacement softening may occur after relative displacements of 5 to 20 mm at the interface. Alternatively, residual interface strengths could be used to produce a conservative analysis.

d. The extended hyperbolic formulation does not model displacements normal to the interface. According to the results from the interface tests performed, dilation takes place at the interface between sand and concrete. Although the model provides accurate estimates of the interface response to simultaneous changes in normal and shear stresses, it cannot predict changes in normal stresses during shear induced by restrained dilation of the interface. Restrained dilation of interfaces is known to occur in rock joints, and rock joint models have been developed that allow the calculation of normal stress changes induced by this phenomenon. However, it is not known whether restrained dilation can occur at a wall-backfill interface. Relatively simple finite element analyses can be performed using SOILSTRUCT-ALPHA to estimate the magnitude of changes in normal stress at the wall-backfill interface due to dilation, and the results can be used to evaluate the importance of these normal stress changes for design of lock walls.

e. If interface dilation is found to be an important issue for design of lock walls or other Corps of Engineers structures, it may be convenient to

develop a new interface element formulation for use in finite element analyses. This new formulation could incorporate features of the extended hyperbolic model and account for coupled tangential and normal displacements. The formulation of the thin layer interface element developed by Desai et al. (1984) could be a convenient starting point for the development of such a coupled interface model.

References

Acar, Y. B., Durgunoglu, H. T., and Tumay, M. T. (1982). "Interface properties of sand," *Journal of the Soil Mechanics and Foundations Division,* ASCE, 108(GT4), 648-654.

American Society for Testing and Materials. (1990). "Standard test method for classification of soils for engineering purposes," Practice No. D2487-90, *1990 Book of ASTM Standards*, 04.08, Philadelphia, PA.

_____. (1991). "Standard test method for minimum index density and unit weight of soils and calculation of relative density," ASTM D4254-91, West Conshohocken, PA.

_____. (1992). "Standard test method for specific gravity of soils," ASTM D854-92, West Conshohocken, PA.

_____. (1993a). "Standard classification of soils for engineering purposes (Unified Soil Classification System)," ASTM D2487-93, West Conshohocken, PA.

_____. (1993b). "Standard practice for description and identification of soils (visual-manual procedure)," ASTM D2488-93, West Conshohocken, PA.

_____. (1993c). "Standard test method for maximum index density and unit weight of soils using a vibratory table," ASTM D4253-93, West Conshohocken, PA.

Bosscher, P. J., and Ortiz, C. (1987). "Frictional properties between sand and various construction materials," *Journal of Geotechnical Engineering,* ASCE, 113(9), 1035-1039.

Brandon, T. L., Duncan, J. M., and Gardner, W. S. (1990). "Hydrocompression settlement of deep fills," *Journal of Geotechnical Engineering*, ASCE, 116(10), 1536-1548.

Brummund, N. F., and Leonards, G. A. (1973). "Experimental study of static and dynamic friction between sand and typical construction materials," *Journal of Testing and Evaluation*, ASTM, 1(2), 162-165.

Clough, G. W., and Duncan, J. M. (1969). "Finite element analyses of Port Allen and Old River Locks," Report No. TE-69-3, U.S. Army Engineer Waterways Experiment Station, Vicksburg, MS.

Clough, G. W., and Duncan, J. M. (1971). "Finite element analyses of retaining wall behavior," *Journal of the Soil Mechanics and Foundations Division,* ASCE, 97(SM12), 1657-1673.

Desai, C. S., and Rigby, D. B. (1997). "Cyclic interface and joint shear device including pore pressure effects," *Journal of Geotechnical and Geoenvironmental Engineering* 123(6), 568-579.

Desai, C. S., Drumm, E. C., and Zaman, M. M. (1985). "Cyclic testing and modeling of interfaces," *Journal of Geotechnical Engineering,* ASCE, 111(6), 793-815.

Desai, C. S., Muqtadir, A., and Scheele, F. (1986). "Interaction analyses of anchor-soil systems," *Journal of Geotechnical Engineering,* ASCE, 112(5), 537-553.

Desai, C. S., Zaman, M. M., Lightner, J. G., and Siriwardane, H. J. (1984). "Thin-layer elements for interfaces and joints," *International Journal for Numerical and Analytical Methods in Geomechanics* 8(1), 19-43.

Duncan, J. M., and Chang, C. Y. (1970). "Nonlinear analysis of stress and strain in soils," *Journal of the Soil Mechanics and Foundations Division,* ASCE, 96(SM5), 1629-1653.

Duncan, J. M., and Clough, G. W. (1971). "Finite element analyses of Port Allen Lock," *Journal of the Soil Mechanics and Foundations Division,* ASCE, 97(SM8), 1053-1067.

Duncan, J. M., Byrne, P., Wong, K. S., and Mabry, P. (1980). "Strength, stress-strain and bulk modulus parameters for finite element analyses of stresses and movements in soil masses," Report No. UCB/GT/80-01, Department of Civil Engineering, University of California, Berkeley.

Duncan, J. M., Williams, G. W., Sehn, A. L., Seed, R. B. (1991). "Estimation earth pressures due to compaction," *Journal of Geotechnical Engineering* 117(12), 1833-1847.

Ebeling, R. M., and Filz, G. M. "Soil-structure interaction analyses of rock founded gravity and cantilevered walls" (in preparation), U.S. Army Engineer Research and Development Center, Vicksburg, MS.

Ebeling, R. M., and Mosher, R. L. (1996). "Red River U-Frame Lock No. 1 backfill-structure-foundation interaction," *ASCE Journal of Geotechnical Engineering* 122(3), 216-225.

Ebeling, R. M., and Wahl, R. E. (1997). "Soil-structure-foundation interaction analysis of new roller-compacted concrete North Lock Wall at McAlpine Locks," Technical Report ITL-97-5, U.S. Army Engineer Waterways Experiment Station, Vicksburg, MS.

Ebeling, R. M., Duncan, J. M., and Clough, G. W. (1990). "Methods of evaluating the stability and safety of gravity earth-retaining structures founded on rock - Phase 2 study," Technical Report ITL-90-7, U.S. Army Engineer Waterways Experiment Station, Vicksburg, MS.

Ebeling, R. M., Pace, M. E., and Morrison, E. E. (1997). "Evaluating the stability of existing massive concrete gravity structures founded on rock," Technical Report REMR-CS-54, U.S. Army Engineer Waterways Experiment Station, Vicksburg, MS.

Ebeling, R. M., Peters, J. F., and Clough, G. W. (1992). "User's guide for the incremental construction soil-structure interaction program SOILSTRUCT," Technical Report ITL-90-6, U.S. Army Engineer Waterways Experiment Station, Vicksburg, MS.

Ebeling, R. M., Peters, J. F., and Mosher, R. L. (1997). "The role of non-linear deformation analyses in the design of a reinforced soil berm at Red River U-Frame Lock No. 1," *International Journal for Numerical and Analytical methods in Geomechanics* 21, 753-787.

Ebeling, R. M., Clough, G. W., Duncan, J. M., and Brandon, T. L. (1992). "Methods for evaluating the stability and safety of gravity earth retaining structures founded on rock," Technical Report REMR-CS-29, U.S. Army Engineer Waterways Experiment Station, Vicksburg, MS.

Ebeling, R. M., Mosher, R. L., Abraham, K., and Peters, J. F. (1993). "Soil-structure interaction study of Red River Lock and Dam No. 1 subjected to sediment loading," Technical Report ITL-93-3, U.S. Army Engineer Waterways Experiment Station, Vicksburg, MS.

Esterhuizen, J. J. (1997). "Progressive failure of slopes in lined waste impoundments," Ph.D. Diss., Geotechnical Engineering Division, Department of Civil Engineering, Virginia Polytechnic Institute and State University, Blacksburg.

Evgin, E., and Fakharian, K. (1996). "Effect of stress paths on the behaviour of sand-steel interfaces," *Canadian Geotechnical Journal* 33(6), 853-865.

Fakharian, K., and Evgin, E. (1995). "Simple shear versus direct shear tests on interfaces during cyclic loading." *Proceedings Third International Conference on Recent Advances in Geotechnical Earthquake Engineering and Soil Dynamics*, St. Louis, MO, April 2-7, 1995. S. Prakash, ed., University of Missouri at Rolla, III, 13-16.

Fakharian, K., and Evgin, E. (1996). "An automated apparatus for three-dimensional monotonic and cyclic testing of interfaces," *Geotechnical Testing Journal* 19(1), 22-31.

_____. (1997). "Cyclic simple-shear behavior of sand-steel interfaces under constant normal stiffness condition," *Journal of Geotechnical and Geoenvironmental Engineering* 123(12), 1096-1105.

Filz, G. M. (1992). "An analytic and experimental study of earth loads on rigid retaining walls," Ph.D. Diss., Geotechnical Engineering Division, Department of Civil Engineering, Virginia Polytechnic Institute and State University, Blacksburg.

Filz, G. M., and Duncan, J. M. (1997). "Vertical shear loads on nonmoving walls. I: Theory," *ASCE Journal of Geotechnical Engineering* 123(9), 856-862.

Filz, G. M., Duncan, J. M., and Ebeling, R. M. (1997). "Vertical shear loads on nonmoving walls. II: Applications," *ASCE Journal of Geotechnical Engineering* 123(9), 863-873.

Gómez, J. E., Filz, G. M., and Ebeling, R. M. (1999). "Development of an improved numerical model for concrete-to-soil interfaces in soil-structure interaction analyses; Report 1, Preliminary study," Technical Report ITL-99-1, U.S. Army Engineer Research and Development Center, Vicksburg, MS.

Goodman, R. E., Taylor, R. L., and Brekke, T. L. (1968). "A model for the mechanics of jointed rock," *Journal of the Soil Mechanics and Foundations Division,* ASCE, 94(SM3), 637-659.

Headquarters, U.S. Army Corps of Engineers. (1994). "Stability of gravity walls, vertical shear," Engineer Technical Letter 1110-2-352, Washington, DC.

_____. "Stability analyses of concrete structures" (in preparation), Engineer Manual 1110-2-2100, Washington, DC.

Heuze, F. E., and Barbour, T. G. (1982). "New models for rock joints and interfaces," *ASCE Journal of the Geotechnical Engineering Division* 108(GT5), 757-776.

Hryciw, R. D., and Irsyam, M. (1993). "Behavior of sand particles around rigid ribbed inclusions during shear," *Soils and Foundations* 33(3), 1-13.

Huck, P. J., and Saxena, S. K. (1981). "Response of soil-concrete interface at high pressure." *Proceedings of the Tenth International Conference on Soil Mechanics and Foundation Engineering*, Stockholm, 15-19 June 1981. A. A. Balkema, Rotterdam, The Netherlands, 2, 141-144.

Jaky, J. (1948). "The coefficient of earth pressure at rest," *Journal of the Society of Hungarian Architects and Engineers*, 1944.

Janbu, N. (1963). "Soil compressibility as determined by oedometer and triaxial tests." *European Conference on Soil Mechanics and Foundation Engineering*, Wiesbaden, Germany, 1, 19-25

Kishida, H., and Uesugi, M. (1987). "Tests of the interface between sand and steel in the simple shear apparatus," *Géotechnique* 37(1), 45-52.

Kondner, R. L. (1963). "Hyperbolic stress-strain response: Cohesive soils," *Journal of the Soil Mechanics and Foundations Division,* ASCE, proc. Paper 3429, 89(SM1), 115-143.

Kondner, R. L., and Zelasko, J. S. (1963). "A hyperbolic stress-strain formulation for sands." *Proceedings, 2nd Pan-American Conference on Soil Mechanics and Foundations Engineering,* Sao Paulo, Brazil, July 16-24 1963. I, 289-324.

Kramer, S. L. (1996). *Geotechnical earthquake engineering.* Prentice-Hall, Upper Saddle River, NJ.

Kulhawy, F. H., and Peterson, M. S. (1979). "Behavior of sand-concrete interfaces." *Proceedings of the 6th Panamerican Conference on Soil Mechanics and Foundation Engineering*, Lima, Peru, December 2-7, 1979. II, 225-236.

Lade, P. V., and Duncan, J. M. (1975). "Elastoplastic stress-strain theory for cohesionless soil," *ASCE Journal of the Geotechnical Engineering Division* 101(GT10), 1037-1053.

_____. (1976). "Stress-path dependent behavior of cohesionless soil," *ASCE Journal of the Geotechnical Engineering Division* 102(GT1), 51-68.

Lee, P. A., Kane, W. F., Drumm, E. C., and Bennett, R. M. (1989). "Investigation and modeling of soil-structure interface properties." *Foundation engineering: Current principles and practice.* ASCE Geotechnical Special Publication 22, 580-587.

Matsui, T., and San, K. C. (1989). "An elastoplastic joint element with its application to reinforced slope cutting," *Soils and Foundations* 29(3), 95-104.

Morrison, C. S. (1995). "The development of a modular finite element program for analyses of soil-structure interaction," Ph.D. Diss., Geotechnical Engineering Division, Department of Civil Engineering, Virginia Polytechnic Institute and State University, Blacksburg.

Peterson, M. S., Kulhawy, F. H., Nucci, L. R., and Wasil, B. A. (1976). "Stress-deformation behavior of soil-concrete interfaces," Contract Report B-49 to Niagara Mohawk Power Corporation, Syracuse, NY.

Potyondy, J. G. (1961). "Skin friction between various soils and construction materials," *Géotechnique* 11(4), 339-353.

Pyke, R. (1979). "Nonlinear soil models for irregular cyclic loadings," *ASCE Journal of the Geotechnical Engineering Division* 105(GT6), 715-726.

Seed, R. B., and Duncan, J. M. (1986). "FE analyses: Compaction-induced stresses and deformations," *Journal of Geotechnical Engineering* 112(1), 23-43.

Sehn, A. L. (1990). "Experimental study of earth pressures on retaining structures," Ph.D. Diss., Geotechnical Engineering Division, Department of Civil Engineering, Virginia Polytechnic Institute and State University, Blacksburg.

Shallenberger, W. C., and Filz, G. M. (1996). "Interface strength determination using a large displacement shear box." *Proceedings of the Second International Congress on Environmental Geotechnics*, Osaka, Japan, 5-8 November 1996. M. Kamon, ed., A. A. Balkema, Rotterdam, The Netherlands.

Stankowski, T., Runesson, K., and Sture, S. (1993). "Fracture and slip of interfaces in cementitious composites. I: Characteristics," *Journal of Engineering Mechanics,* ASCE, 119(2), 292-314.

Stark, T. D., Ebeling, R. M., and Vettel, J. J. (1994). "Hyperbolic stress-strain parameters for silts," *Journal of Geotechnical Engineering,* ASCE, 120(2), 420-441.

Stark, T. D., Williamson, T. A., and Eid, H. T. (1996). "HDPE geomembrane/geotextile interface shear strength," *Journal of Geotechnical Engineering* 122(3), 197-203.

Uesugi, M., and Kishida, H. (1985). "Discussion: Cyclic testing and modeling of interfaces," *Journal of Geotechnical Engineering,* ASCE, 113(9), 1086-1087.

_____. (1986a). "Frictional resistance at yield between dry sand and mild steel," *Soils and Foundations* 26(4), 139-149.

_____. (1986b). "Influential factors of friction between steel and dry sands," *Soils and Foundations* 26(2), 33-46.

Uesugi, M., Kishida, H., and Tsubakihara, Y. (1988). "Behavior of sand particles in sand-steel friction," *Soils and Foundations* 28(1), 107-118.

_____. (1989). "Friction between sand and steel under repeated loading," *Soils and Foundations* 29(3), 127-137.

Uesugi, M., Kishida, H., and Uchikawa, Y. (1990). "Friction between dry sand and concrete under monotonic and repeated loading," *Soils and Foundations* 30(1), 115-128.

Wilson, E. L. (1975). "Finite elements for foundations, joints and fluids." *Finite Elements in Geomechanics*. G. Gudehus, ed., John Wiley, London.

Wong, P. C., Kulhawy, F. H., and Ingraffea, A. R. (1989). "Numerical modeling of interface behavior for drilled shaft foundations under generalized loading." *Foundation Engineering: Current Principles and Practice*, ASCE Geotechnical Special Publication 22, 565-579.

Wood, D. M. (1990). *Soil behavior and critical state soil mechanics*. Cambridge University Press, New York.

Yoshimi, Y., and Kishida, T. (1981). "A ring torsion apparatus for evaluating friction between soil and metal surfaces," *Geotechnical Testing Journal* 4(4), 145-152.

Yuan, Z., and Chua, K. M. (1992). "Exact formulation of axisymmetric-interface-element stiffness matrix," *Journal of Geotechnical Engineering* 118(8), 1264-1271.

Zaman, M. M., Desai, C. S., and Drumm, E. C. (1984). "Interface model for dynamic soil-structure interaction," *Journal of Geotechnical Engineering* 110(9), 1257-1273.

Appendix A
Results of Triaxial and Consolidation Tests

Triaxial and consolidation tests were performed on specimens of the soils used for interface testing. The objectives of these tests were as follows:

a. Determination of the internal friction angle of the soils.

b. Determination of the hyperbolic parameters of the soils.

c. Evaluation of hydrocompression strains induced by inundation of the soils.

This appendix describes the procedures and results of the tests performed on specimens of Density sand and Light Castle sand. The procedure for the determination of the internal friction angle of the soils from the results of the triaxial tests is presented. Hydrocompression properties of the soils are evaluated based on the results of the consolidation tests. The procedure for determination of the hyperbolic parameter values of each of the soils is presented in Appendix B.

A.1 Triaxial Tests

Two different sands were used for the tests:

a. *Density sand*. It is a fine to medium silica sand with subrounded to rounded grains, available commercially for in situ density determinations.

b. *Light Castle sand*. It is a fine to medium sand with subangular to angular grains.

A more complete description of the properties of these soils is presented in Chapter 3 of this report.

Drained triaxial (CD) tests were performed to determine the internal friction angle and hyperbolic parameter values of the Density sand and the Light Castle sand for a range of relative densities. Sets of medium dense and dense specimens

were prepared by pluviation for each type of sand. After preparation, each sample was subjected to an internal manometric pressure of -15 to -20 kPa, which was gradually removed during application of the cell pressure. The samples were de-aired using carbon dioxide, inundated with de-aired distilled water, and back-pressure saturated. The samples in each set were consolidated under effective confining pressures ranging from 45 to 280 kPa. These values are representative of the estimated values of confining pressure within the backfill of typical lock walls. Shearing was performed at a strain rate of 0.25 $^{\%}/_{\text{min}}$, which was found to be appropriate for pore pressure dissipation during previous trials.

The results of the tests are presented graphically in Figures A1 to A4.[1] All the specimens exhibited dilation during shear and strain softening after mobilization of the peak strength. Because the peak strength envelopes of both soils are curved, the value of secant friction angle ϕ for a given confining pressure σ'_3, can be calculated from the following expression (Duncan et al. 1980):[2]

$$\phi = \phi_o - \Delta\phi \cdot log_{10}\left(\frac{\sigma'_3}{p_a}\right) \tag{A1}$$

where

ϕ_o = peak secant friction at a confining pressure of 101.4 kPa (1 atm)

$\Delta\phi$ = reduction in the peak friction angle value for a tenfold increase in σ'_3

p_a = atmospheric pressure

The values of friction parameters ϕ_o and $\Delta\phi$ are determined using diagrams of secant friction angle versus normalized confining pressure σ_3/p_a such as those shown in Figures A1c, A2c, A3c, and A4c.

The procedure for the determination of the hyperbolic parameter values of the soils is presented in Appendix B.

A.2 Consolidation Testing

Consolidation tests were performed on specimens of Density sand and Light Castle sand to provide additional data on their mechanical properties and determine their susceptibility to hydrocompression (Brandon, Duncan, and Gardner 1990).

Two specimens of each type of sand were prepared at different relative densities in a dry condition. Each specimen was consolidated under a series of vertical stress increments. Once a predetermined stress was reached, the specimen

[1] For convenience, symbols are listed and defined in the Notation (Appendix F).

[2] References cited in this Appendix are included in the References at the end of the main text.

was inundated after primary consolidation was attained. The results of these tests are presented as strain versus stress diagrams in Figures A5 to A8.

During inundation, compressive vertical strain was observed in all specimens tested. The strain that takes place during inundation includes deformation due to secondary compression of the sand and collapse of the structure due to inundation. The value of the strain induced by hydrocompression in each test was determined from strain versus time plots following the procedure suggested by Brandon, Duncan, and Gardner (1990).

Figure A9 is a diagram of hydrocompression strain versus relative density determined from the consolidation tests on Light Castle Sand specimens. Two specimens, prepared at different relative densities, were inundated under a vertical stress of 32.3 kPa. It is seen that hydrocompression strains decrease for increasing soil densities. A straight line was drawn through the data points corresponding to these two tests and extended through the entire range of relative densities shown. Lines parallel to this extended line were drawn through the single data points corresponding to vertical stresses of 7.8 and 17 kPa.

In the Instrumented Retaining Wall (IRW) described in Chapter 5, the vertical stress in the backfill ranges from zero at the top of the backfill to 33.6 kPa at the bottom. The extended lines shown in Figure A9 allow the estimation of hydrocompression strains throughout the height of the backfill. It can be seen that hydrocompression strains may range from zero to 0.0015 for a relative density of 100 percent. Assuming an average vertical stress of 17 kPa, the average hydrocompression strain of the backfill during inundation is 0.0002. This value corresponds to a vertical settlement at the top of the backfill of less than 0.5 mm. This is consistent with the negligible settlements observed during inundation in the IRW test.

It must be noted that the procedure followed for estimation of hydrocompression strains in the IRW backfill is only approximate. There is not enough information to support the assumed linear relationship between hydrocompression strains and relative density. In addition, an accurate estimate of the backfill settlement can be obtained only by integration of the hydrocompression strains over the height of the backfill. However, given the relatively small height of the IRW backfill, it can be assumed that the error in the estimation of the hydrocompression settlement is small.

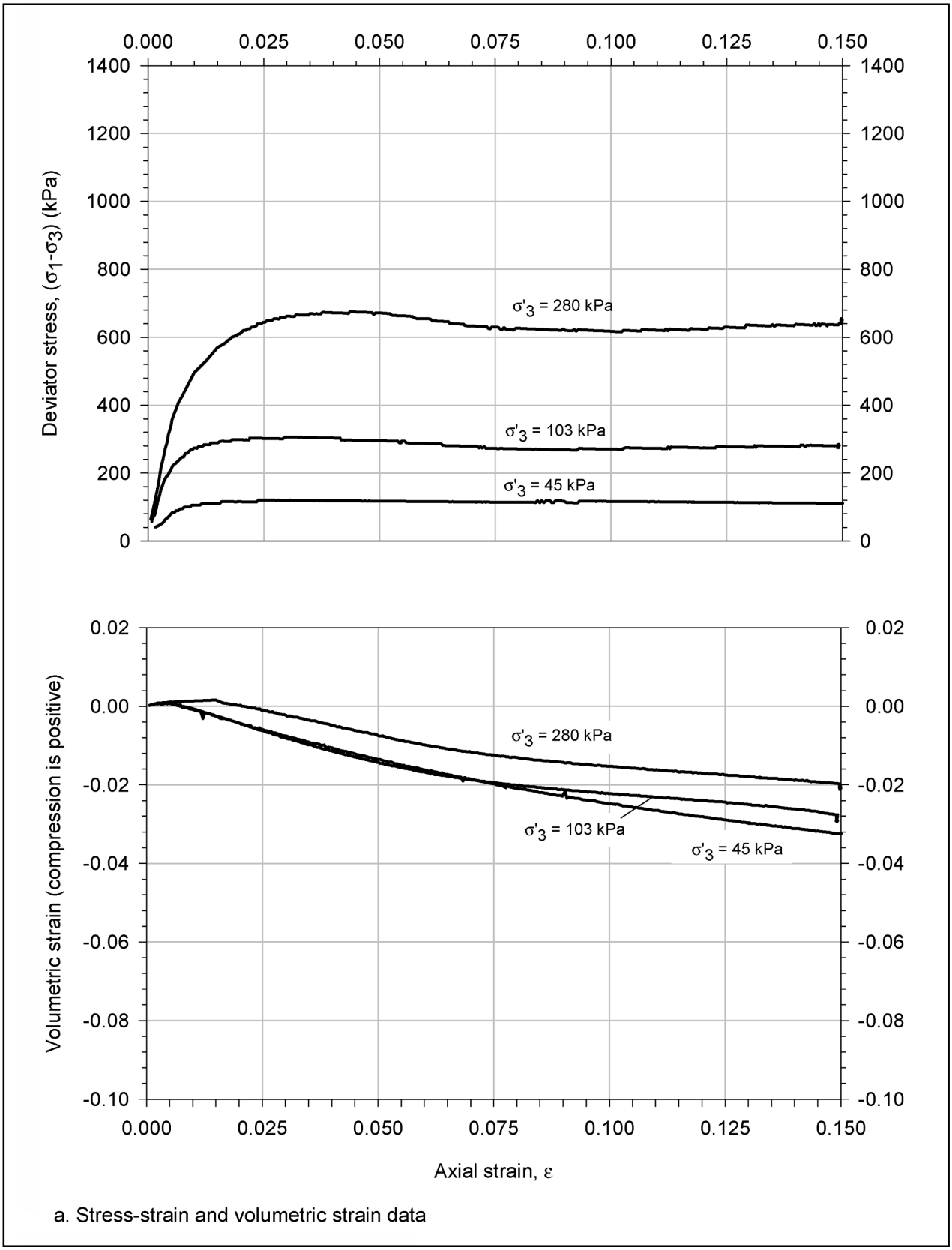

a. Stress-strain and volumetric strain data

Figure A1. Results of CD triaxial tests on medium-dense Density sand (Sheet 1 of 3)

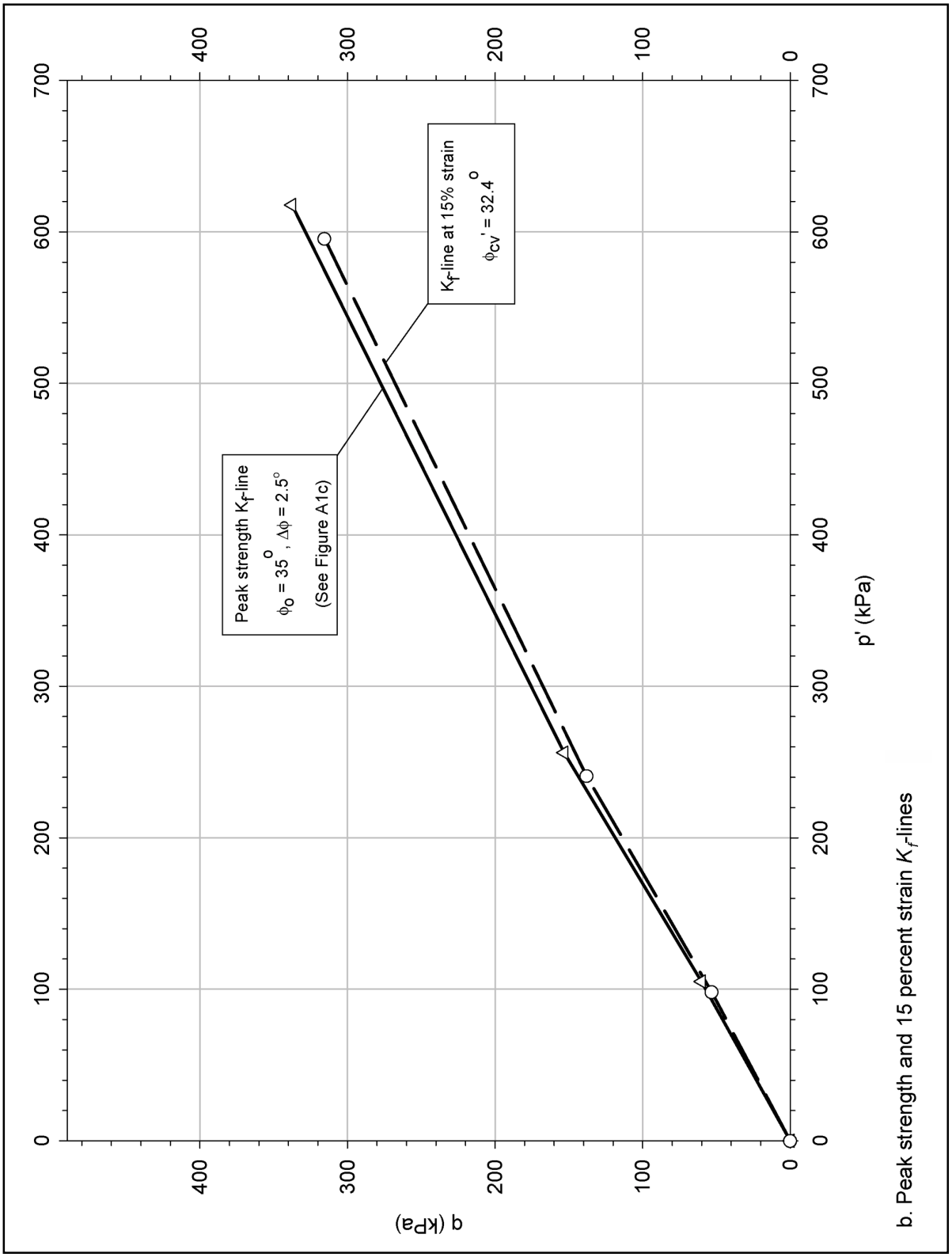

b. Peak strength and 15 percent strain K_f-lines

Figure A1. (Sheet 2 of 3)

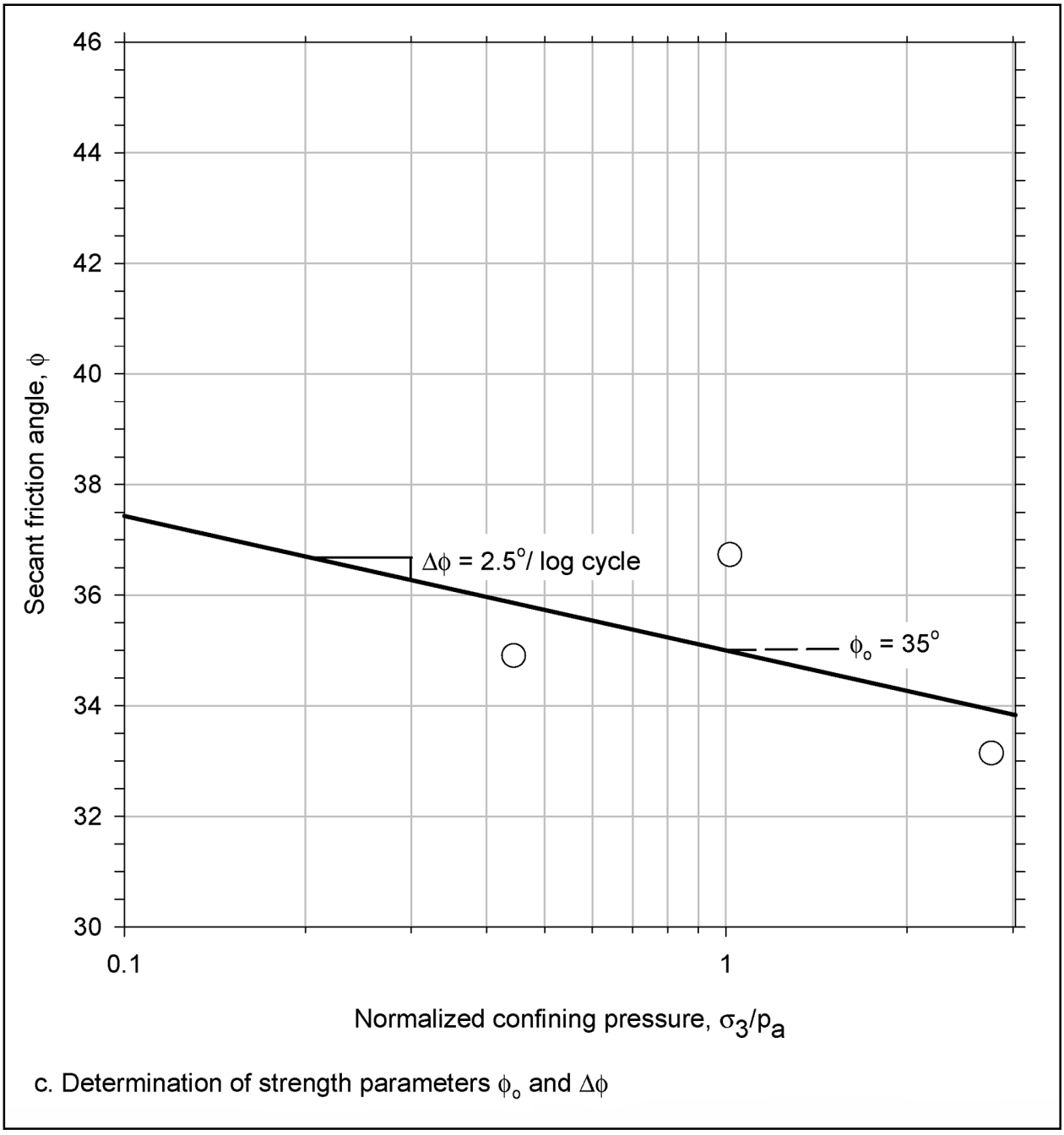

Figure A1. (Sheet 3 of 3)

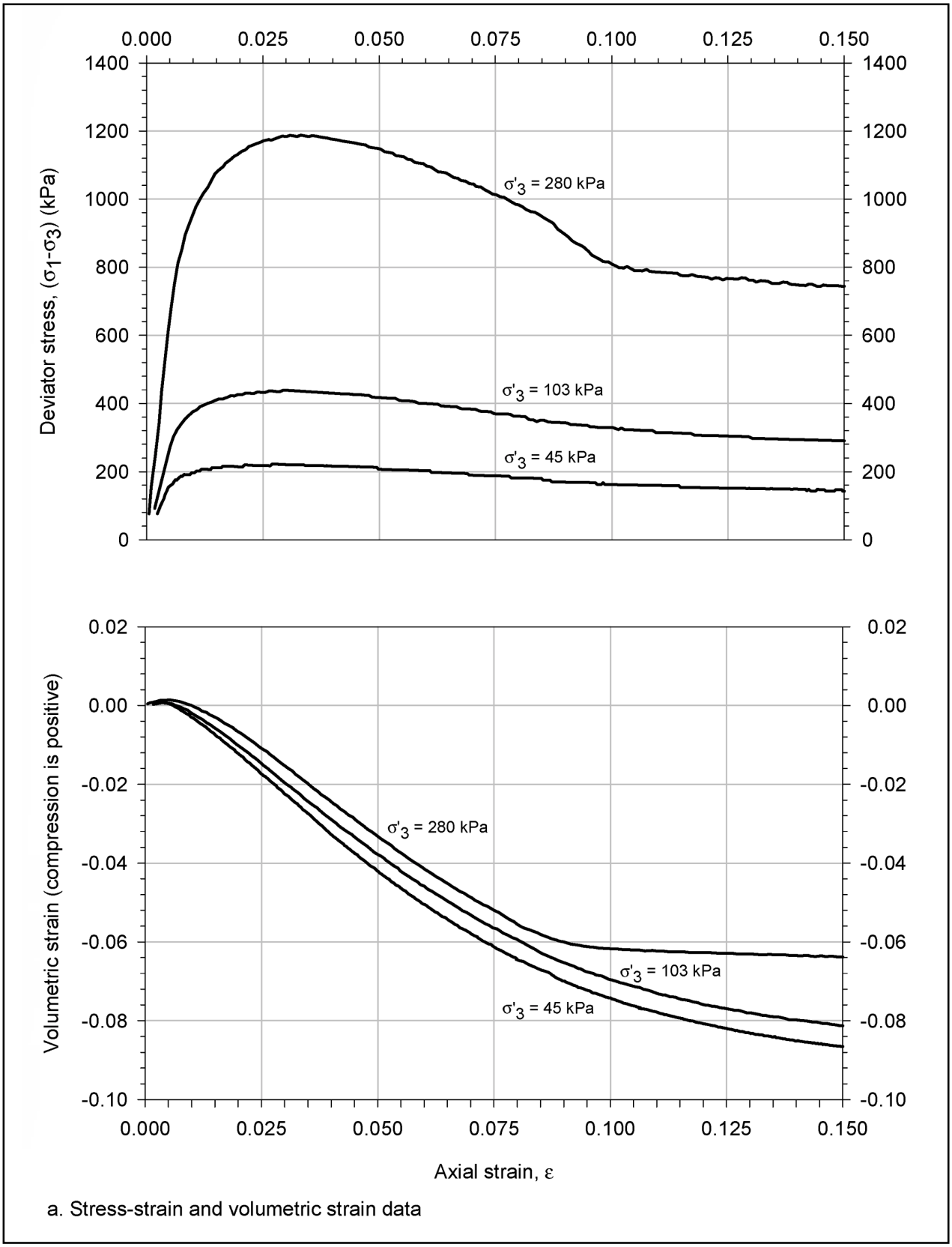

a. Stress-strain and volumetric strain data

Figure A2. Results of CD triaxial tests on dense Density sand (Sheet 1 of 3)

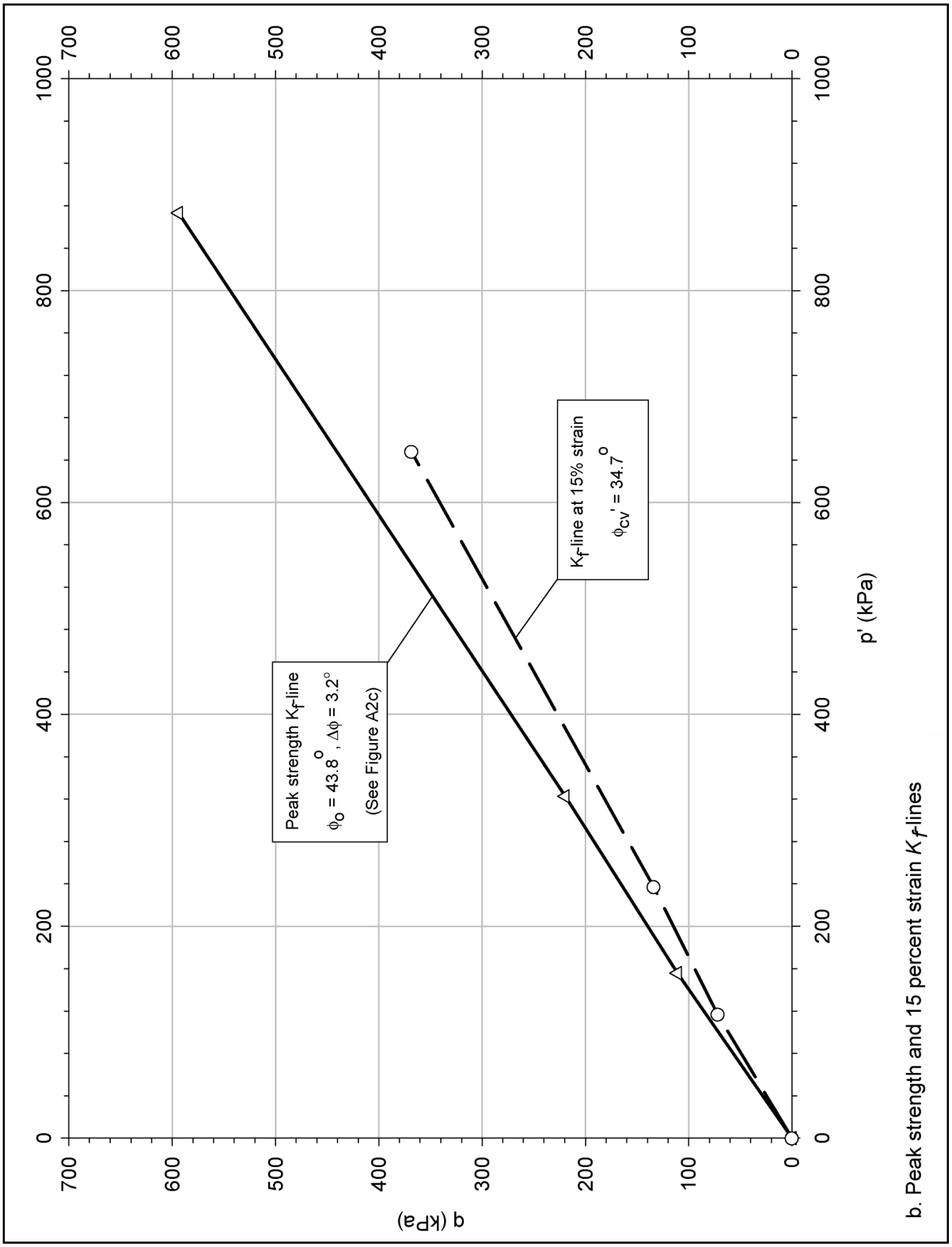

b. Peak strength and 15 percent strain K_f-lines

Figure A2. (Sheet 2 of 3)

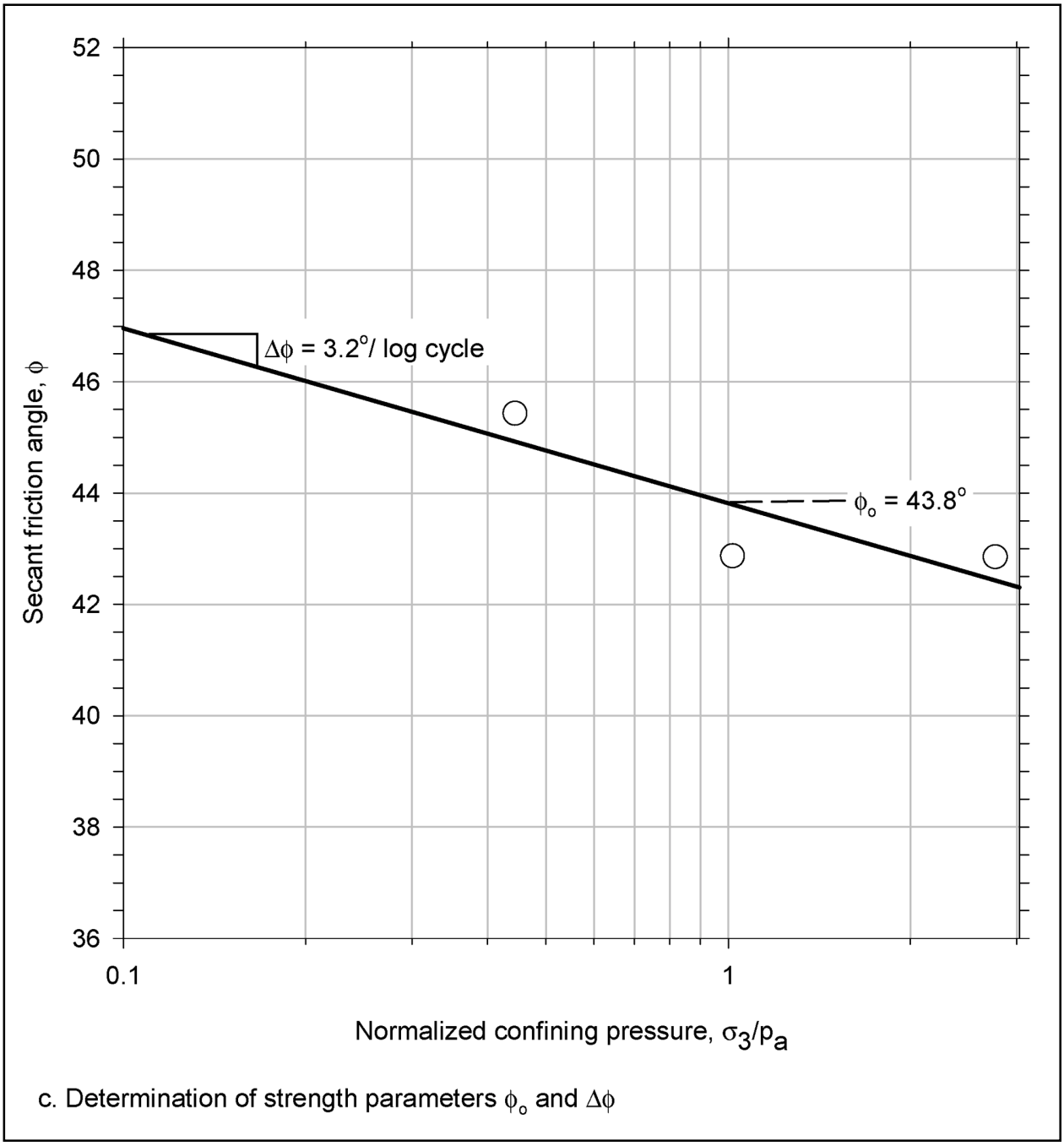

Figure A2. (Sheet 3 of 3)

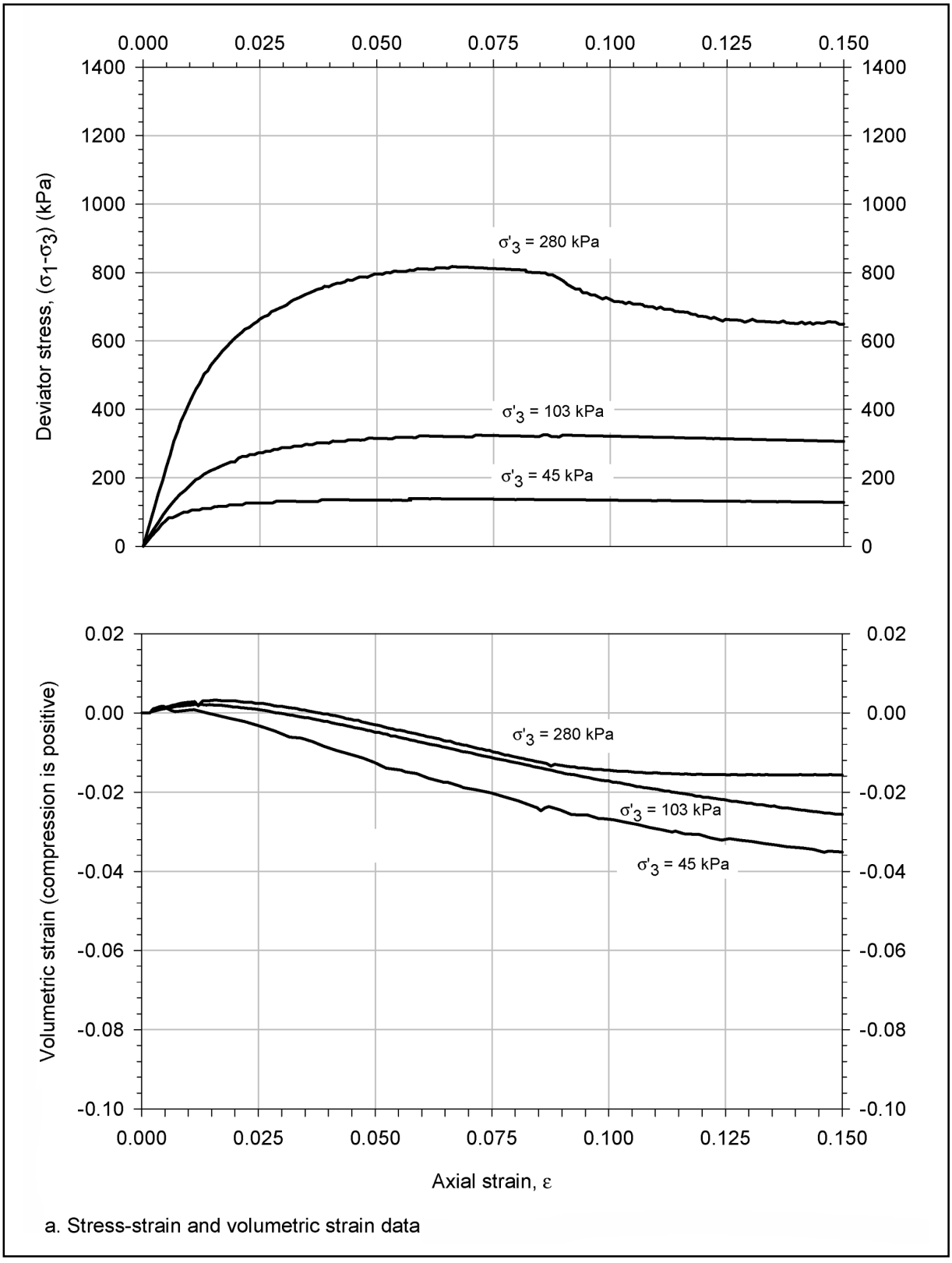

Figure A3. Results of CD triaxial tests on medium-dense Light Castle sand (Sheet 1 of 3)

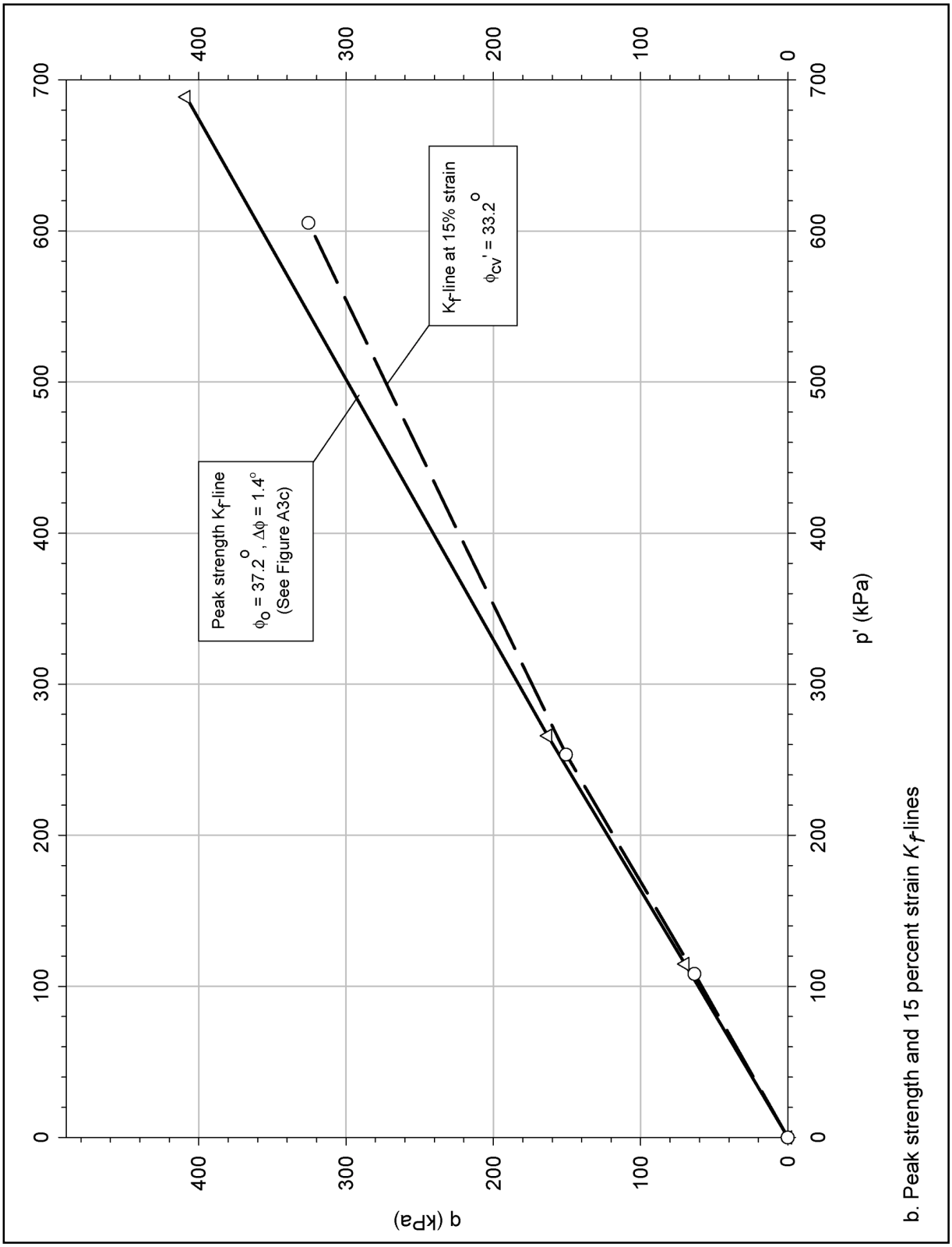

b. Peak strength and 15 percent strain K_f-lines

Figure A3. (Sheet 2 of 3)

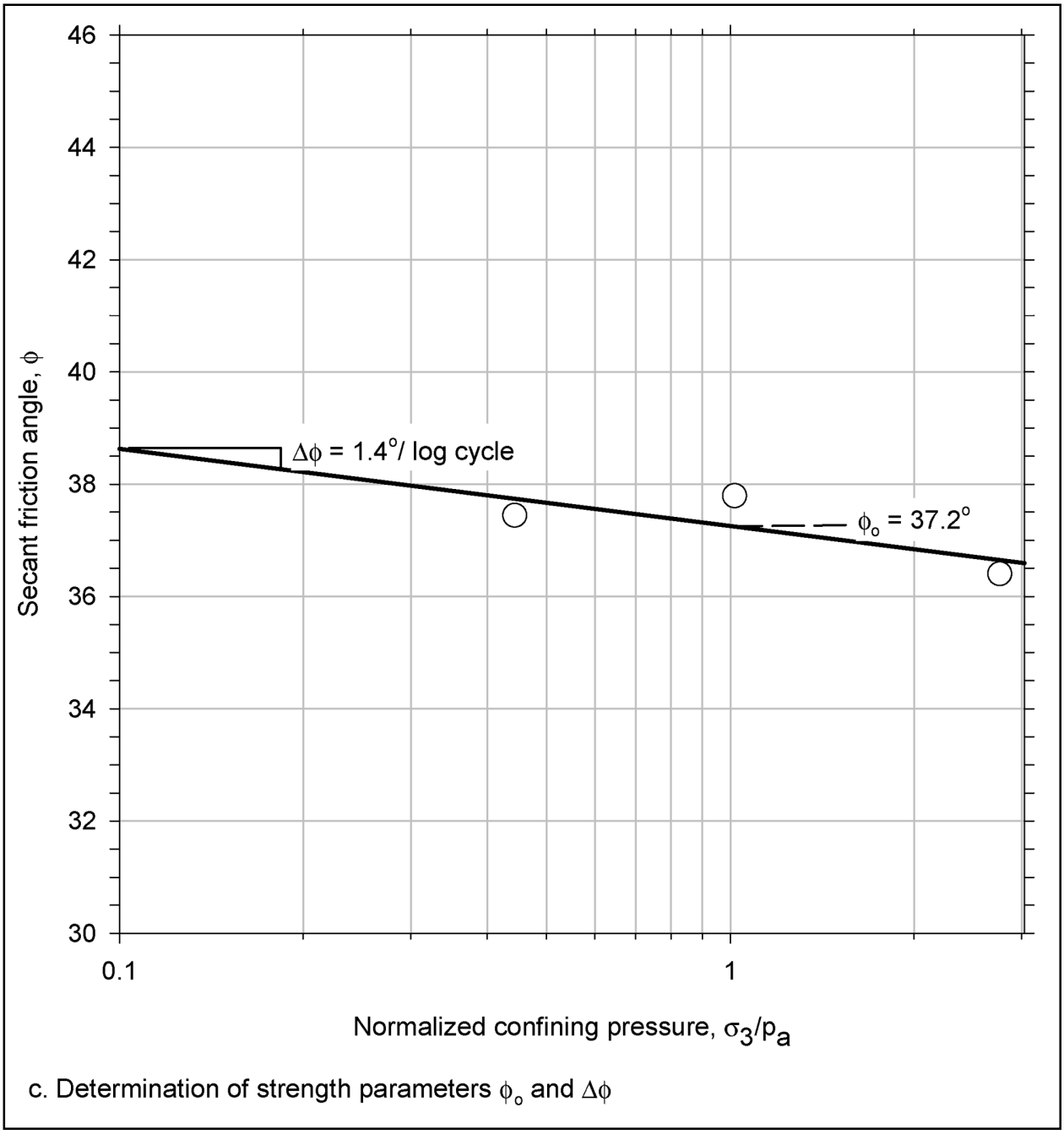

Figure A3. (Sheet 3 of 3)

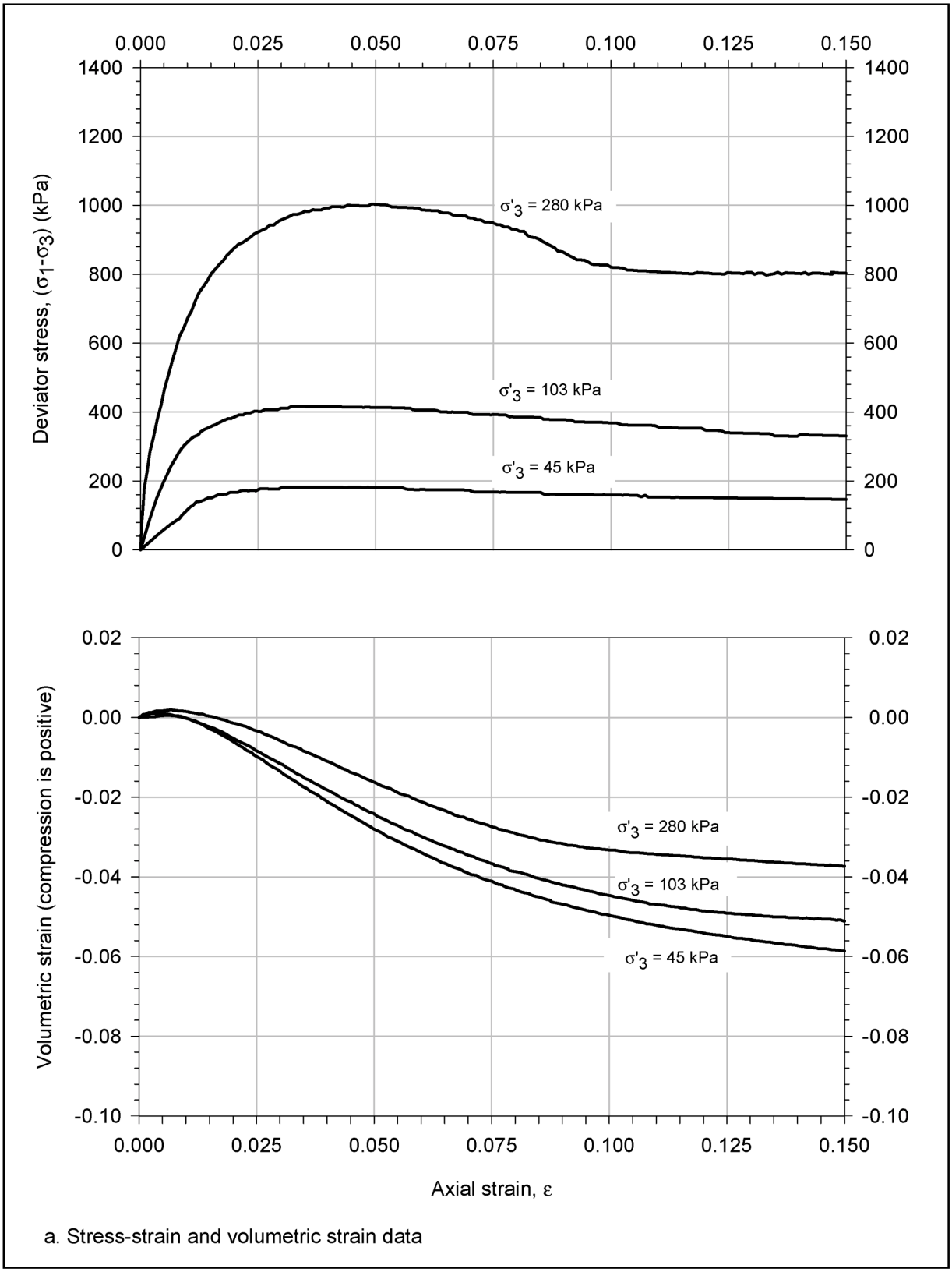

a. Stress-strain and volumetric strain data

Figure A4. Results of CD triaxial tests on dense Light Castle sand (Sheet 1 of 3)

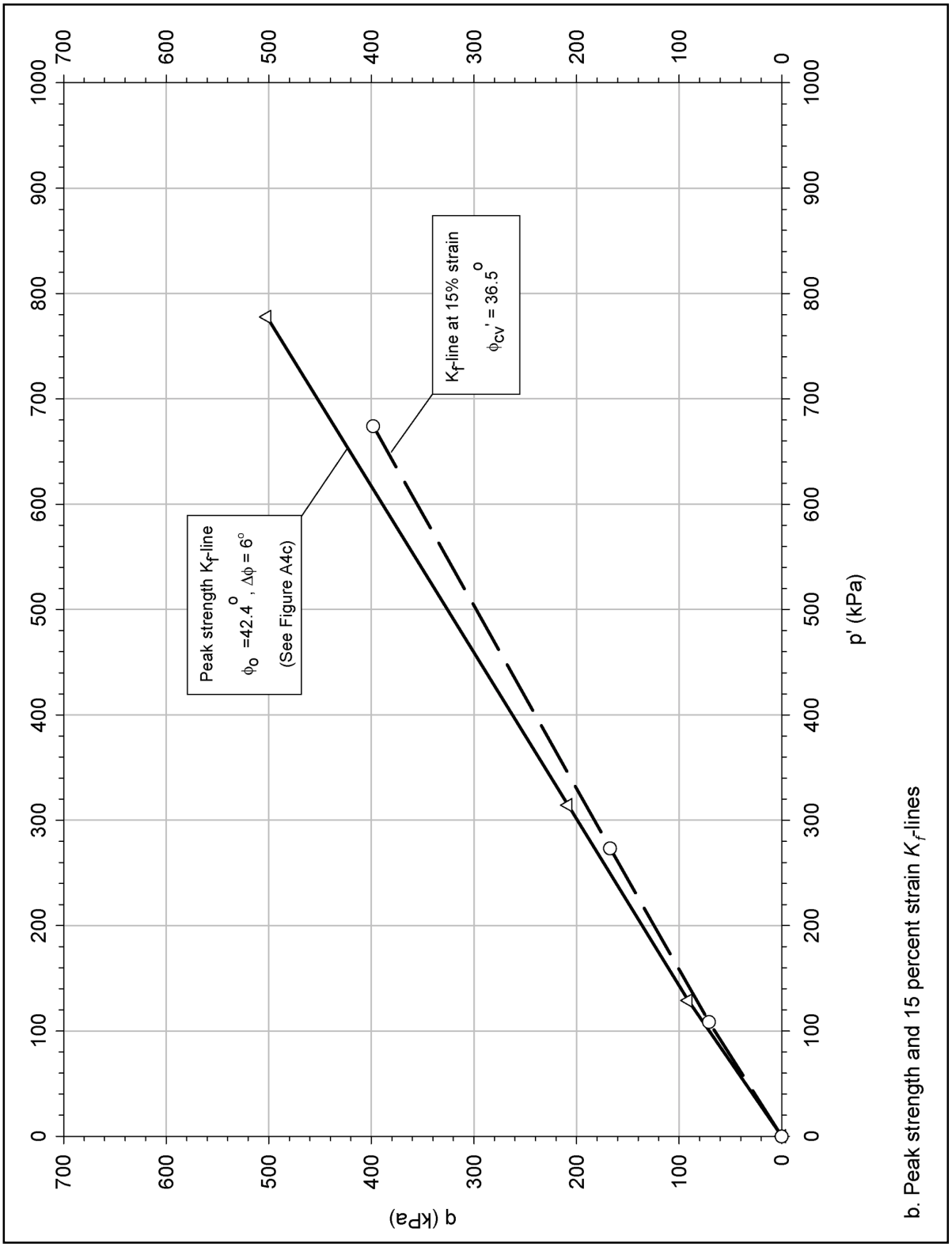

Figure A4. (Sheet 2 of 3)

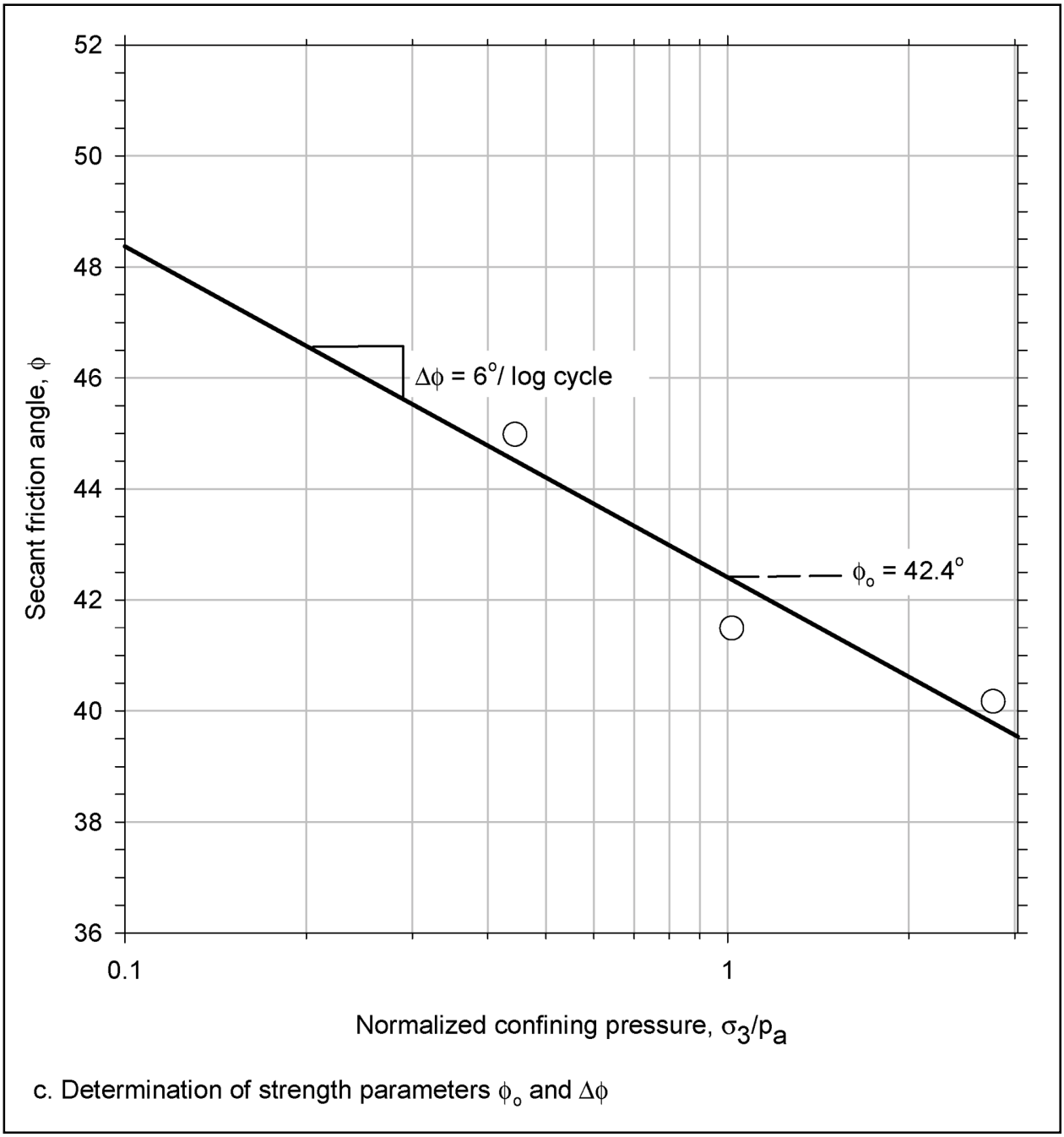

Figure A4. (Sheet 3 of 3)

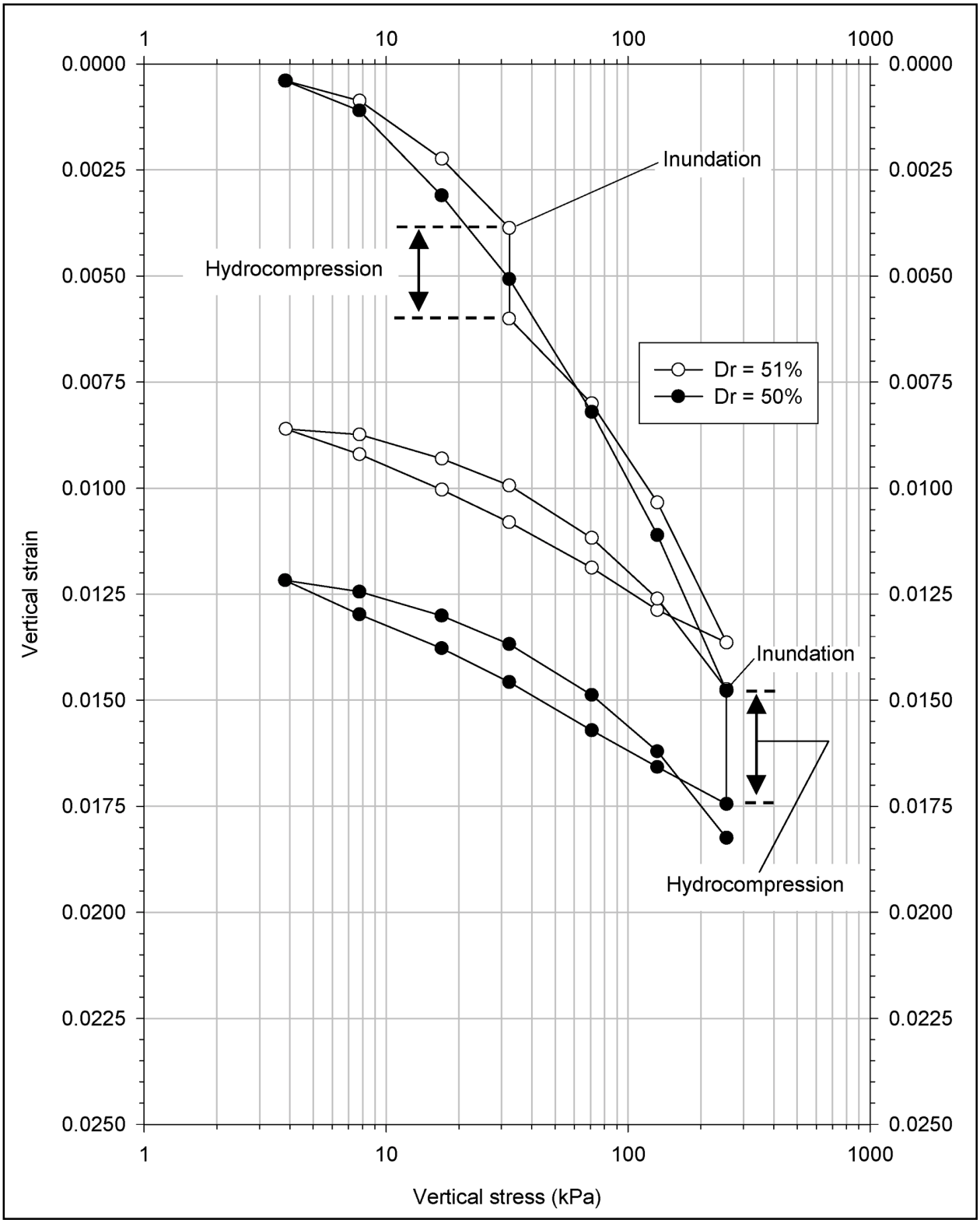

Figure A5. Results of consolidation tests on medium-dense Density sand

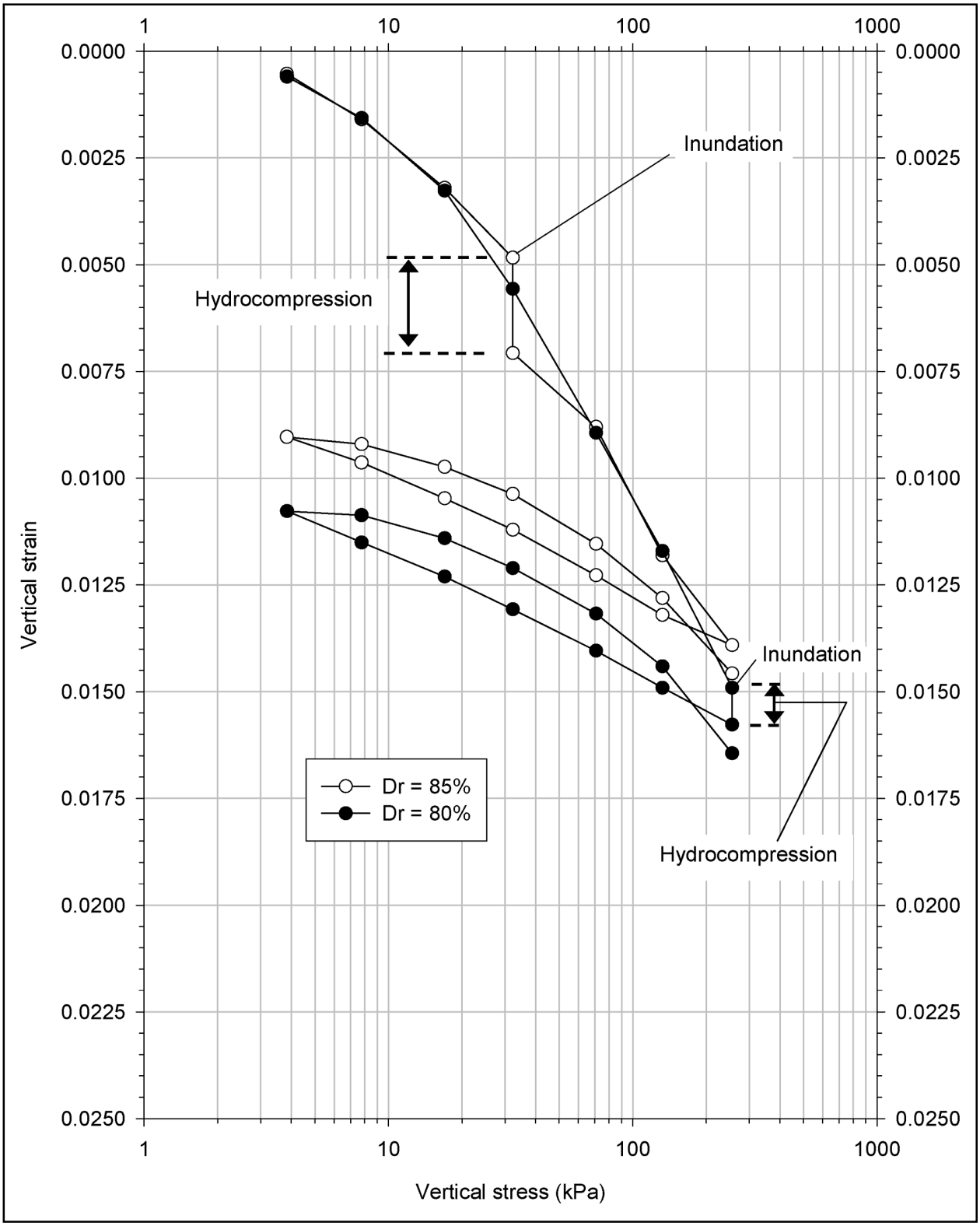

Figure A6. Results of consolidation tests on dense Density sand

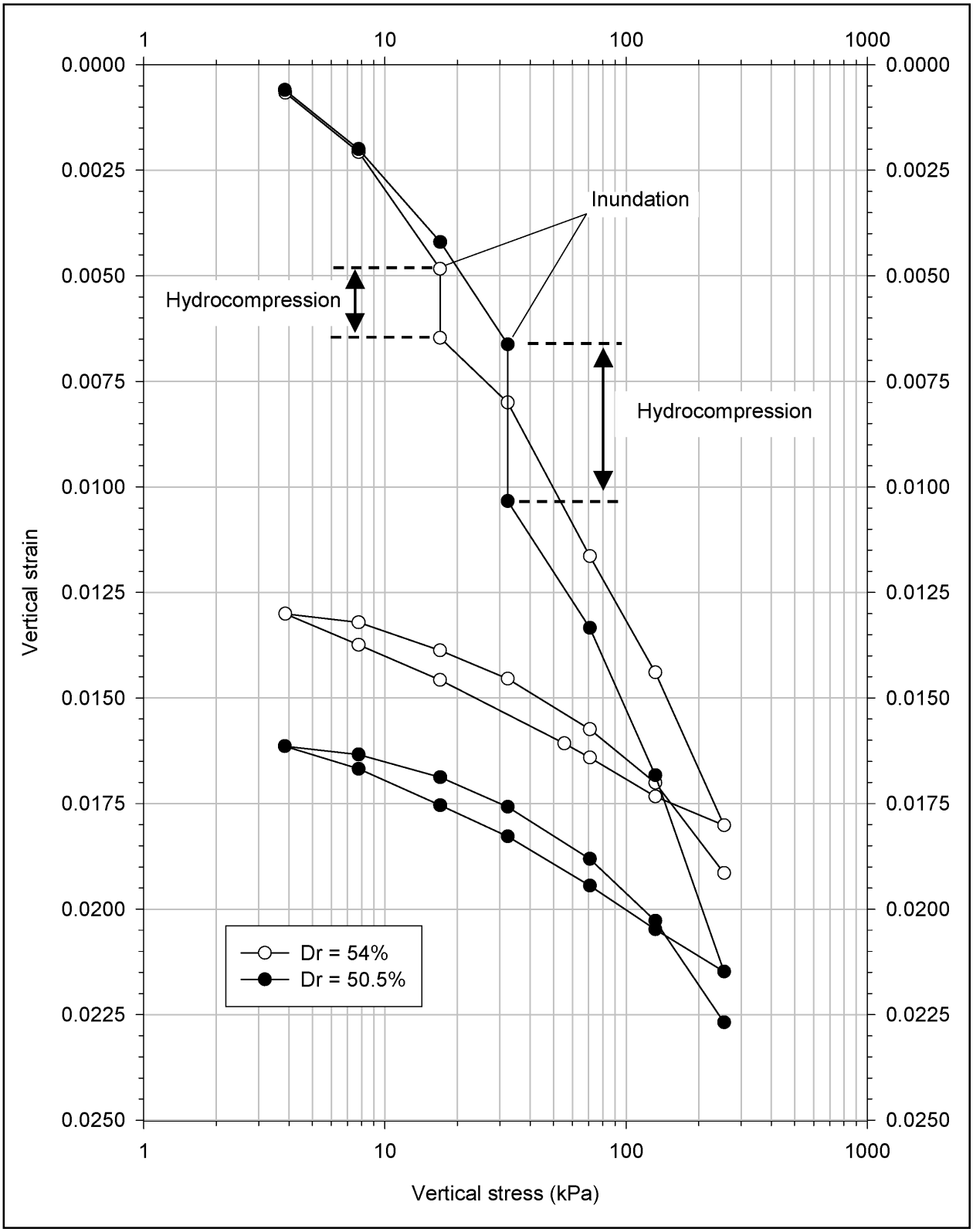

Figure A7. Results of consolidation tests on medium-dense Light Castle sand

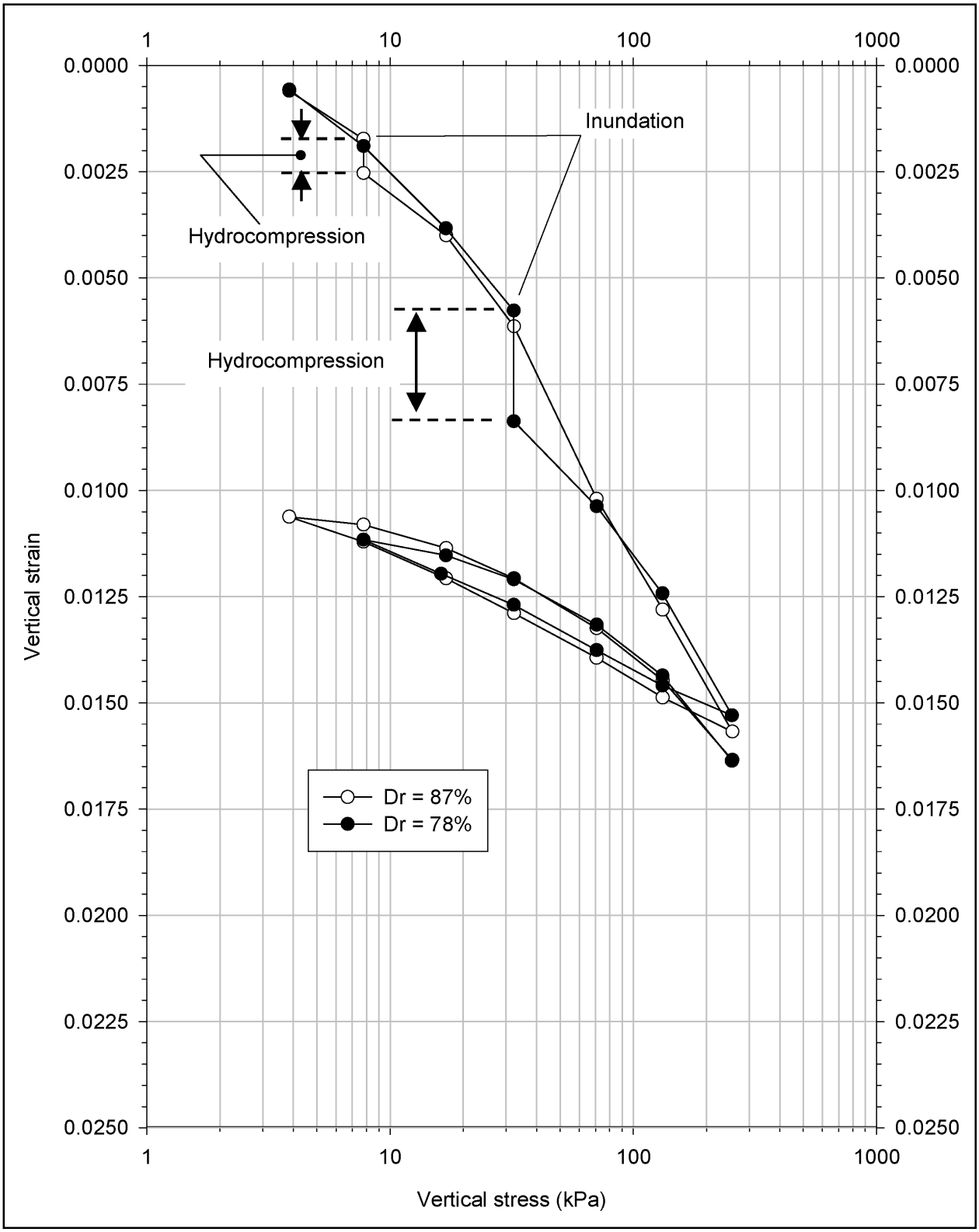

Figure A8. Results of consolidation tests on dense Light Castle sand

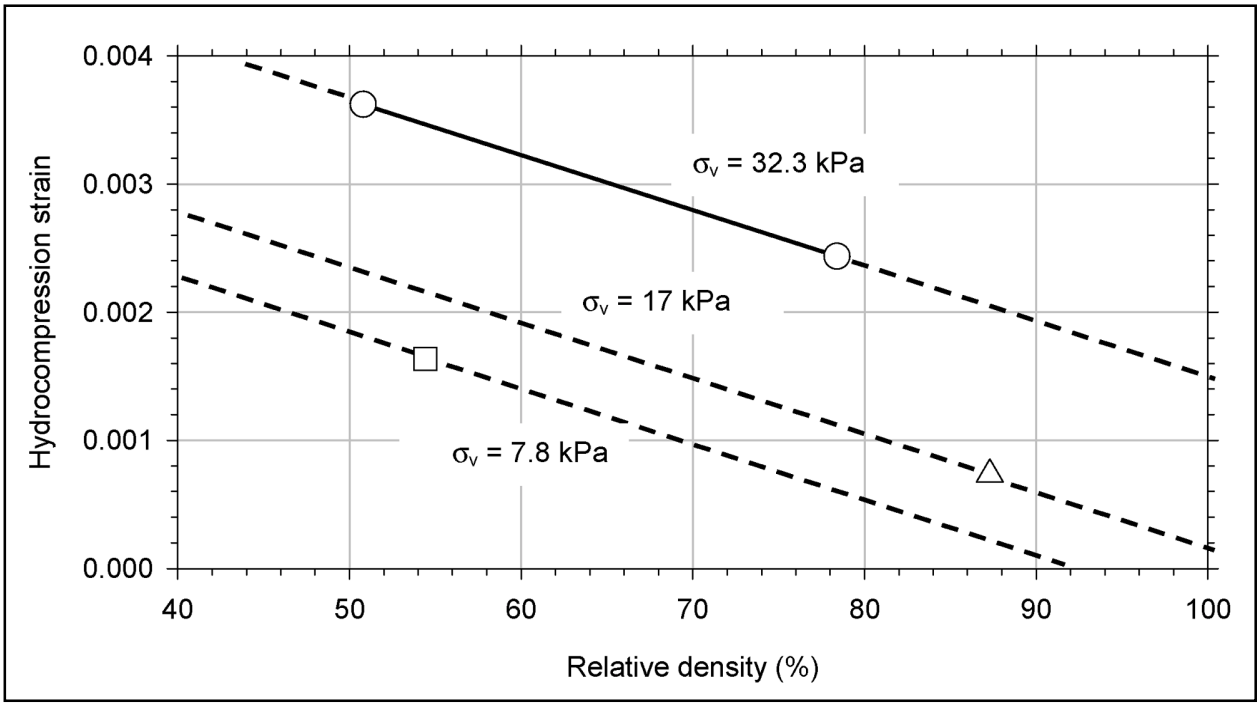

Figure A9. Relationship between hydrocompression strain and relative density for Light Castle sand

Appendix B
Determination of Hyperbolic Parameter Values of Soils

This appendix describes the procedure suggested by Duncan et al. (1980)[1] for the determination of hyperbolic parameter values for soils from results of triaxial tests. Hyperbolic parameter values of Density sand and Light Castle sand are determined based on the results of the triaxial tests presented in Appendix A. Figures B1 through B16 show the determination of the hyperbolic parameter values for all the sands tested. Figures B1 through B4, corresponding to the determination of parameter values for medium-dense Density sand, are used in the following description to illustrate the procedure followed. Example calculations of hyperbolic parameter values for dense Light Castle sand are presented in the last section of this appendix.

B.1 Transformed Plots

The procedure for the determination of hyperbolic parameter values of medium-dense Density sand is illustrated in Figures B1 through B4. The triaxial test stress-strain data shown in Figure A1 of Appendix A is represented in a transformed plot in Figure B1. In this transformed diagram, the value of axial strain[2] ε measured during the test is divided by the corresponding value of deviator stress σ_1-σ_3 and plotted against the axial strain. If the stress-strain relationship measured during the triaxial test is hyperbolic, the transformed diagram is a straight line. The intercept a of this straight line on the $\varepsilon/(\sigma_1 - \sigma_3)$ axis is the reciprocal of the initial Young's modulus E_i of the soil specimen. The slope b of the line is the reciprocal of the asymptotic deviator stress $(\sigma_1 - \sigma_3)_{ult}$.

The stress-strain relationship of a soil usually differs from a hyperbola. Duncan et al. (1980) indicated that the values of parameters a and b can be determined from a straight line passing through the points in the transformed plot that correspond to 70 and 95 percent of the strength.

---

[1] References cited in this Appendix are included in the References at the end of the main text.

[2] For convenience, symbols are listed and defined in the Notation (Appendix F).

The transformed plot in Figure B1 shows the 70 and 95 percent strength data points for each of the tests performed on medium-dense Density sand. Straight lines are drawn through each pair of these points. For comparison, the complete set of transformed data from the tests is also shown in the figure. It is seen that the lines drawn through the 70 and 95 percent data points match closely the transformed data sets. Such a comparison may be useful for minimizing errors in the determination of hyperbolic parameter values that can arise from inconsistencies in the data. Transformation of the entire set of test data is easily achieved in an electronic spreadsheet. The use of a spreadsheet also facilitates modification of the values of parameters *a* and *b* to obtain the best possible fit to the data.

B.2 Hyperbolic Parameter Values

B.2.1 Determination of *K* and *n*

The values of the parameters *a* and *b* determined from the transformed plots are presented in the table included in Figure B1. The values of initial Young's modulus and asymptotic deviator stress are determined using the following equations:

$$E_i = \frac{1}{a} \tag{B1}$$

$$\left(\sigma_1 - \sigma_3\right)_{ult} = \frac{1}{b} \tag{B2}$$

The values of E_i and $(\sigma_1 - \sigma_3)_{ult}$ for each of the tests performed on medium-dense Density sand are presented in the table in Figure B1. It can be seen that the values of initial Young's modulus E_i increase with increasing confining pressure σ'_3. Janbu (1963) suggested the following relationship between the initial Young's modulus and confining pressure:

$$E_i = K \cdot p_a \left(\frac{\sigma'_3}{p_a}\right)^n \tag{B3}$$

where

K = modulus number

p_a = atmospheric pressure

n = modulus exponent

Equation B3 can be used for both undrained and drained compression. For undrained compression, the value of σ_3 is used instead of σ'_3. This relationship implies that there is a linear relationship between the logarithm of the initial

Young's modulus and the logarithm of the confining pressure. Figure B2 is a logarithmic diagram showing the values of normalized Young's modulus E_i/p_a, determined from the table in Figure B1, represented against the values of normalized confining stress σ'_3/p_a. A best-fit straight line is drawn through the data points. The value of the modulus number K is equal to the value of normalized Young's modulus given by this best-fit line for a confining stress of one atmosphere. The slope of the line is the modulus exponent n.

B.2.2 Determination of R_f

The table in Figure B1 shows the values of deviator stress at failure $(\sigma_1 - \sigma_3)_f$, determined from the stress-strain plots of the tests, which are presented in Figure A1 of Appendix A. It can be seen in the table that the values of $(\sigma_1 - \sigma_3)_{ult}$ are larger than the values of $(\sigma_1 - \sigma_3)_f$ in all the tests. The value of the failure ratio, R_f, for each of the tests is determined from the following expression:

$$R_f = \frac{(\sigma_1 - \sigma_3)_f}{(\sigma_1 - \sigma_3)_{ult}} \tag{B4}$$

The table contains the values of R_f determined for each of the tests. For modeling, an average value of R_f is determined from the test results as shown at the bottom of the table. Typical values of R_f range between 0.5 and 0.9 for most soils (Duncan et al. 1980).

B.2.3 Determination of K_b and m

In the hyperbolic model, it is assumed that the value of bulk modulus B is independent of stress level and dependent of confining pressure (Duncan et al. 1980). The following expression is used for the calculation of the bulk modulus:

$$B = \frac{(\sigma_1 - \sigma_3)}{3 \cdot \varepsilon_v} \tag{B5}$$

where $(\sigma_1 - \sigma_3)$ is the deviator stress and ε_v is the volumetric strain.

In reality, application of deviator stress during a triaxial test induces volume changes in the soil specimen. Consequently, the value of bulk modulus determined from triaxial test data depends on which points on the stress-strain and volumetric strain-axial strain curves are selected for the calculation. The following criteria are used for the selection of points in the volumetric strain-axial strain data (Duncan et al. 1980):

a. If the volumetric strain-axial strain data plot does not reach a horizontal tangent (zero volume change) before mobilization of 70 percent of the strength, the points on the stress-strain and volumetric strain-axial strain

curves corresponding to a stress level of 70 percent are used for bulk modulus determination.

b. If the volumetric strain-axial strain curve reaches a horizontal tangent before mobilization of 70 percent of the strength, the point where the volumetric strain-axial strain curve becomes horizontal and the corresponding point on the stress-strain curve are used for bulk modulus determination.

For Density sand and Light Castle sand, it was found that dilation was significant and that the volumetric strain-axial strain curve presented a horizontal tangent before mobilization of 70 percent of the strength. Therefore, the second criterion was used for the determination of the bulk modulus *B* for all the specimens tested, as shown in Tables B1 through B4.

Table B1
Determination of Bulk Modulus for Medium-Dense Density Sand

Confining Stress σ_3' kPa	Deviator Stress (σ_1 - σ_3) kPa	Volumetric Strain ε_v %	Bulk Modulus B [1] kPa
45	78.6	0.073	36146
103	133.7	0.082	54107
280	388.5	0.158	82023

[1] $B = \frac{(\sigma_1 - \sigma_3)}{\varepsilon_v}$

Table B2
Determination of Bulk Modulus for Dense Density Sand

Confining Stress σ_3' kPa	Deviator Stress (σ_1 - σ_3) kPa	Volumetric Strain ε_v %	Bulk Modulus B [1] kPa
45	120.8	0.071	56471
103	184.0	0.067	91446
280	684.2	0.140	163358

[1] $B = \frac{(\sigma_1 - \sigma_3)}{\varepsilon_v}$

Table B3
Determination of Bulk Modulus for Medium-Dense Light Castle Sand

Confining Stress σ_3' kPa	Deviator Stress (σ_1 - σ_3) kPa	Volumetric Strain ε_v %	Bulk Modulus B [1] kPa
45	72.8	0.170	14277
103	210.7	0.210	33451
280	555.9	0.320	57901

[1] $B = \frac{(\sigma_1 - \sigma_3)}{\varepsilon_v}$

Table B4
Determination of Bulk Modulus for Dense Light Castle Sand

Confining Stress σ_3' kPa	Deviator Stress $(\sigma_1 - \sigma_3)$ kPa	Volumetric Strain ε_v %	Bulk Modulus B [1] kPa
45	73.8	0.047	52340
103	199.2	0.109	60917
280	548.3	0.190	96192

[1] $B = \dfrac{(\sigma_1 - \sigma_3)}{\varepsilon_v}$

It can be seen in Tables B1 through B4 that the values of bulk modulus increase with confining pressure. The relationship between bulk modulus and confining pressure is approximated by the following relationship:

$$B = K_b \cdot p_a \left(\frac{\sigma_3'}{p_a} \right)^m \tag{B6}$$

where K_b is the bulk modulus number and m is the bulk modulus exponent.

The values of K_b and m are determined in a logarithmic diagram of normalized bulk modulus B/p_a versus normalized confining stress σ_3'/p_a. The values presented in Table B1 for the medium-dense Density sand were used to create the B/p_a versus σ_3'/p_a diagram of Figure B3. A best-fit straight line was drawn through the data points. The value of bulk modulus number K_b is equal to the value of normalized bulk modulus given by this best-fit line for a confining stress of 1 atm. The slope of the line is the bulk modulus exponent m.

B.3 Comparison of Model to Test Data

Once the hyperbolic parameter values are determined, it is necessary to compare the model response to the test data. The stress-strain response from the model is calculated using the following expression:

$$(\sigma_1 - \sigma_3) = \frac{\varepsilon}{\dfrac{1}{K \cdot p_a \left(\dfrac{\sigma_3'}{p_a} \right)^n} + R_f \cdot \dfrac{\varepsilon}{(\sigma_1 - \sigma_3)_f}} \tag{B7}$$

The deviator stress at failure $(\sigma_1 - \sigma_3)_f$ is calculated from the following equation:

$$(\sigma_1 - \sigma_3)_f = 2\frac{\sigma_3 \cdot \sin\phi'}{1 - \sin\phi'} \quad \text{(B8)}$$

where ϕ' is the internal friction angle.

The volumetric strain-axial strain response is calculated using the following equation:

$$\varepsilon_v = \frac{(\sigma_1 - \sigma_3)}{3 \cdot K_b \cdot p_a \cdot \left(\frac{\sigma_3'}{p_a}\right)^m} \quad \text{(B9)}$$

The stress-strain and volumetric strain-axial strain responses of the sands tested were calculated using Equations B7, B8, and B9, and the hyperbolic parameters determined following the procedure described previously. Figures B4, B8, B12, and B16 compare the test data and the calculated hyperbolic response. In the figures, the stress-strain hyperbolas are interrupted at the value of deviator stress at failure $(\sigma_1 - \sigma_3)_f$. A horizontal stress-strain relationship, i.e., zero Young's modulus, is used to model the response of the soil at failure.

It can be seen that the hyperbolic model provides an accurate approximation to the stress-strain response measured during the tests. The volumetric strain-axial strain response calculated using the hyperbolic model also provides a good approximation to the test data for the initial stages of shear, in which compression takes place. It does not model subsequent dilation of the soils.

B.4 Example Calculations of Hyperbolic Parameter Values

This section presents an example of the determination of hyperbolic parameter values. The data from the CD triaxial tests performed on dense specimens of Light Castle sand are used for this example. The example follows the procedure described by Duncan et al. (1980).

The first step in the determination of hyperbolic parameter values is checking for inconsistencies in the data from the CD triaxial tests. Figure B17 shows the results of the tests performed on dense Light Castle sand. The data shown in the figure are identical to those shown in Figures A4 and B16. Close examination of Figure B17 reveals that the data present some minor inconsistencies. To minimize these inconsistencies, a smooth response of the soil to triaxial testing was assumed for the determination of the hyperbolic parameter values. This assumed response corresponds to the solid lines in Figure B17.

The next step is the determination of the deviator stress at failure $(\sigma_1 - \sigma_3)_f$ for each confining stress. The values of $(\sigma_1 - \sigma_3)_f$ can be determined from the deviator stress-axial strain plots of the tests. Column (2) in the table presented in

Figure B18 contains the values of deviator stress at failure determined from Figure B17. The values of deviator stress corresponding to 70 and 95 percent of $(\sigma_1-\sigma_3)$ are calculated as shown in columns (3) and (6), respectively.

The values of axial strain corresponding to 70 and 95 percent of the strength are determined from the deviator stress-axial strain plots. Columns (4) and (7) in Figure B18 contain the strain values determined as shown in Figure B17.

The values in columns (2), (3), (4), (6), and (7) are the basis for the determination of the values of initial Young's modulus E_i and failure ratio R_f. The sequence of calculations leading to the determination of the values of E_i and R_f is shown in Figure B18, and corresponds to the procedure presented in the previous sections.

It must be noted that in the method presented in Figure B18 the data are not plotted in transformed coordinates. Only the two data points corresponding to 70 and 95 percent of the strength are transformed as shown in columns (5) and (8). Although not strictly necessary, it is recommended always to plot the complete data set in transformed coordinates. The transformed plots are useful to check the data for inconsistencies and for verifying the values of Young's modulus and failure ratio determined from the procedure presented in Figure B18. Transforming the data following the procedure described previously in this appendix can be accomplished easily with electronic spreadsheets.

The value of failure ratio R_f to be used for modeling is the average of the values determined in Figure B18. The values of K and n are determined by plotting the normalized values of initial Young's modulus against the normalized confining stress in logarithmic scale as shown in Figure B19.

Figures B17 and B18 also illustrate the determination of the values of bulk modulus B from the triaxial test data. If the volumetric strain-axial strain plot does not reach a horizontal tangent before mobilization of 70 percent of the strain, the volumetric strain corresponding to 70 percent of the strength is used for the determination of B. If the volumetric strain-axial strain plot reaches a horizontal tangent before mobilization of 70 percent of the strength, the maximum value of volumetric strain is used for the determination of B.

The volumetric strain-axial strain plots of dense Light Castle sand shown in Figure B17 reach a horizontal tangent before mobilization of 70 percent of the strength. The maximum values of volumetric strain are determined as shown in the figure. They are copied to column (10) of the table in Figure B18. The deviator stress corresponding to the point of maximum volumetric strain is also determined from the figure and copied to column (9) in Figure B18. These two values are used to determine the value of B for each of the confining stresses applied. The values of K_b and m are determined from a logarithmic plot of normalized bulk modulus versus normalized confining stress, as shown in Figure B20.

It must be noted that none of the values presented in Figure B18 was determined graphically. They were obtained directly or by interpolation of data in an

electronic spreadsheet. Although graphical determination of values of stress and strain from a figure such as B17 may provide less significant decimal places than their numerical determination, the overall precision of the values of the hyperbolic parameters is similar using both procedures. The use of an electronic spreadsheet is recommended, not for increased precision, but for ease in the calculations and verification of the results.

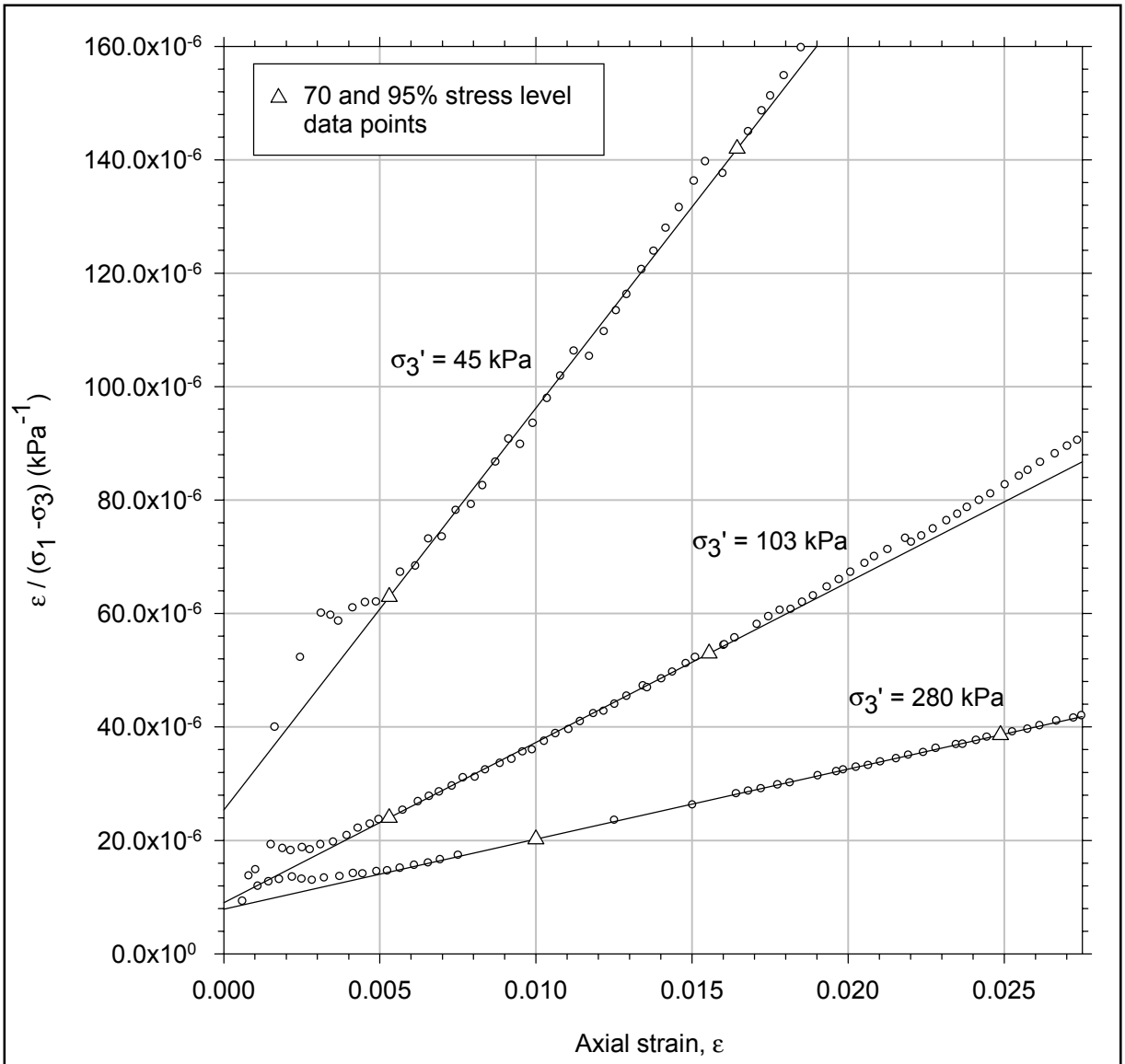

σ_3' (kPa)	a $(kPa)^{-1}$	E_i (kPa)	b $(kPa)^{-1}$	$(\sigma_1 - \sigma_3)_{ult}$ (kPa)	$(\sigma_1 - \sigma_3)_f$ (kPa)	R_f
45	2.54×10^{-5}	39407	7.09×10^{-3}	141.1	120.4	0.853
103	9.02×10^{-6}	110847	2.83×10^{-3}	353.7	306.5	0.866
280	7.84×10^{-6}	127560	1.24×10^{-3}	808.9	675.3	0.835

Average $R_f = 0.852$

Figure B1. Transformed stress-strain plots from triaxial test data on medium-dense Density sand and determination of hyperbolic parameter values

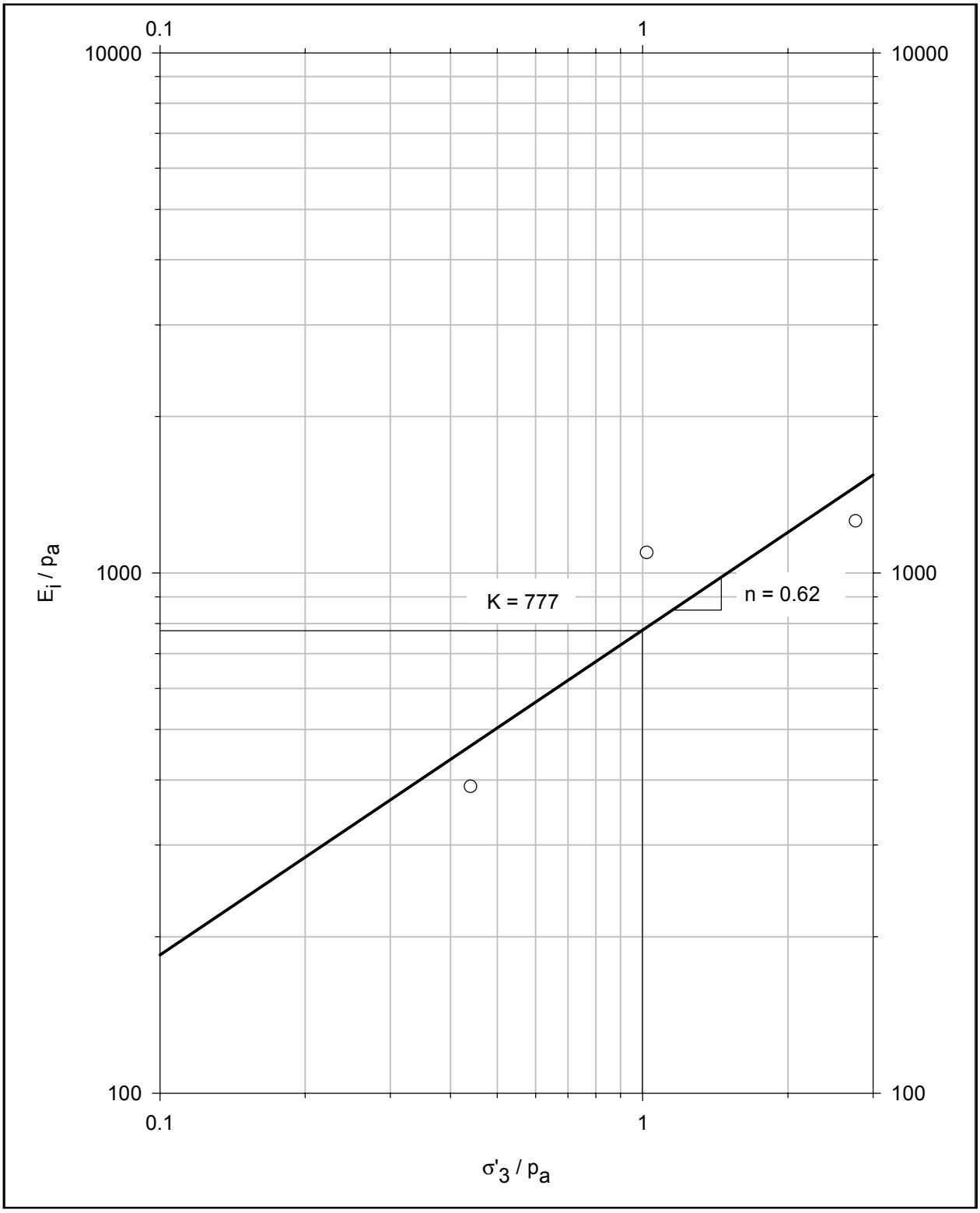

Figure B2. Determination of hyperbolic parameters *K* and *n* for medium-dense Density sand

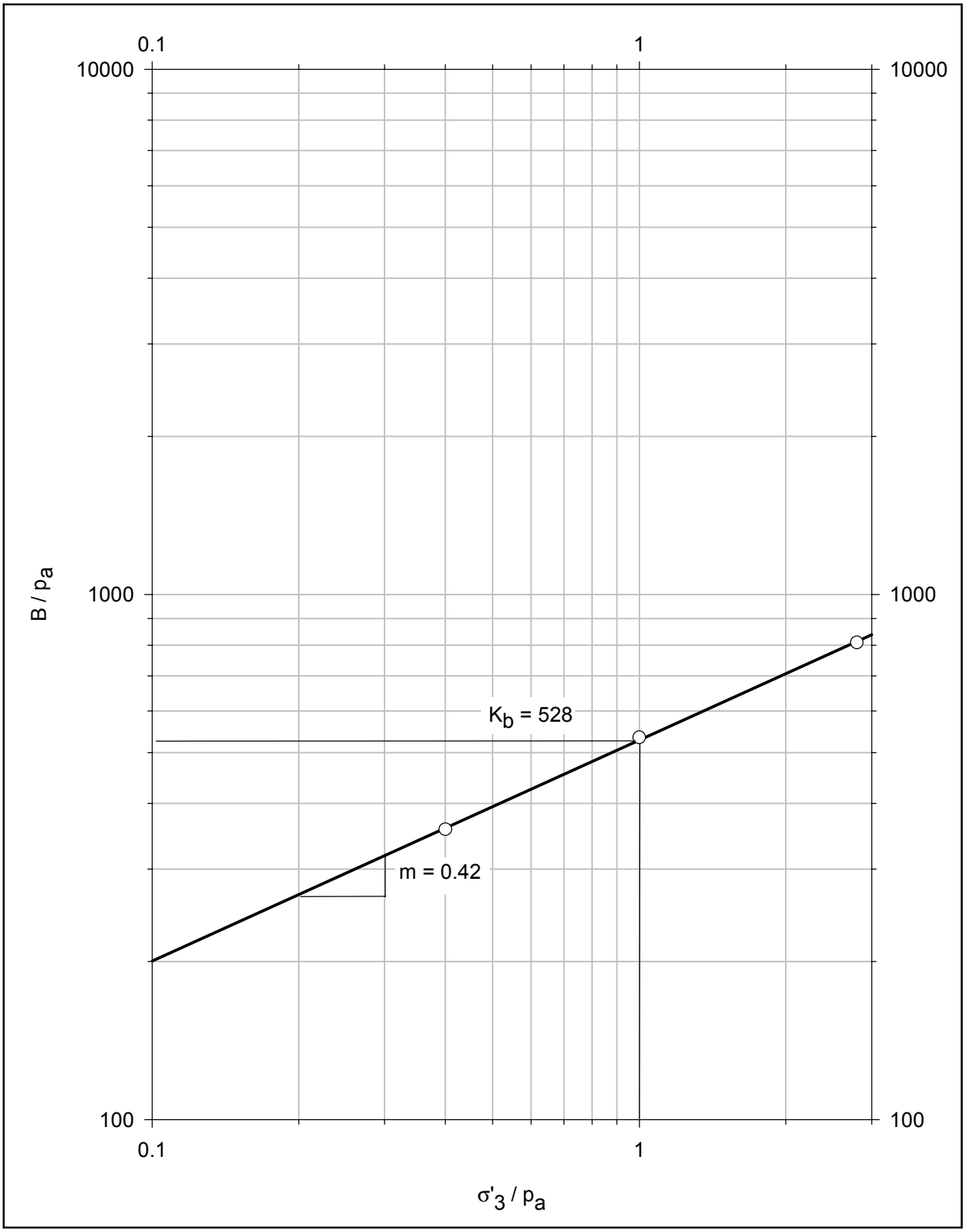

Figure B3. Determination of hyperbolic parameters K_b and m for medium-dense Density sand

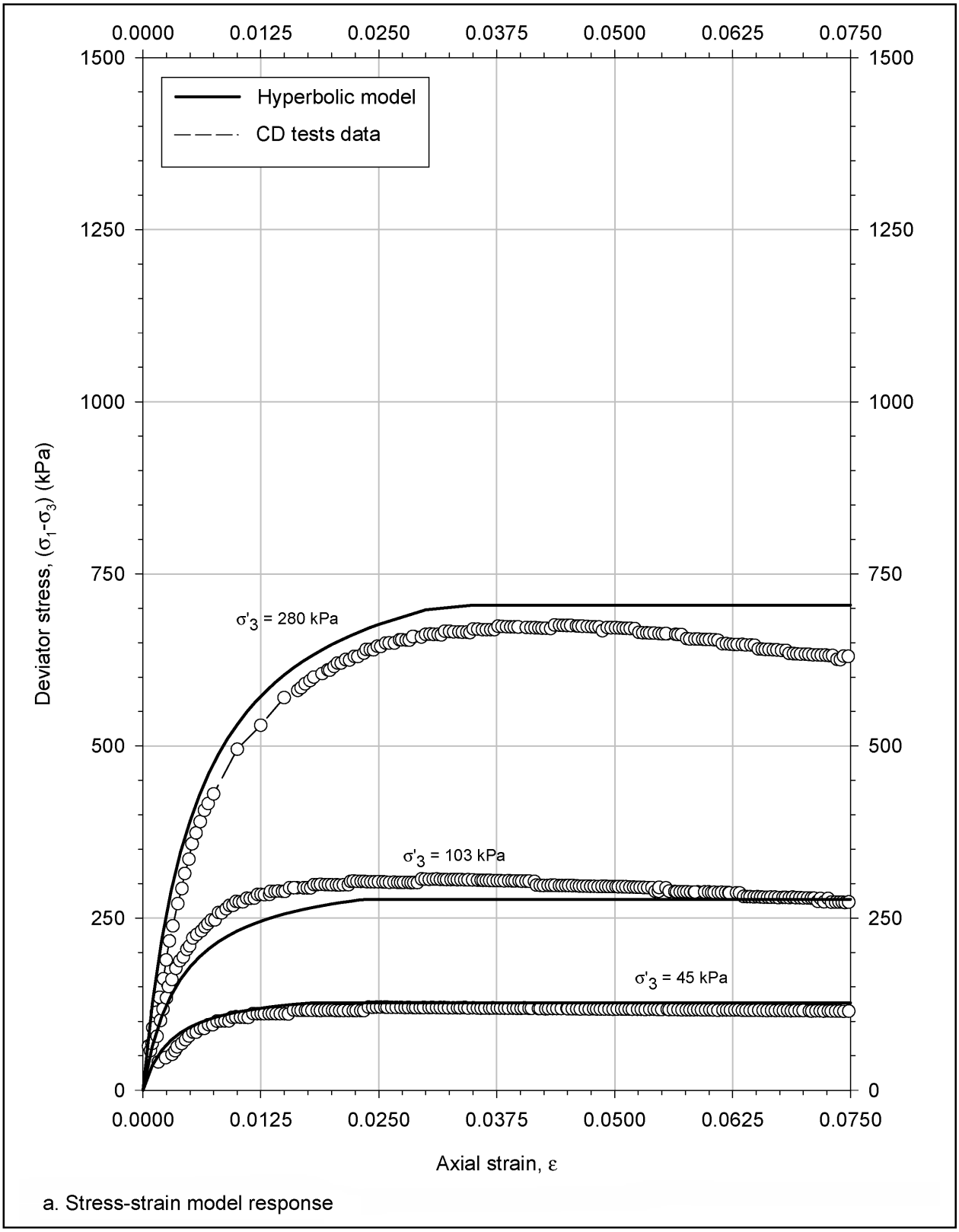

a. Stress-strain model response

Figure B4. Hyperbolic model for medium-dense Density sand and comparison to CD triaxial test data (Continued)

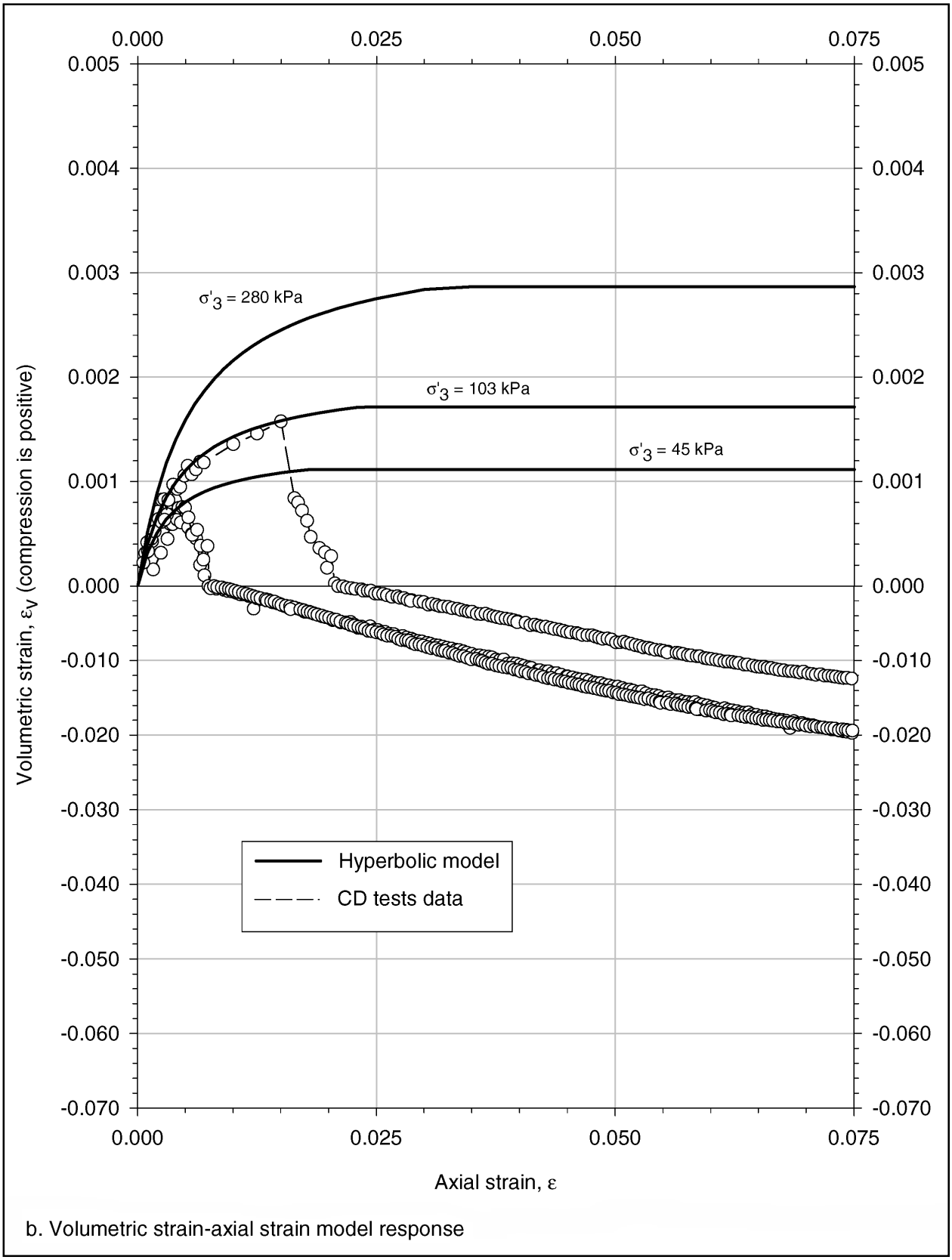

b. Volumetric strain-axial strain model response

Figure B4. (Concluded)

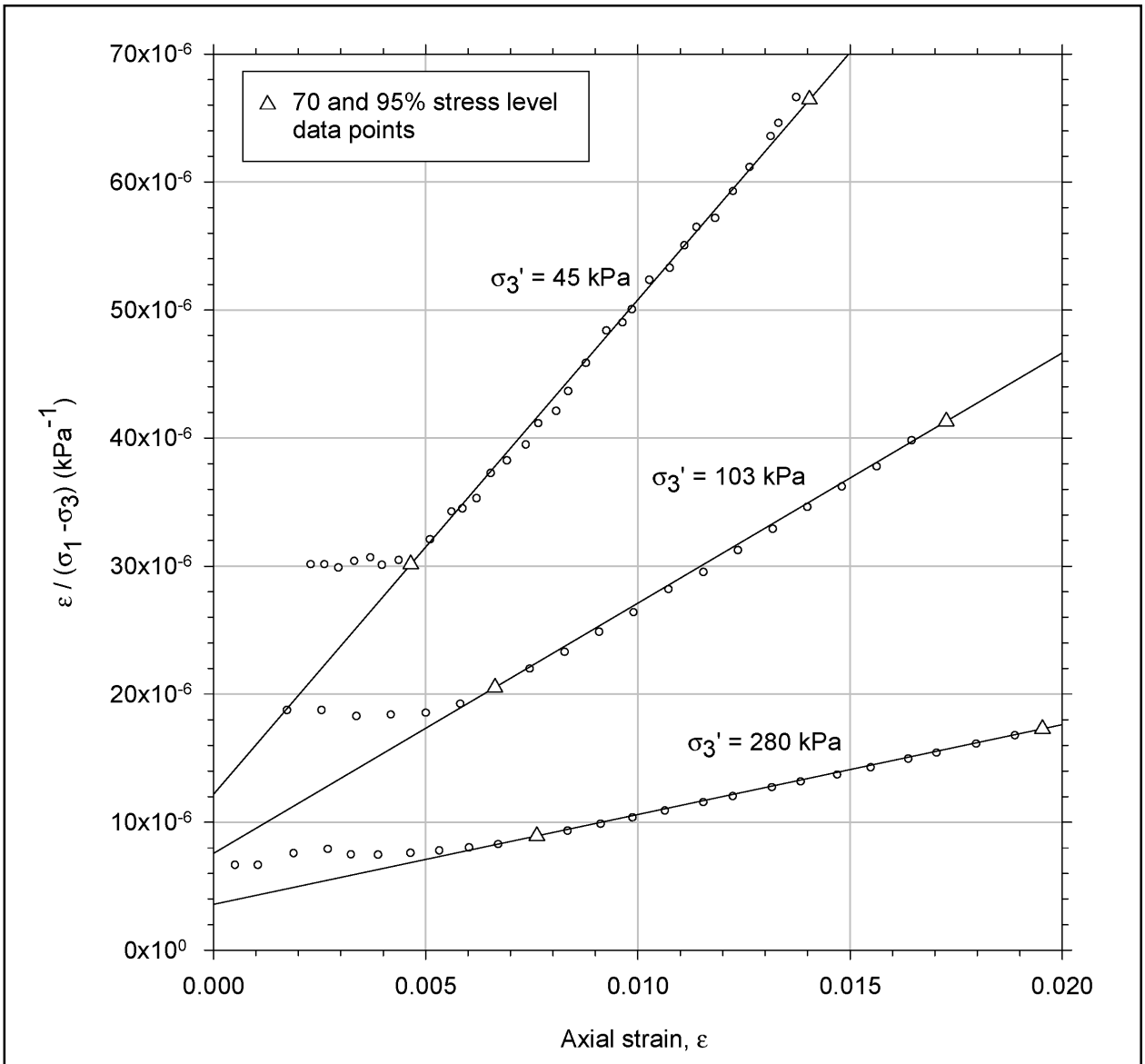

σ_3' (kPa)	a $(kPa)^{-1}$	E_i (kPa)	b $(kPa)^{-1}$	$(\sigma_1 - \sigma_3)_{ult}$ (kPa)	$(\sigma_1 - \sigma_3)_f$ (kPa)	R_f
45	1.22×10^{-5}	82035	3.86×10^{-3}	258.9	222.0	0.858
103	7.56×10^{-6}	132274	1.95×10^{-3}	511.6	439.1	0.858
280	3.58×10^{-6}	279539	7×10^{-4}	1425.1	1187.7	0.833

Average R_f = 0.850

Figure B5. Transformed stress-strain plots from triaxial test data on dense Density sand and determination of hyperbolic parameter values

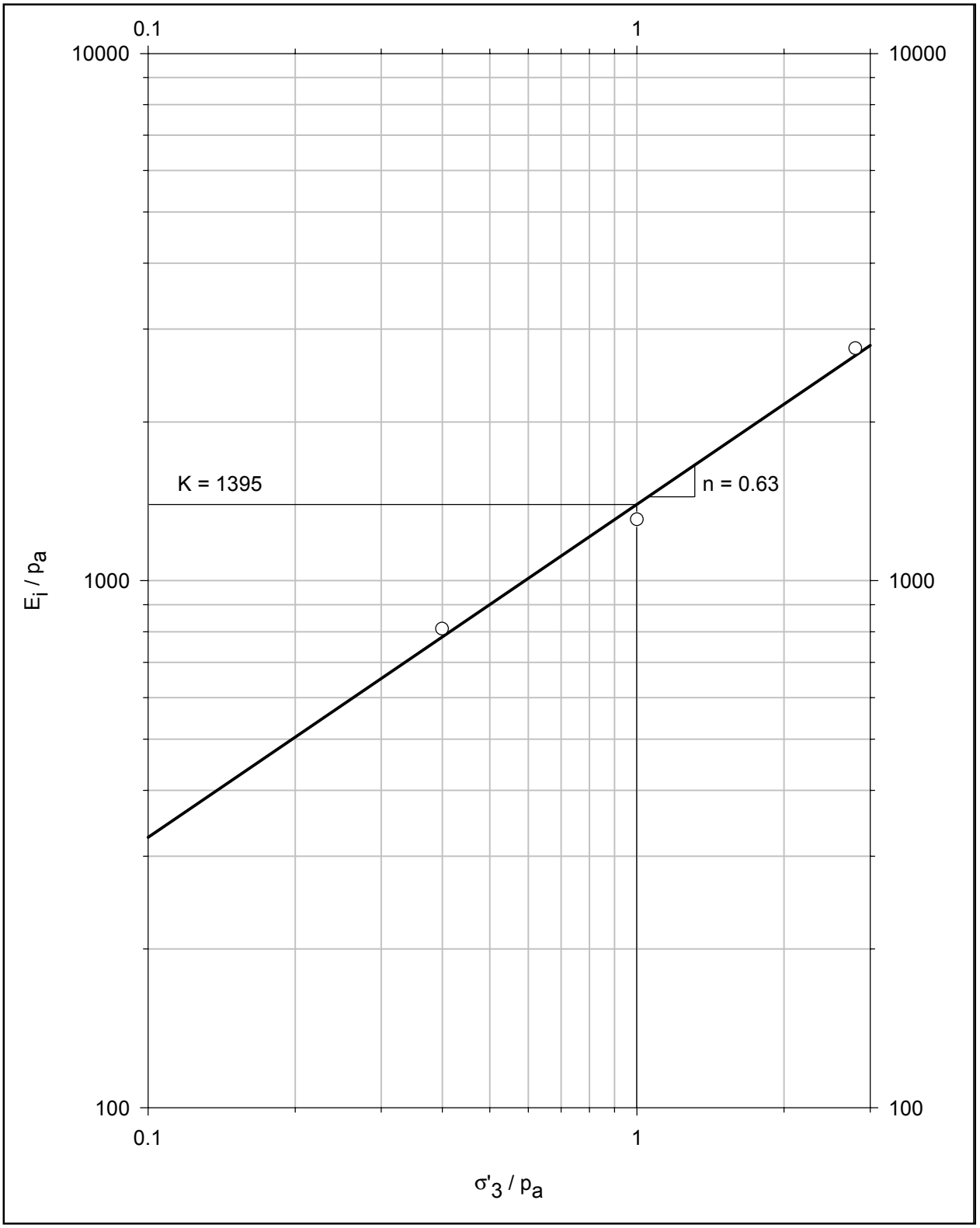

Figure B6. Determination of hyperbolic parameters *K* and *n* for dense Density sand

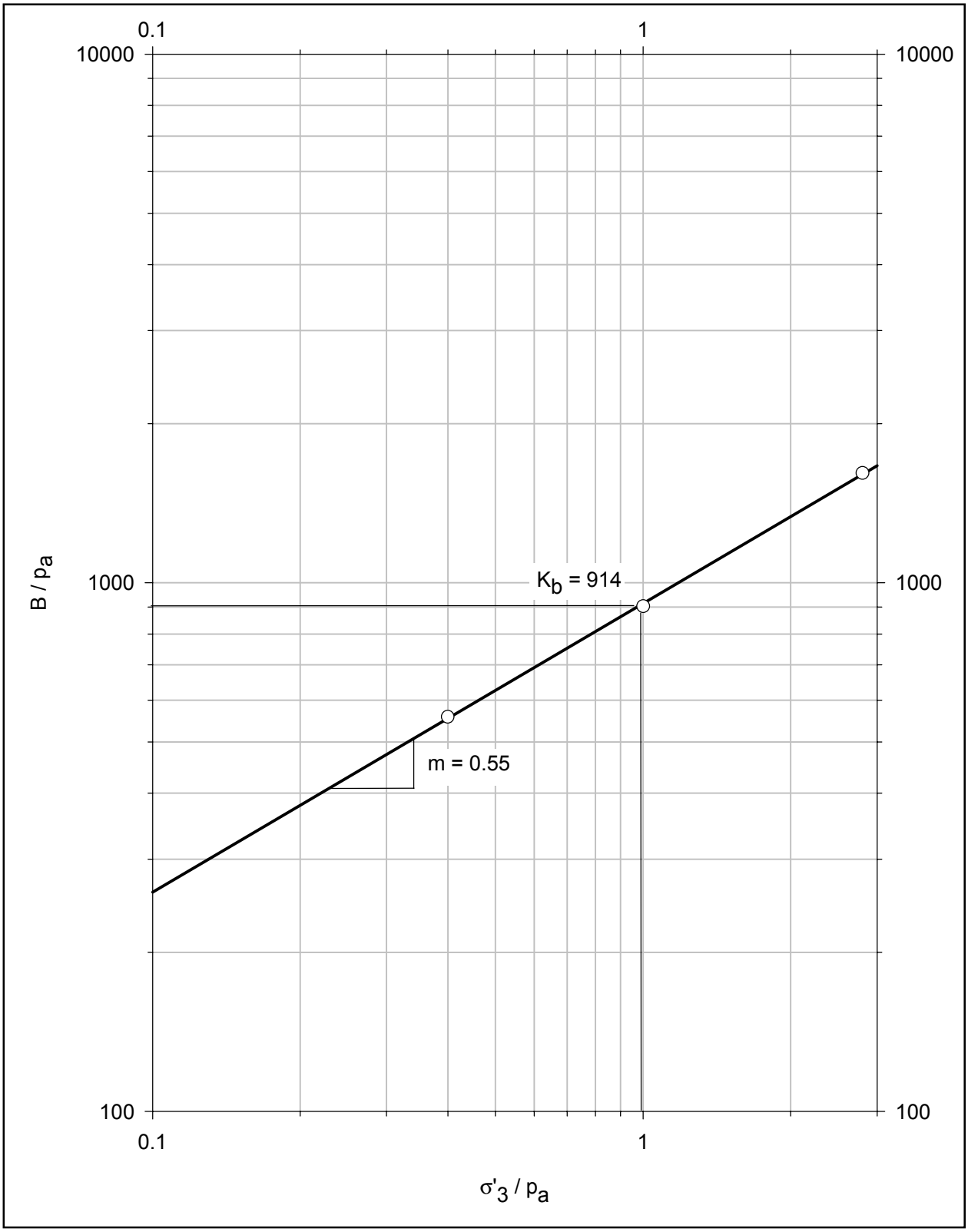

Figure B7. Determination of hyperbolic parameters *K* and *m* for dense Density sand

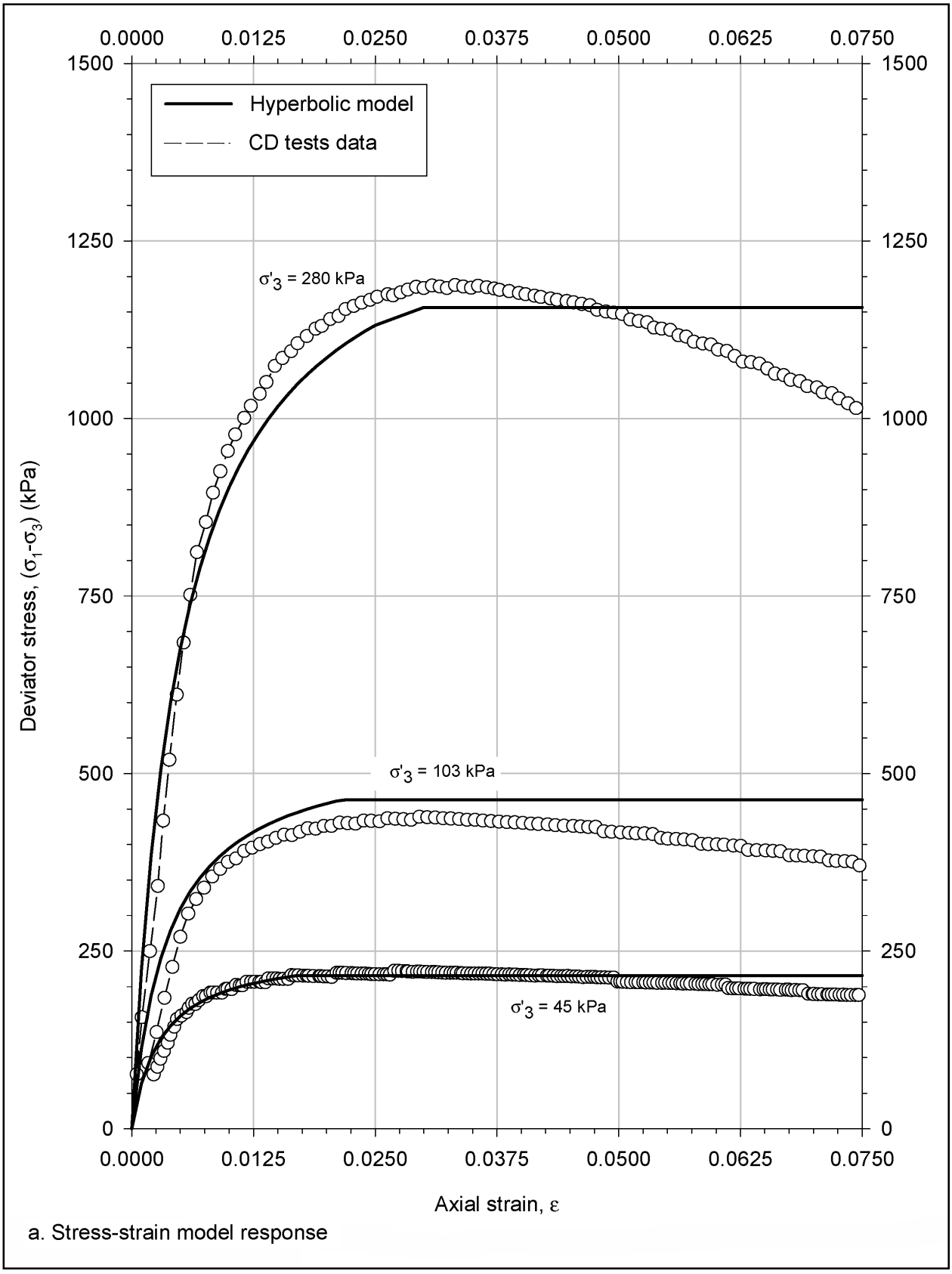

a. Stress-strain model response

Figure B8. Hyperbolic model for dense Density sand and comparison to CD triaxial test data (Continued)

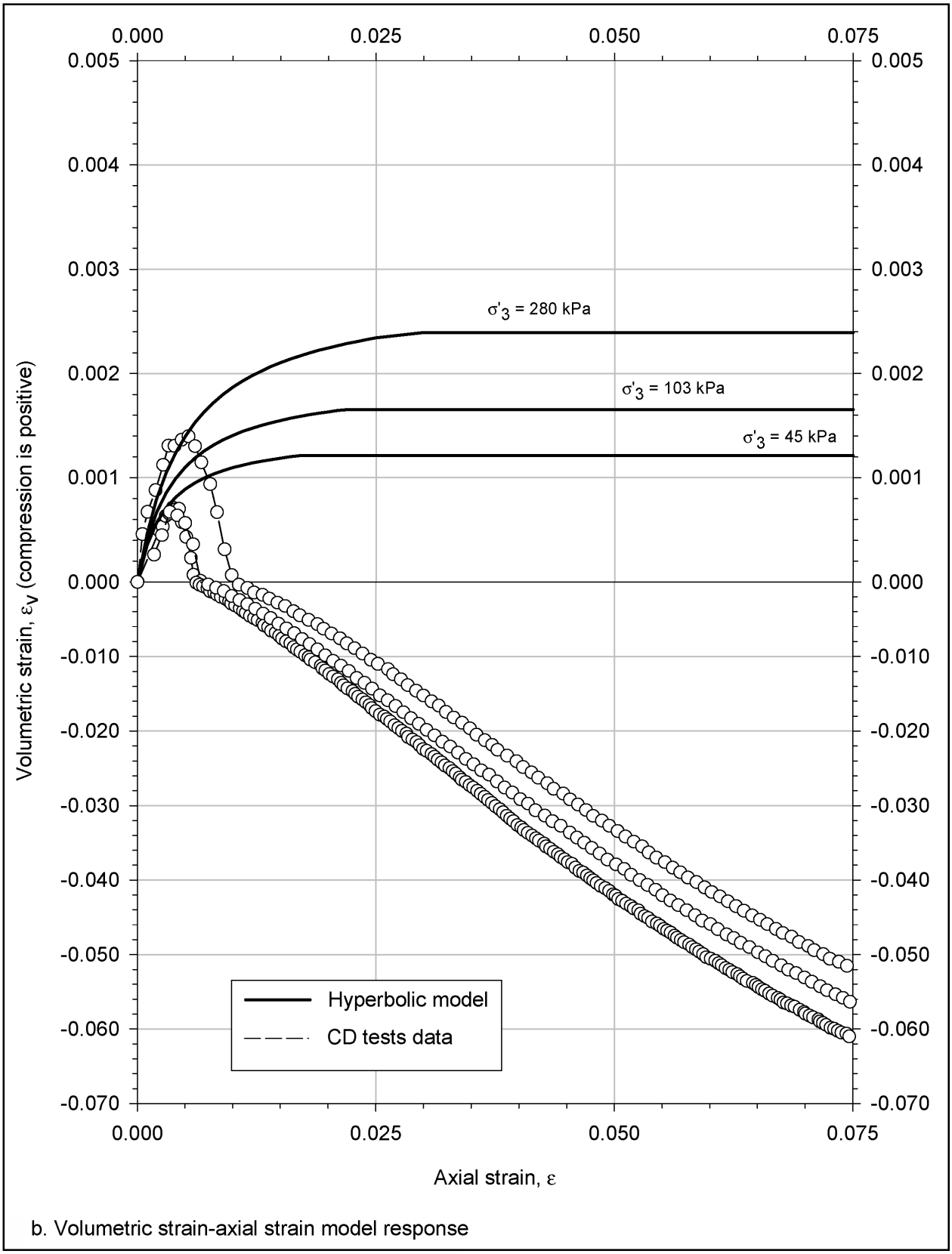

b. Volumetric strain-axial strain model response

Figure B8. (Concluded)

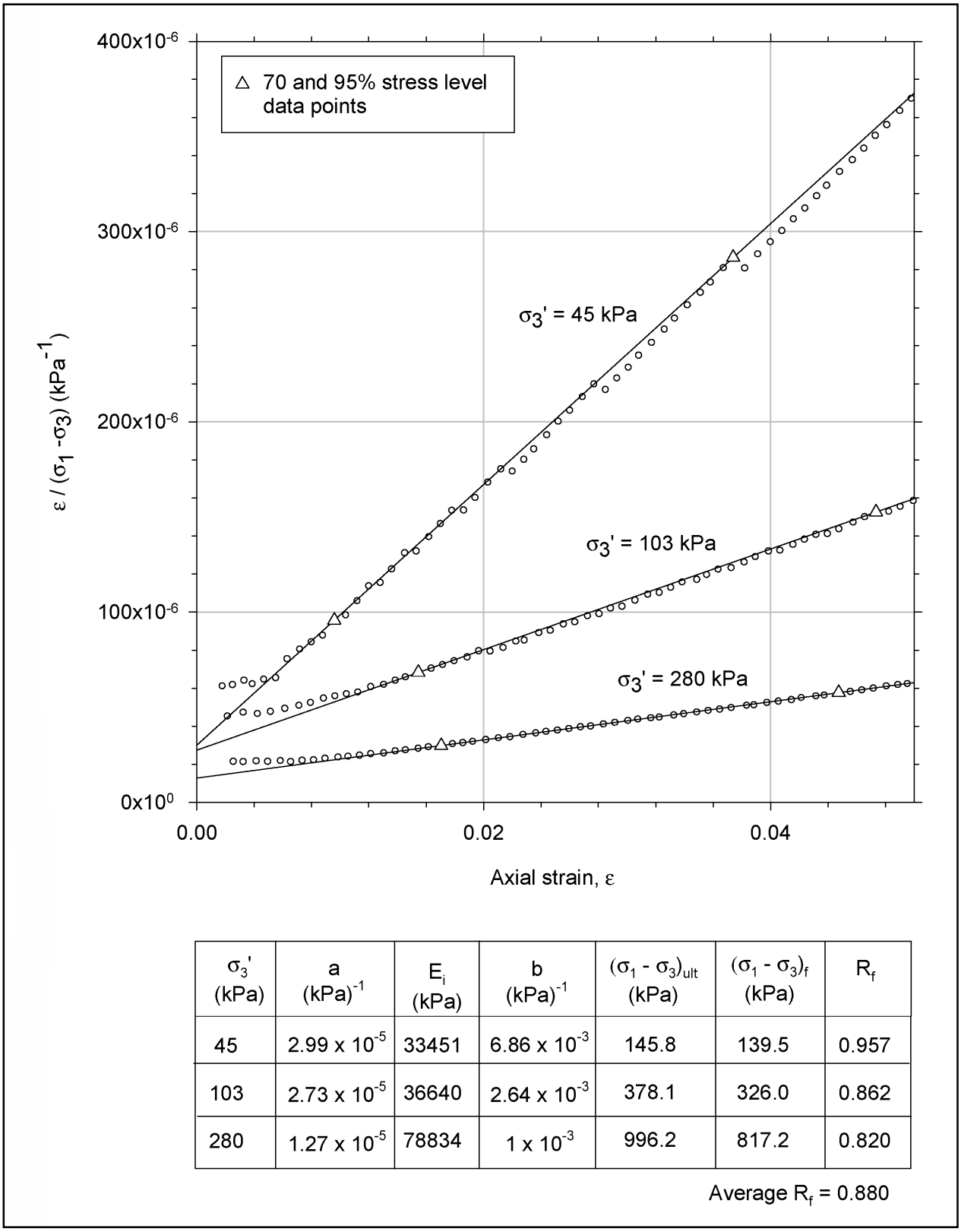

σ_3' (kPa)	a $(kPa)^{-1}$	E_i (kPa)	b $(kPa)^{-1}$	$(\sigma_1 - \sigma_3)_{ult}$ (kPa)	$(\sigma_1 - \sigma_3)_f$ (kPa)	R_f
45	2.99×10^{-5}	33451	6.86×10^{-3}	145.8	139.5	0.957
103	2.73×10^{-5}	36640	2.64×10^{-3}	378.1	326.0	0.862
280	1.27×10^{-5}	78834	1×10^{-3}	996.2	817.2	0.820

Average $R_f = 0.880$

Figure B9. Transformed stress-strain plots from triaxial test data on medium-dense Light Castle sand and determination of hyperbolic parameter values

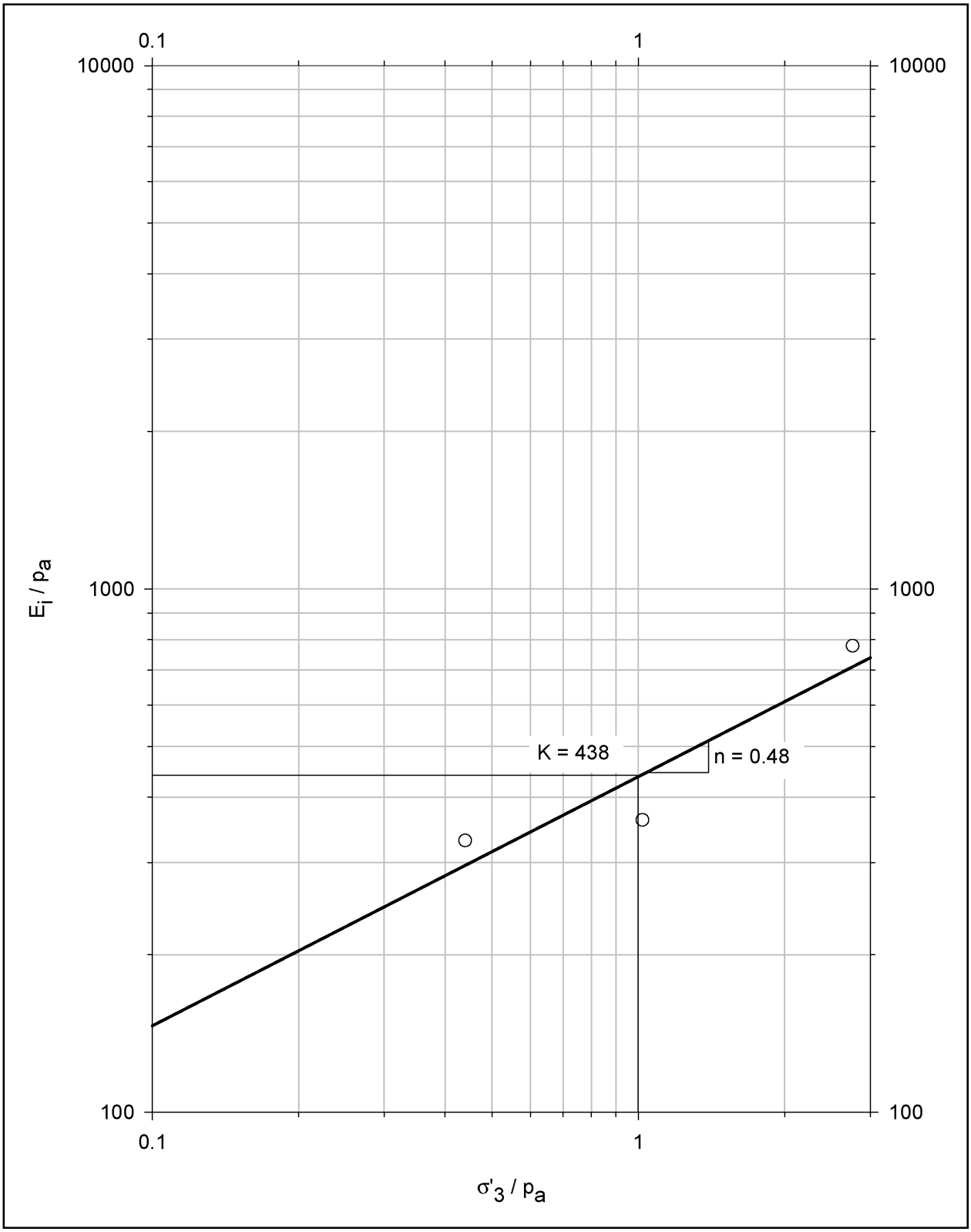

Figure B10. Determination of hyperbolic parameters *K* and *n* for medium-dense Light Castle sand

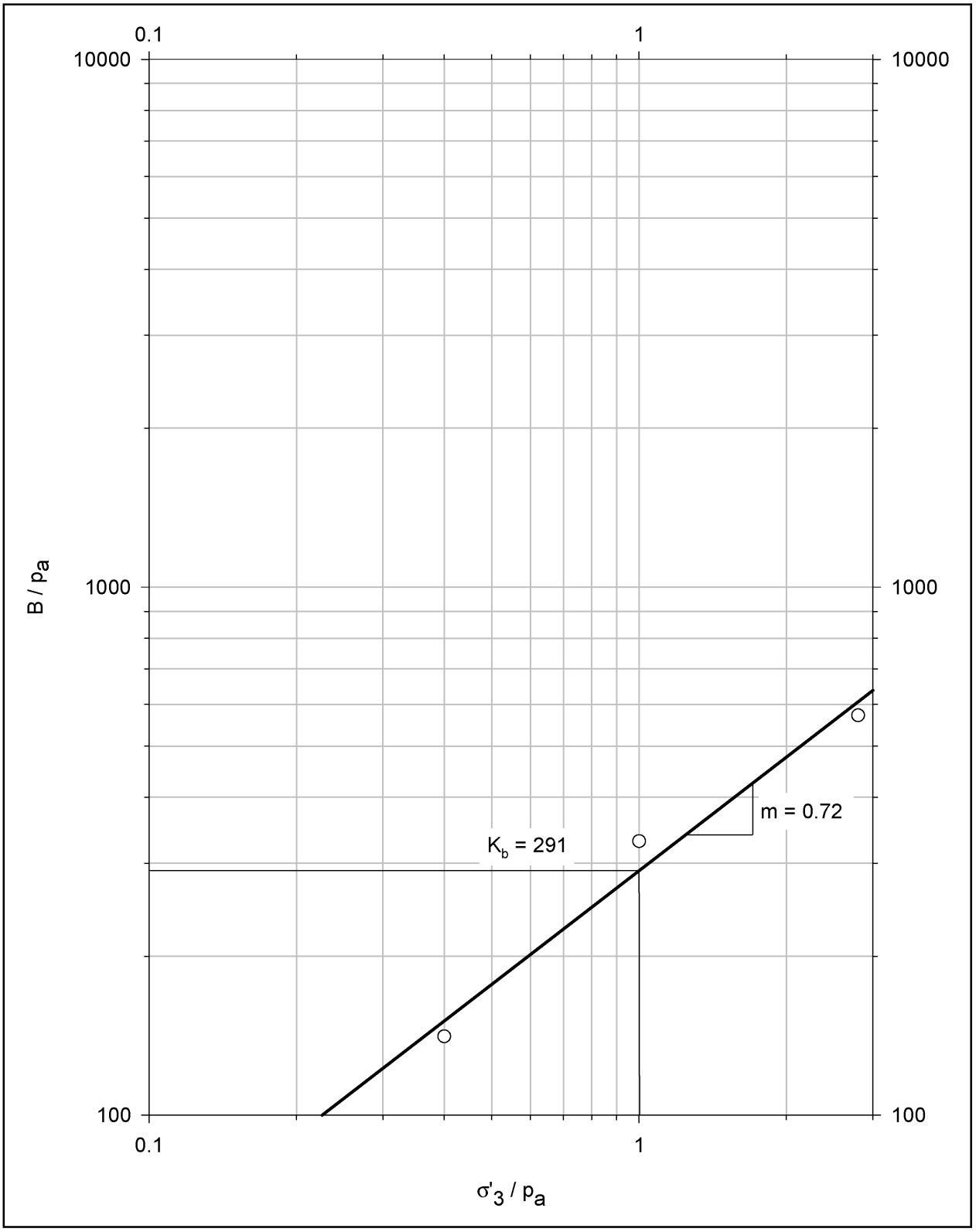

Figure B11. Determination of hyperbolic parameters K_b and m for medium-dense Light Castle sand

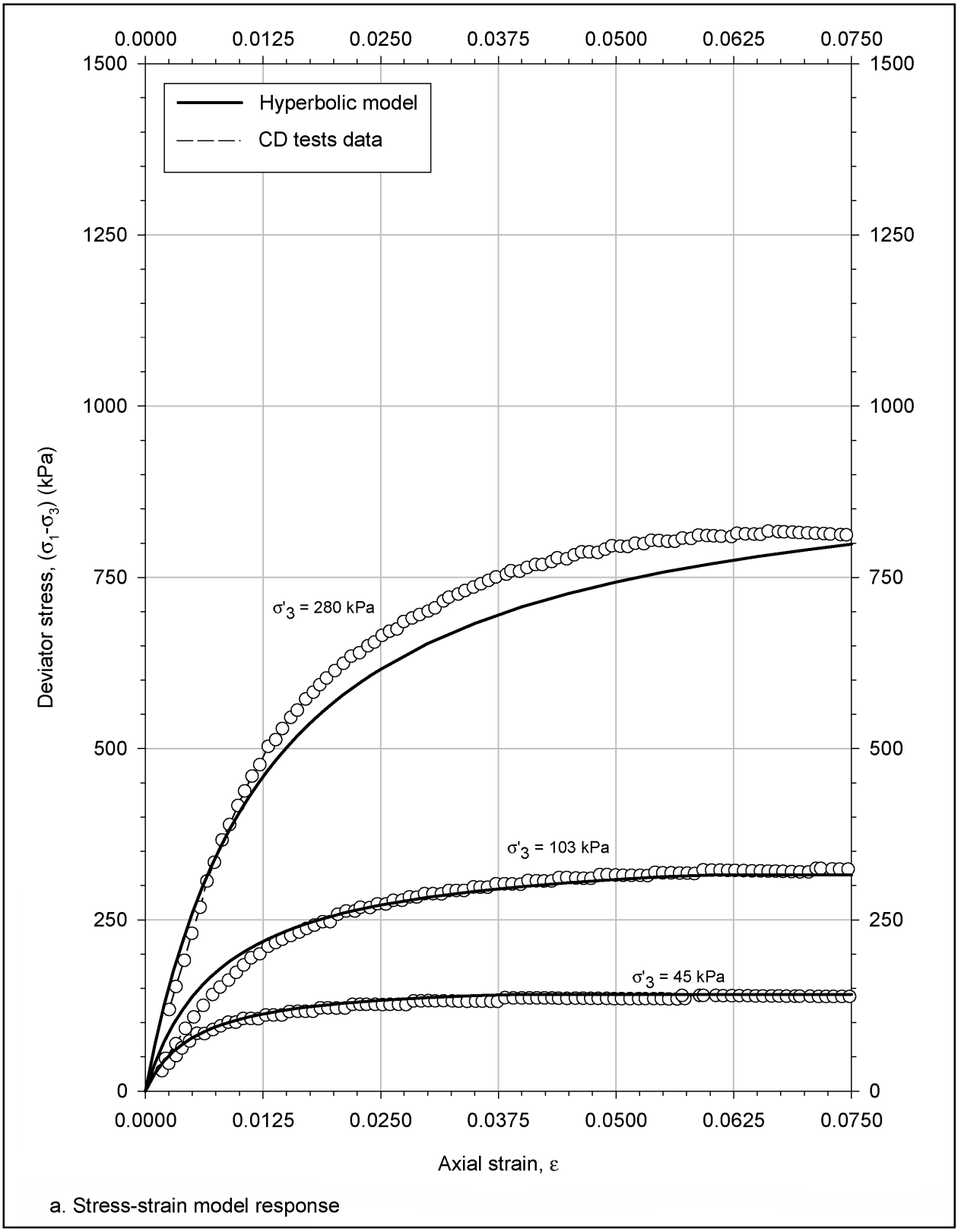

a. Stress-strain model response

Figure B12. Hyperbolic model for medium-dense Light Castle sand and comparison to CD triaxial test data (Continued)

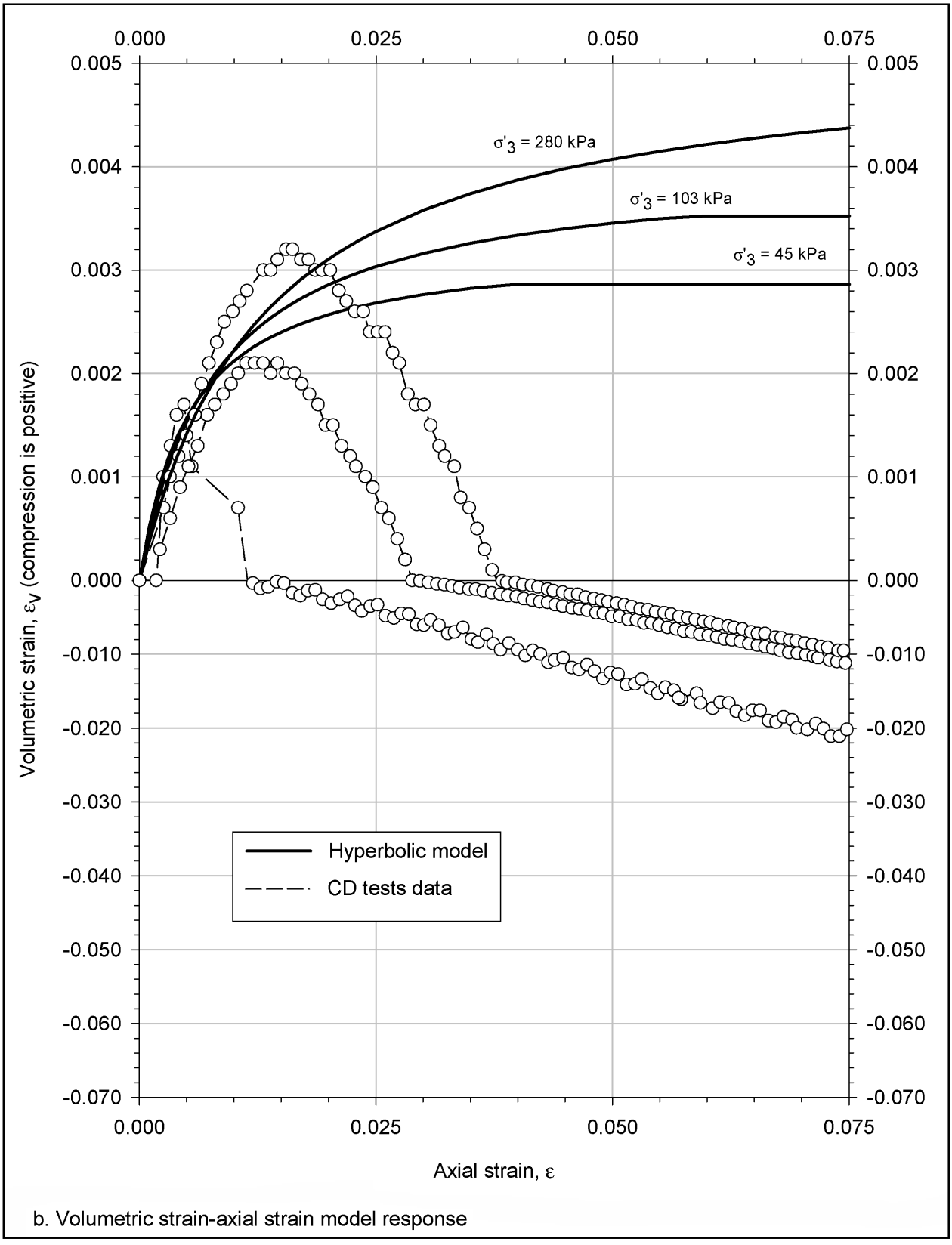

b. Volumetric strain-axial strain model response

Figure B12. (Concluded)

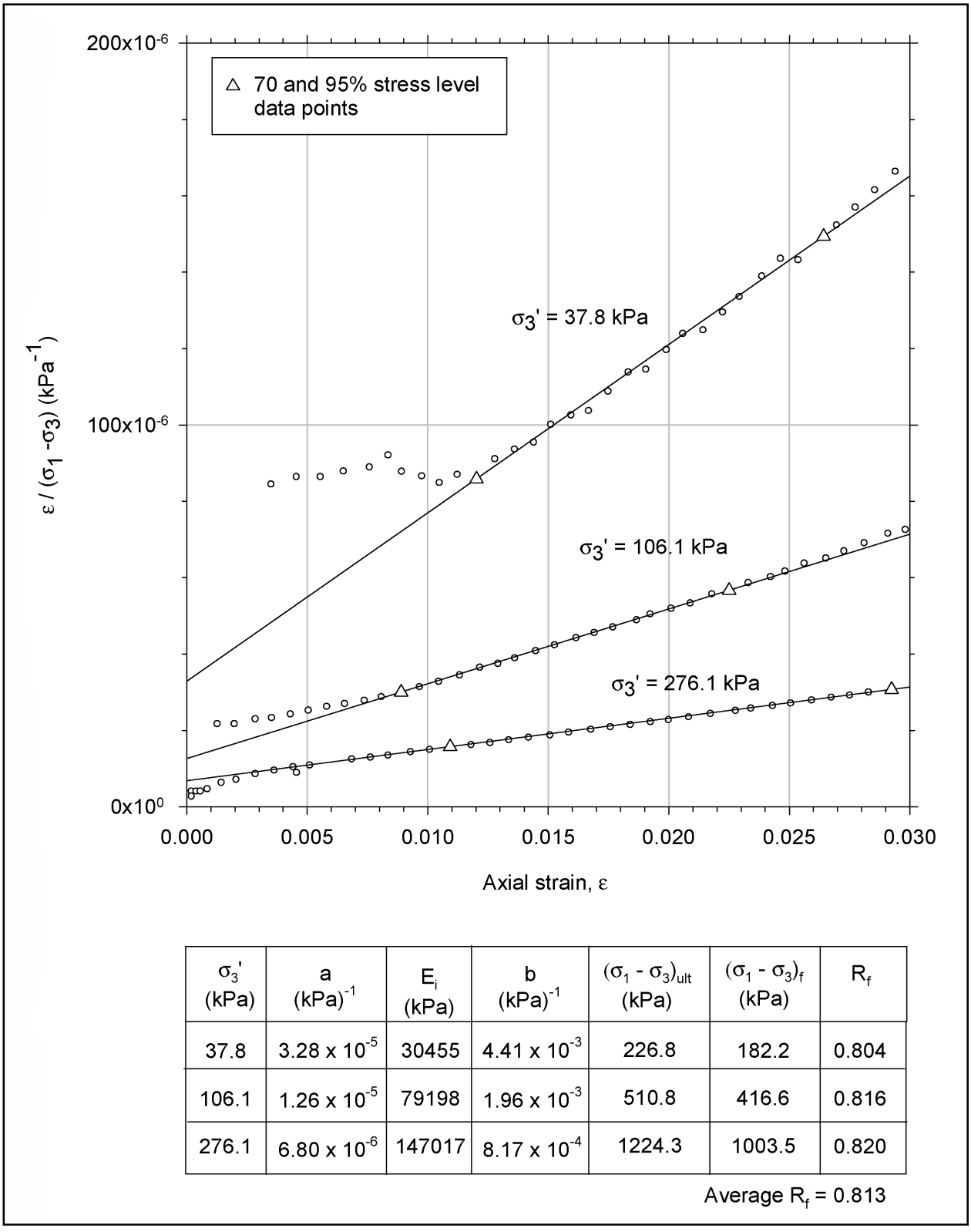

σ_3' (kPa)	a $(kPa)^{-1}$	E_i (kPa)	b $(kPa)^{-1}$	$(\sigma_1 - \sigma_3)_{ult}$ (kPa)	$(\sigma_1 - \sigma_3)_f$ (kPa)	R_f
37.8	3.28×10^{-5}	30455	4.41×10^{-3}	226.8	182.2	0.804
106.1	1.26×10^{-5}	79198	1.96×10^{-3}	510.8	416.6	0.816
276.1	6.80×10^{-6}	147017	8.17×10^{-4}	1224.3	1003.5	0.820

Average R_f = 0.813

Figure B13. Transformed stress-strain plots from triaxial test data on dense Light Castle sand and determination of hyperbolic parameter values

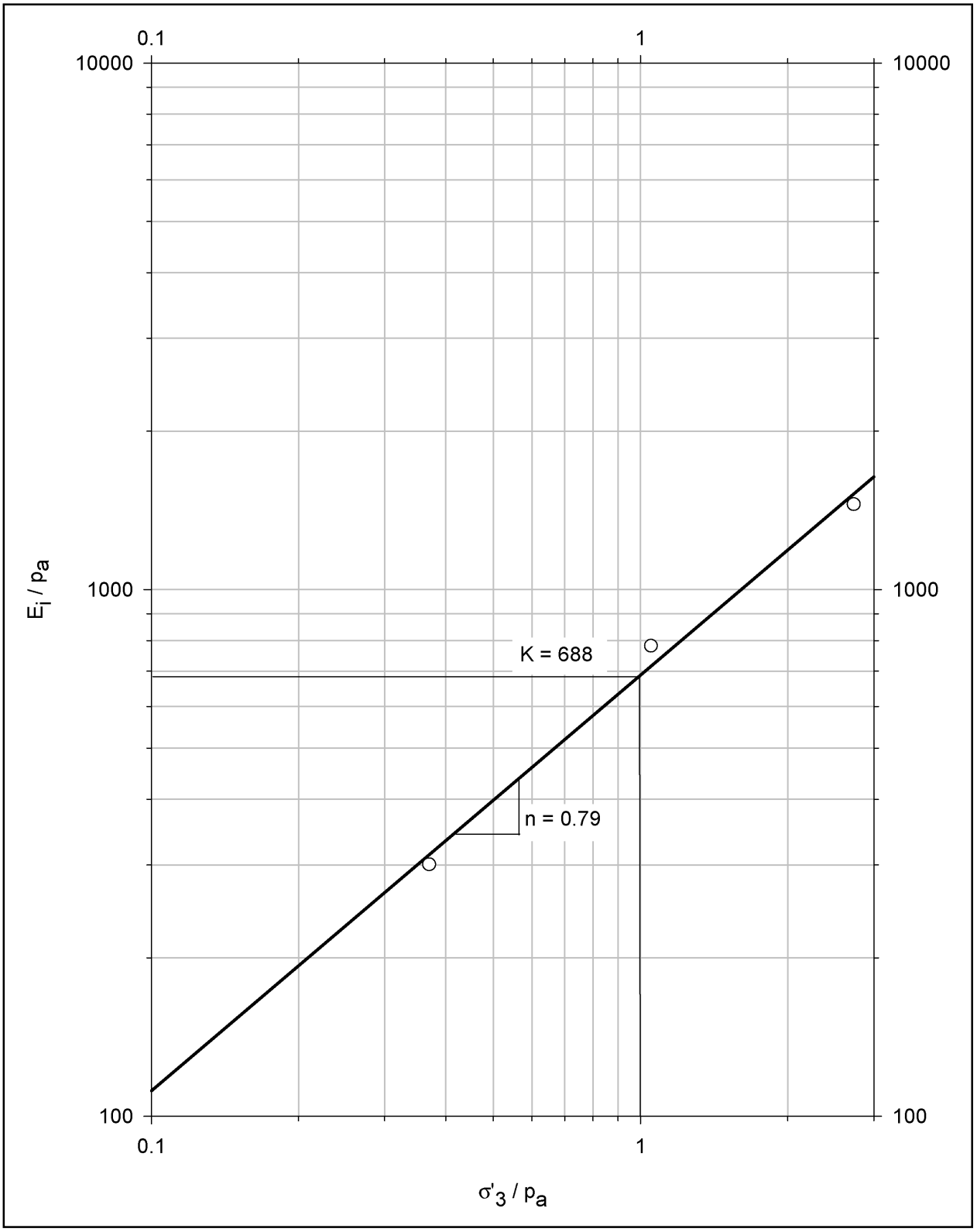

Figure B14. Determination of hyperbolic parameters *K* and *n* for dense Light Castle sand

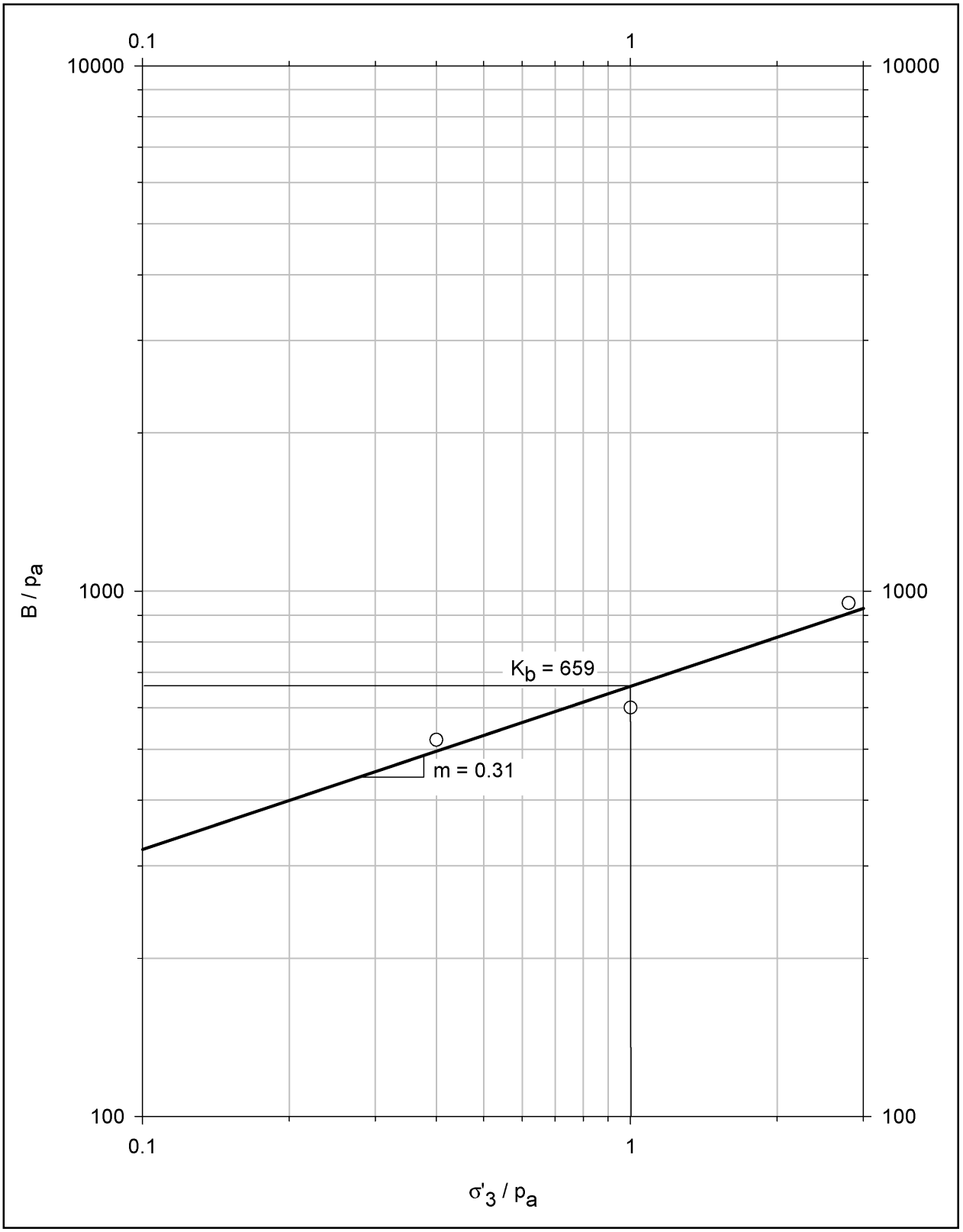

Figure B15. Determination of hyperbolic parameters K_b and m for dense Light Castle sand

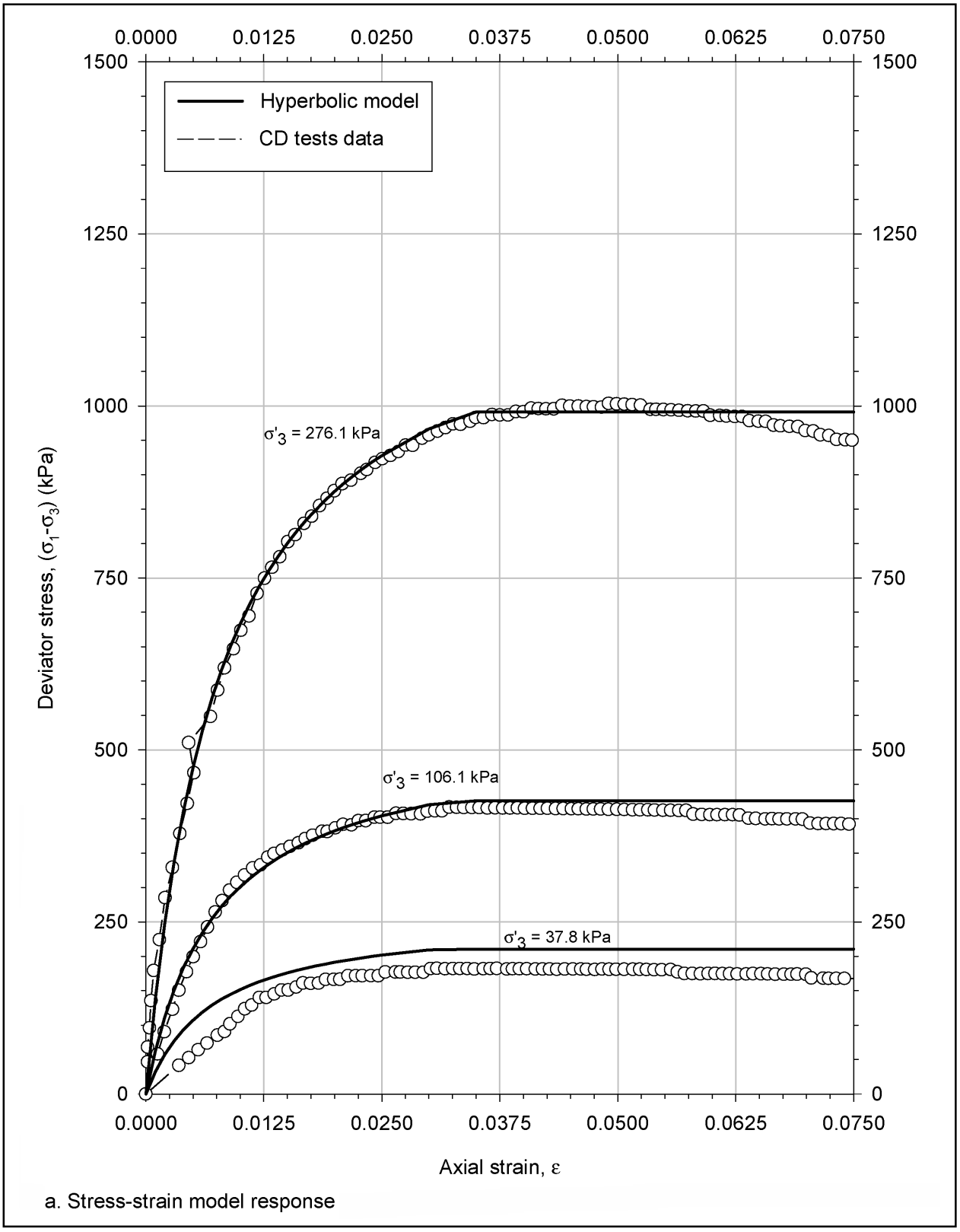

a. Stress-strain model response

Figure B16. Hyperbolic model for dense Light Castle sand and comparison to CD triaxial test data (Continued)

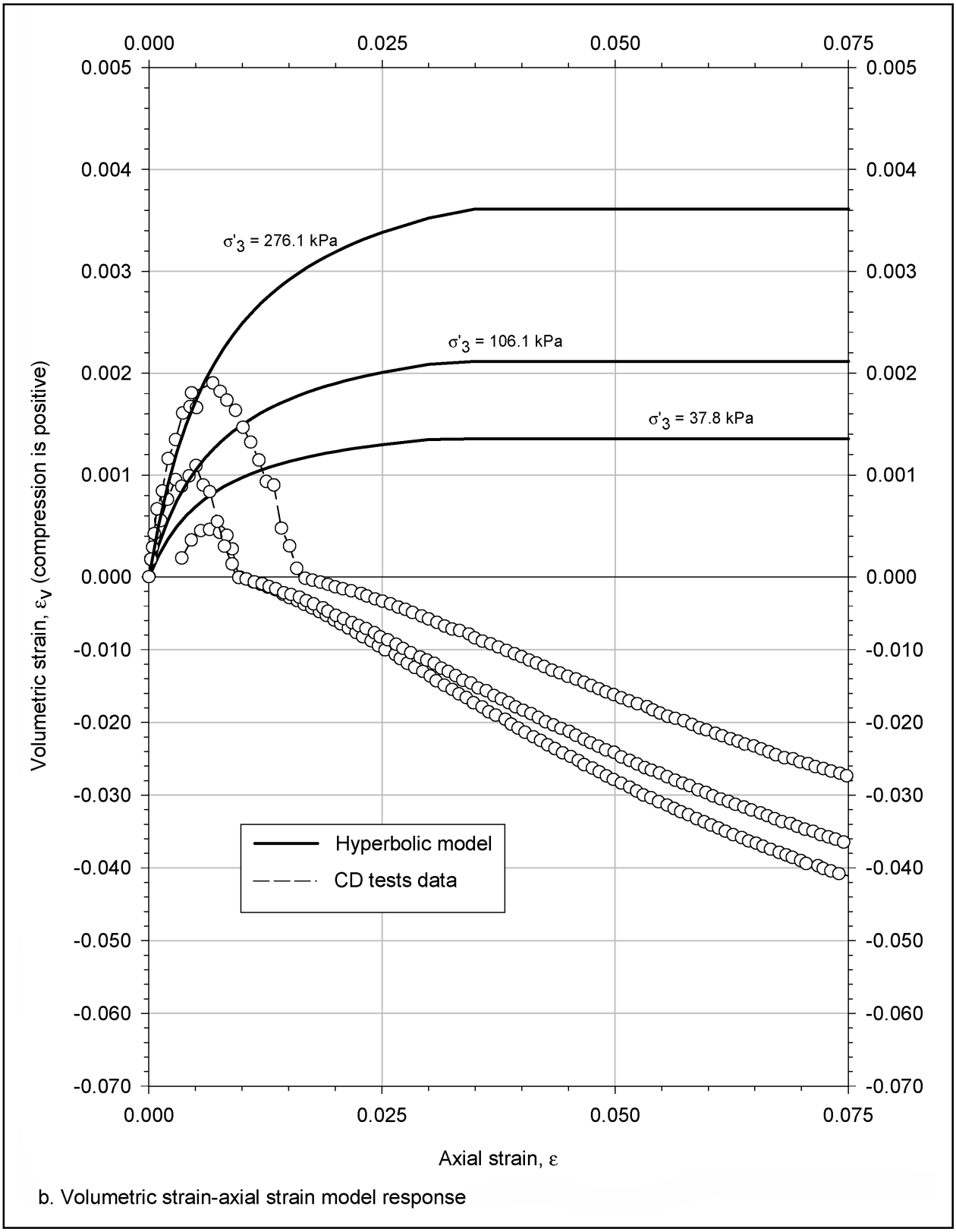

b. Volumetric strain-axial strain model response

Figure B16. (Concluded)

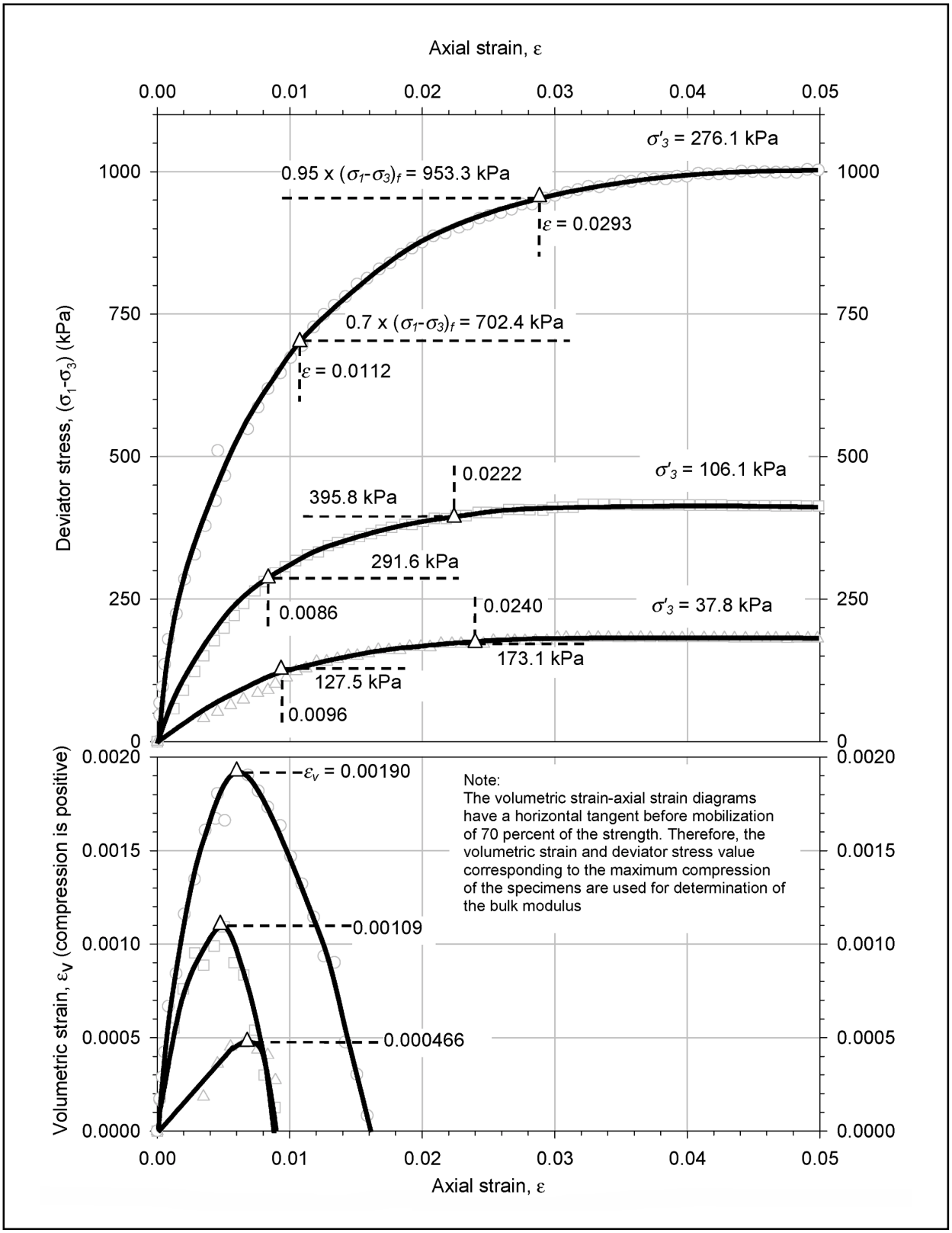

Figure B17. Example determination of axial and volumetric strain values at 70 and 95 percent of strength. Data from CD triaxial tests on dense Light Castle sand

σ'_3 (kPa)	$(\sigma_1-\sigma_3)_f$ (kPa)	Data for Determination of Hyperbolic Parameters K and n						Data for Determination of Hyperbolic Parameters K_b and m		
		70% Stress Level			95% Stress Level					
		$(\sigma_1-\sigma_3)$ (kPa)	ε	$\frac{\varepsilon}{(\sigma_1-\sigma_3)}$ (kPa^{-1})	$(\sigma_1-\sigma_3)$ (kPa)	ε	$\frac{\varepsilon}{(\sigma_1-\sigma_3)}$ (kPa^{-1})	$(\sigma_1-\sigma_3)$ (kPa)	ε_v	$\frac{(\sigma_1-\sigma_3)}{3\cdot\varepsilon_v}$ (kPa)
(1)	(2)	(3)	(4)	(5)	(6)	(7)	(8)	(9)	(10)	(11)
38	182.2	127.5	0.0096	7.53×10^{-5}	173.1	0.0240	1.39×10^{-4}	73.8	0.00047	52340
106	416.6	291.6	0.0086	2.95×10^{-5}	395.8	0.0222	5.61×10^{-5}	199.2	0.00109	60917
276	1003.5	702.4	0.0112	1.59×10^{-5}	953.3	0.0293	3.07×10^{-5}	548.3	0.00190	96192

$\frac{\sigma'_3}{pa}$ (12)	$\frac{1}{(\sigma_1-\sigma_3)_{ult}}$ (kPa^{-1}) (13)	R_f (14)	$\frac{E_i}{pa}$ (15)	$\frac{B}{pa}$ (16)
0.38	4.42×10^{-3}	0.805	300	517
1.05	1.96×10^{-3}	0.816	782	601
2.72	8.18×10^{-4}	0.820	1465	950

Notes:
- pa = 101.3 kPa
- Figure B17 illustrates the procedure for the determination of the values of deviator stress, axial strain, and volumetric strain for this example
- See Appendix B for a complete explanation of the hyperbolic model and procedure for determination of hyperbolic parameter values
- In this example, the organization of calculations is based on Figure 21 of Duncan et al. (1980). Numerical values correspond to the dense Light Castle Sand used for this investigation

(1) Confining stress. Use effective confining stress, σ'_3, for effective stress analyses. Use total confining stress, σ_3, for total stress analyses

(2) Deviator stress at failure. Determined from the deviator stress-axial strain plots of the data of each test.

(3) 70 percent of $(\sigma_1-\sigma_3)_f$ **(4)** Axial strain corresponding to (3) determined as illustrated in Figure B17 **(5)** $\frac{\varepsilon}{(\sigma_1-\sigma_3)} = \frac{(4)}{(3)}$

(6) 95 percent of $(\sigma_1-\sigma_3)_f$ **(7)** Axial strain corresponding to (6) determined as illustrated in Figure B17 **(8)** $\frac{\varepsilon}{(\sigma_1-\sigma_3)} = \frac{(7)}{(6)}$

(9) Deviator stress for determination of bulk modulus, B. Use (3) if the ε_v-ε curve does not reach a horizontal tangent in compression before (3) is mobilized. Otherwise, use $(\sigma_1-\sigma_3)$ corresponding to the maximum ε_v (compression) as illustrated in Figure B17

(10) Volumetric strain for determination of B. Use ε_v corresponding to (3) if the ε_v-ε curve does not reach a horizontal tangent in compression before (3) is mobilized. Otherwise, use the maximum ε_v (compression) as illustrated in Figure B17

(11) $\frac{(\sigma_1-\sigma_3)}{3\cdot\varepsilon_v} = \frac{(9)}{3\cdot(10)}$ **(12)** $\frac{\sigma'_3}{pa} = \frac{(1)}{101.3kPa}$ **(13)** $\frac{1}{(\sigma_1-\sigma_3)_{ult}} = \frac{(8)-(5)}{(7)-(4)}$ **(14)** $R_f = (2)\cdot(13)$ **(15)** $\frac{E_i}{pa} = \frac{2}{(5)+(8)-(13)\cdot[(4)+(7)]}\cdot\frac{1}{pa}$

(16) $\frac{B}{pa} = \frac{(11)}{pa}$

Figure B18. Determination of the normalized values of E_i and B for each of the CD triaxial tests performed on dense Light Castle sand (adapted from Duncan et al. 1980)

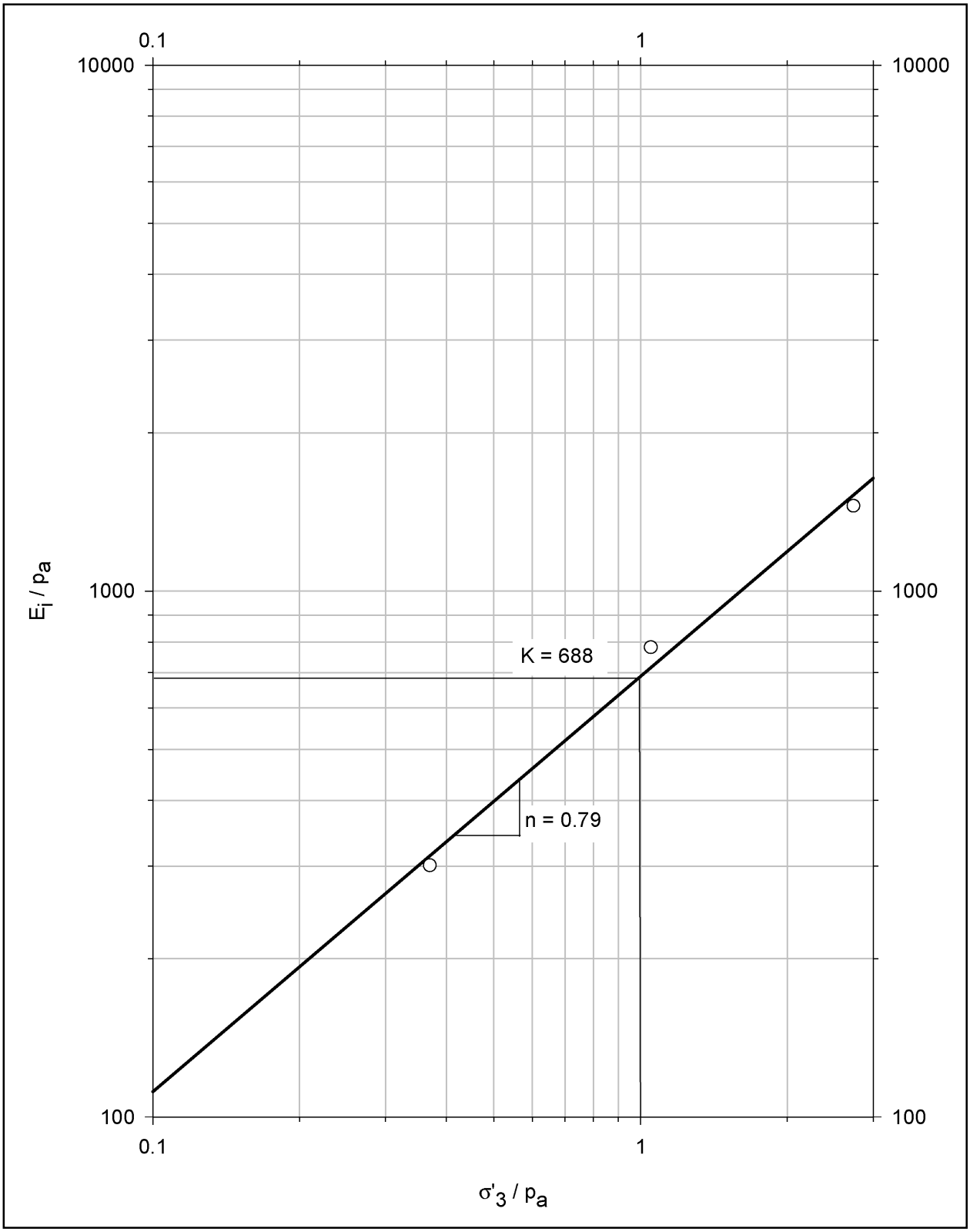

Figure B19. Determination of hyperbolic parameters *K* and *n* from the E_i/p_a values determined in column (15) of Figure B18

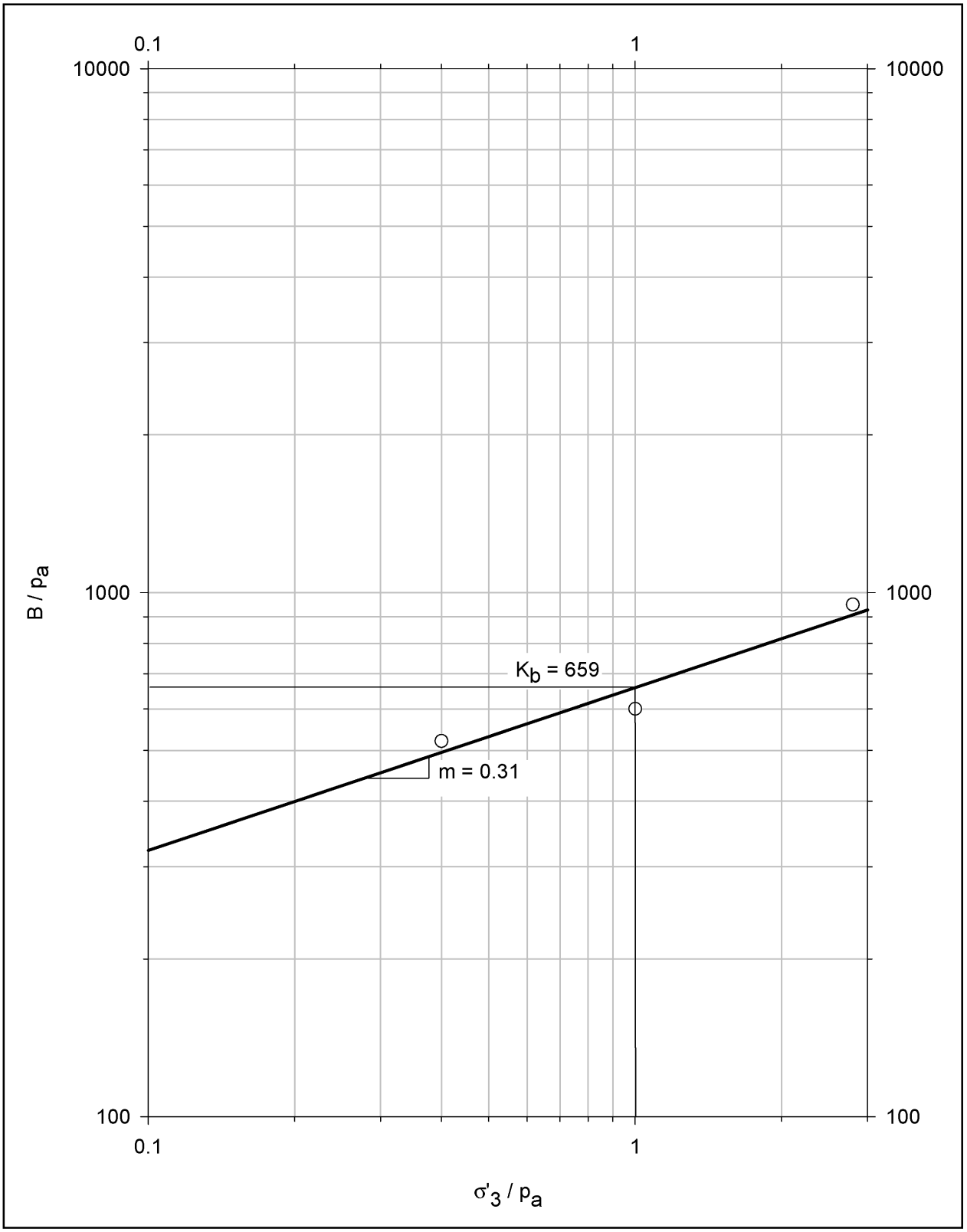

Figure B20. Determination of hyperbolic parameters K_b and m from the B/p_a values determined in column (16) of Figure B18